Relaxin Addition Therapy To Combat Muscle Fibrosis Associated With Duchenne Muscular Dystrophy

MPhil Thesis

September 2019

Yee King Leong

Supervisors: Dr. Linda Popplewell, Prof. George Dickson

Advisor: Dr Pavlos Alifragis,

School of Biological Sciences

Royal Holloway University of London

DECLARATION

This work presented in this thesis was carried out in School of Biological Sciences, at Royal Holloway University of London. I confirm that all the content in this work is my own hard work and has not been shown to any other.

Yee King Leong

ACKNOWLEDGEMENTS

The studies in this thesis were an exciting learning process and fantastic insight into gene therapy. Although, many challenges in this project, I feel grateful about the support from multiple group of people who provide scientific guideline, scientific research assistance, discussions, sharing idea and all excellent friendship experiences:

I would like to full-heartedly appreciate my supervisors Dr Popplewell Linda who provide not just professional guidance, excellent mentoring, scientific inspiration, research mentoring and most important believing in me. Next, Professor George Dickson with his many years of scientific research experiences in the field of gene therapy for Duchenne Muscular Dystrophy. And also, to my previous MSc supervisor Dr Takis Athanasopoulos.

All of the lab members of Dickson and Linda lab including all the post-doc Ngoc, Shan, Alberto, Pradeep, Lukacz, Betty, previous post-doc Susie, Hayder, Jamuna and Anita, previous PhD Marc and Golnoush, PhD student Arjun, Nertiyan, Rebeca, James, Ona, Viktorija and Master student Julia, Leoni and Chiara. Besides, the lab members from lab 203a Alaa, Anila, Aminder, Jade and Ilde; 4-04 office member Joe, Versha, Ellie, Sashar, Eleanor, Judith, Erwann, Anthony and George.

SPECIAL DEDICATION

My very special thanks to my parents Yeok Poo Leong and Cheng Cher Lee for all the support throughout my life.

René Descartes

“ I think / resist , therefore I exist!”

Jean-Paul Sartre

ABSTRACT

The progressive X-linked genetic disorder Duchenne Muscular Dystrophy (DMD) is caused by a defect in the myofibre subsarcolemmal protein dystrophin. The malfunction of dystrophin leads to myofibre membrane fragility and myofibre necrosis. Currently, there is no cure for DMD available, which affects 1 in 3500 live male birth worldwide.

Here, we test the hypothesis that overexpression of the hormone relaxin is able to reduce muscular fibrosis. For this purpose, we use conventional plasmids or adeno-associated viral (AAV) vectors based plasmids to express mouse relaxin 1 isoforms in mouse muscle cells (C2C12 cells) and in mouse muscle fibroblasts (MH cells). We assessed the expression of relaxin, as well as the relaxin downstream effect on fibrotic related genes, in transfected cells through real-time quantitative PCR or Western Blot analysis. In addition, we performed *in vitro* wound scratch assays to examine whether overexpression of relaxin decreases the migration potential of fibroblasts. We show that an increased expression of relaxin reduces the fibrotic response of muscle fibroblasts *in vitro*.

On the basis of this cellular work, overexpression of relaxin may have the potential to reduce muscle fibrosis in *in vivo* models of DMD. Further studies will be carried out in mouse models to fully explore the potential of overexpressed relaxin as a novel anti-fibrotic therapy in patients suffering from DMD.

GLOSSARY OF ABBREVIATIONS

AAV	Adeno associated virus
Amp	Ampicillin
BSA	Bovine serum albumin
cDNA	complementary DNA
CO	Codon optimised
DMD	Duchenne muscular dystrophy
DMEM	Dulbecco Modified Eagle Media
DNA	Deoxyribonucleic acid
ECM	Extracellular matrix
FBS	Fetal bovine serum
GFP	Green fluorescent protein
kb	Kilobase
kDa	Kilidalton
LB	Luria-Bertani
µ	Micro
mRln1	mouse relaxin 1
NCO	non-codon optimised
ng	nanogram
nm	Nanometre
NP-40	Nonidet P-40
ori	Originate of replicate
pDNA	Plasmid DNA
PBS	Phophaste buffered saline
PCR	Polymerase chain reaction
PEI	Polyethylenimine
mRNA	Messenger RNA
mRln1	Mouse relaxin 1
RNA	Ribonucleic acid
rpm	Revolutions per minute
scAAV	Self-complementary AAV
Spc512	Muscle specific synthetic promoter
ssAAV	Single stranded AAV
SV40	Simian virus 40
SyBr	N',N'-dimethyl-N-[4-[(E)-(3-methyl-1,3-benzothiazol-2-ylidene)methyl]-1-phenylquinolin-1-ium-2-yl]-N-propylpropane-1,3-diamine
TAE	Tris base, acetic acid and EDTA buffer
TRE	Tetracycline respond element
UV	Ultraviolet

TABLE OF CONTENT

LIST OF FIGURES

LIST OF TABLES

CHAPTER 1: INTRODUCTION

1.1 GENE THERAPY

1.1.1 Overview of gene therapy

The idea of gene therapy was first mentioned by Dr. Marshall Nirenberg around 1960, who suggested that "genetic surgery" might be a cure to treat human diseases (Nirenberg, 1967). Gene therapy involves the transfer of genetic material into the host, such as humans. The purpose of a gene therapy is to either alter the expression of a specific gene or to correct a mutation in a malfunctioning gene.

The first patient, who was successfully cured through a gene therapy was a four year old girl, who suffered from severe immunodeficiency syndrome. In 1990, this patient received *ex vivo* a corrected version of adenosine deaminase through white blood cells. The gene therapy was successful and cured her disease long-term (Bordignon, et al., 1995; Sutton, R., 2018). However, there are also challenges to consider when conducting a gene therapy. In 1999, Jesse Gelsinger, who received an adenovirus vector that expressed ornithine transcarbamylase, suffered from a massive anaphylactic reaction, which lead to his death after four days (Sibbald, B., 2001). The case of Jesse Gelsinger caused a reconsideration in gene therapy and led to a higher safety standard.

To date, there have been worldwide around 2600 gene therapy clinical trials approved or completed. Most of these studies take place either in the USA (64.9%) or in Europe (23%). The main focus of gene therapy are various forms of cancer (65 % of the studies), monogenetic diseases (11.1 % studies) and cardiovascular diseases (6.9 % of the studies). Only a few gene therapies have passed through clinical trials and are now available on the market; the gene therapy Luxturna (Spark Therapeutics) improves the vision in patients suffering from Leber congenital amaurosis or retinitis pigmentosa. In addition, Kymriah (Norvatis) and Yescarta (Kite Pharma Inc/Gilead) has been developed to treat leukemia or B-cell lymphoma, respectively (Gene and Cell Therapy FAQ's, 2018). In 2012, Glybera launched their gene therapy against a rare lipoprotein lipase deficiency in Europe, however it was withdrawn in 2017 due to the enormous cost for each patients (1 million euro) (Morrison, 2015; Senior, 2017). Despite the

enormous therapeutic benefits of gene therapy, there are still many challenges, such as high-costs, that have to be overcome in the future.

1.1.2 Gene Therapy Vectors

Gene therapy is achieved by delivering genetic material to specific cells through the viral or non-viral systems route. In non-viral delivery systems, the genetic material is delivered into the cells through electroporation (genetic material is transferred into cells through high voltage), passive delivery (endocytosis of the genetic material into cells) or ballistic delivery (sheer mechanical force delivering genetic material into cells) (Gene and Cell Therapy FAQ's, 2018).

Non-viral vectors based gene therapy relies on the import of exogenous genetic material into the cell nucleus through physical or chemical systems. Non-viral vectors offer lower immune responses compared to viral vectors. In addition, non-viral vectors have no limitation on exogenous transgene capacity and are relatively easy to apply. There are several modified viruses available that can be used to transfer genetic material into cells. The main focus of this thesis are naked plasmid DNA systems (non-viral delivery). In addition, we plan to test Adeno-Associated Virus (AAV) (viral delivery) in *in vivo* experiments. The AAV viral delivery systems are more effective to deliver genetic materials where AAV viral normally have lower immunogenic respond compare to other types of viral vector (Naso, *et al*., 2017).

1.1.2.1 Viral vectors

In viral vectors disease-causing and –associated genes are removed from the viral genome, only leaving genes that are important for the structure of the virus. Subsequently, potential therapeutic transgenes are integrated into the genome of the virus to create recombinant viral vectors (Thomas *et al*., 2003). The common viral vector adeno-associated virus (AAV) and retrovirus (RV)/lentivirus (LV) vectors have been modified by removing the viral gene that is essential for replication (Daya & Berns, 2008). There are many properties that

contribute to an ideal viral vector for gene therapy such as immunological silence, easy to scale up production, tissue-specific targeting, capability to transduce dividing/non-dividing cells and the capability to integrate the transgene. The capability to integrate the transgenes into host is a double-edged knife where it can cause random insertional mutation mutagenesis (Ramamoorth and Narvekar, 2015). On the other hand, integrating transgene into the host genome is useful for stable long-term transgene expression therapy (Braun, *et al*., 2014), as it provides permanent transgene expression in the host. Each type of viral vector offers advantages as well as disadvantages (**Table 1.1**). More than 70% of all gene therapies in clinical studies are conducted using the viral vectors Adenovirus (AV), Lentivirus (LV)/ Retrovirus (RV) and AAV (Wiley, 2017). This suggests that viral delivery systems are for some treatments the more promising strategy.

Particle characteristics	**Adenovirus**	**Adeno-associated virus**	**Alphavirus**	**Herpesvirus**	**Retrovirus /Lentivirus**	**Vaccinia virus**
Genome	dsDNA	ssDNA	ssRNA (+)	dsDNA	ssRNA (+)	dsDNA
Capsid	Icosahedral	Icosahedral	Icosahedral	Icosahedral	Icosahedral	Complex
Coat	Naked	Naked	Enveloped	Enveloped	Enveloped	Enveloped
Virion polymerase	Negative	Negative	Negative	Negative	Positive	Positive
Virion diameter	70 – 90 nm	18 – 26 nm	60 – 70 nm	150 – 200 nm	80 – 130 nm	170 – 200 X 300 – 450 nm
Genome size	39 – 38 kb	5 kb	12 kb	120 – 200 kb	3 – 9 kb	130 – 280 kb
Gene Therapy Properties						
Family	*Adenoviridae*	*Parvoviridae*	*Togaviridae*	*Herpesviridae*	*Retroviridae*	*Poxviridae*
Infection/tropism	Dividing and non-diving cells	Dividing and non-diving cells	Dividing and non-diving cells	Dividing and non-diving cells	Dividing cells	Dividing and non-diving cells
Host genome interaction	Non-integrating	Non-integrating	Non-integrating	Non-integrating	Integrating	Non-integrating
Transgene expression	Transient	Potential long lasting	Transient	Potential long lasting	Long lasting	Transient
Packaging capacity	7.5 kb	4.5 kb	7.5 kb	> 30kb	6 kb	25 kb

Table 1.1 A comparison of different types of viral vectors used in gene therapy dsDNA: double-stranded DNA, **ssDNA**: single-stranded DNA, **ssRNA**: single-stranded RNA. (Gene Therapy Net, 2017).

1.1.2.2 Adeno-Associated Viral (AAV) vectors

1.1.2.2.1 AAV structure

Adeno-associated virus (AAV) is a single-stranded deoxyribonucleic acid virus (viral genome size: ~4.7 kb) that belongs to the *parvoviridae sub*family (genus: *Dependoparvovirus*) (Büning *et al*., 2008). The AAV was firstly discovered as a contamination during AV preparation (Atchison, 1965). This virus has a very small size (~20nm), which is smaller than naked plasmid DNA. Another important feature of the AAV is that it requires another virus, which is termed helper virus, for its replication. Helper viruses include for example AV, herpes simplex virus or human papillomavirus. The unmodified genome of AAV (wild type AAV) consists of two genes: *rep* (replication) and *cap* (capsid) genes. Additionally, inverted terminal repeats (ITR) can be found N- and C-terminal of the AAV genome (**Figure 1.1**).

The Inverted terminal repeat (ITRs) consists of a 125 bp long palindromic hairpin structure which contains recognition signals for replication and packaging into AAV particle. The *rep* gene encodes for four proteins driven by p5, p19 and p40 promoter (Qiu, & Pintel, 2008), which play an important role in viral DNA replication, integration and packaging. The four different proteins are generated through alternative splicing (Saraiva, et al., 2016). The gene product of the *cap* gene is transcribed through P40 promoter and alternatively spliced to produce structural proteins that form the capsid: viral protein 1 (VP1), viral protein 2 (VP2), viral protein 3 (VP3) and Assembly-activating protein (APP) (Sonntag, et al., 2010). In the absence of a helper virus, the Rep proteins, Rep78 or Rep68, bind to ITR and integrate the viral genome into the human chromosome 19 at the site AAVS1 (MaCarty, et al., 2004). When there is also another virus present, that can function as a helper virus (such as adenovirus and herpesvirus), the AAV will start to replicate and will produce more viral particles. Different types of elements are provided by adenovirus (E1a, E1b, E2a, E4 and VA RNA) or herpesvirus (DNA polymerase, helicase) for helper function which is absent in the AAV genome (Daya and Berns, 2008).

In modified viruses, which are used in gene therapy, both the *rep* and *cap* genes are removed and replaced with transgenes that have gene therapy functions. A summary of the main strategies involved in gene therapy is shown in **Table 1.2**. During the AAV viral vector production, triple transfection of three plasmids that express: 1) *rep* and *cap* genes, 2) ITRs with transgenes and 3) helper genes which facilitates small scale virus production in the human embryonic kidney cell line (HEK293 cells) (Michael, *et al*., 2017).

Types of Gene Therapy	Details
Gene addition	Insert another copy of functional or modified protein to treat disease
Gene correction	Modifying genetic material through gene editing tools for gene correction
Gene silencing	Reducing gene expression through RNA interference
Reprogramming	Changing the characteristic of a cell into another type of cell by adding one or more genes
Cell elimination	Introduce "suicide gene" into tumour cells to induce cell death

Table 1.2 Main gene therapy strategies. A summary of the main type of gene therapy strategies used therapeutically (Adapted from Gene and Cell Therapy FAQ's, 2018).

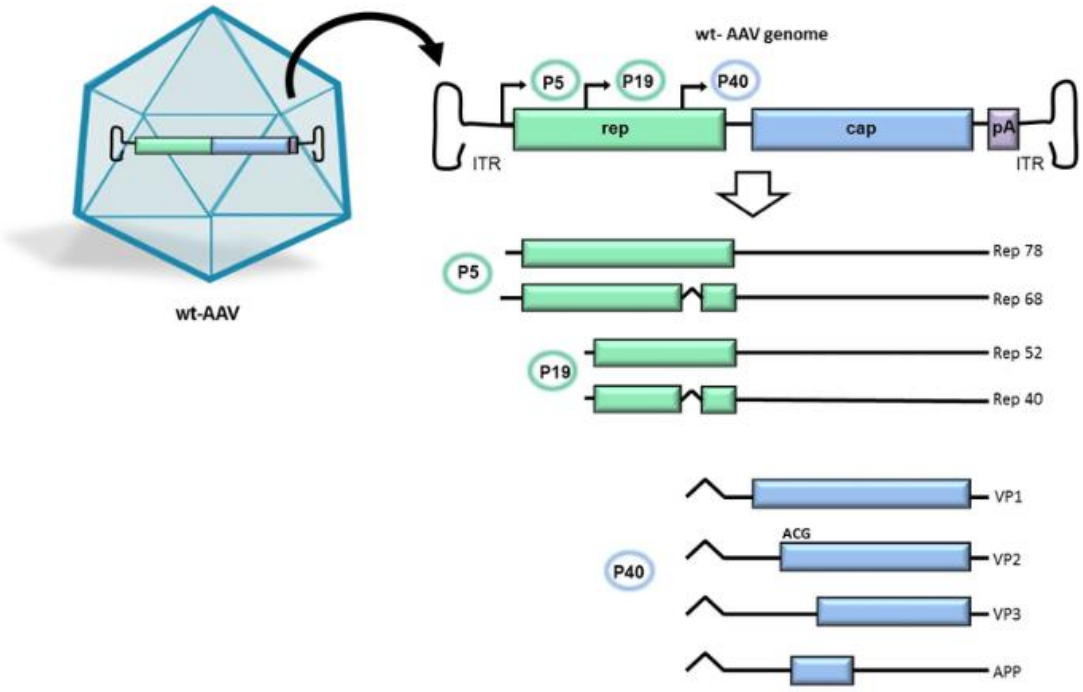

Figure 1.1 A representative illustration of wild-type adeno-associated virus (wt-AAV) viral genome and mRNA transcript. The wt-AAV viral genome containing two inverted terminal repeat (**ITR**), two ORF with *rep* (green) and *cap* (blue) genes and polyadenylation site (**pA**). Four rep genes are transcribed by the P5 promoter (Rep78 and Rep68) or P19 promoter (Rep52 and Rep40). The *cap* genes are driven by the P40 promoter to produce 4 viral proteins (VP, VP2, VP3 and APP). (Image taken from Saraiva, et al., 2016).

1.1.2.2.2 AAV serotypes

Currently, there have been 100 AAV variants identified, which can be categorised into twelve different serotypes. Most of these have been modified and engineered into viral vectors (Wang *et al*., 2016). AAV variants can be distinguished based on their capsid structure that also defines the transduction efficiency of the virus. Various types of AAV capsids bind specific cellular receptors and co-receptors that facilitates the viral internalization into mammalian cells (Chakrabarty, *et al*., 2013). There are few serotypes (1, 6, 7, 8 and 9) that are suitable for recombinant AAV (rAAV) and incorporate with the specific muscle cell targeting "promoter enhancer murine muscle creatine kinase (CK)" (Salva *et al*., 2007). Another muscle-specific promoter consists of a combination of the muscle creatine kinase (MCK) enhancer and the synthetic muscle promoter C5-12 (Wang, et al., 2008). Viral delivery systems derived from the serotype AAV-8 show the highest efficiency to deliver gene therapy throughout whole organisms (Evans *et al*., 2011), whereas viral vectors of the serotypes AAV1 and AAV6 are more efficient for local muscular gene delivery (Wang *et al*., 2005). In three of the DMD clinical trial involved in systemic delivery of micro-dystrophin with AAV-rh74 (similar to AAV-8 serotype) or AAV-9 are the most preferred AAV serotypes (Duan, 2018). Other serotypes of AAV such as ancestral reconstruct AAV Anc80 is an ancestral AAV reconstructed through bioinformatics. The AAV Anc80 is relate to AAV serotypes 1, 2, 8 and 9 (Zinn et al., 2015) which might be an excellent AAV viral vector for muscle-targeting gene therapy with lower immunogenicity.

1.1.3 Gene therapy for muscle cells

In humans, muscles make up approximate 40% to 50% of total body weight. There are a wide range of proteins produced, secreted or processed in muscle cells. Various types of muscular targeted gene therapies have been studied, from decreasing the progression of muscular disorders to immunization through the delivery of an antibody that contributes to a passive vaccine (Paulk, *et al*., 2018). In addition, therapeutic delivery of the factor IX to muscle

cells has been proposed to be beneficial for the treatment of hemophilia (Buchlis, *et al*., 2012). The ideal of using skeletal muscle as a gene therapy target emerged when new target organs were studied to apply gene therapy to patients that suffer from liver diseases, such as Hepatitis B or C. To target a gene therapy specifically to muscle cells it is pivotal to employ a muscle-specific promotor. Non-specific transgenes expression in non-targeted cell types might induce unwanted immune responses or unknown side effects (Munch, *et al*., 2015). Muscle-specific promoters include muscle creatine kinase (MCK) promoter, desmin promoter, CK6 promoter, Syn promoter and Spc512 promoter (Dickson, *et al*., 2017). These have been tested using luciferase activity expression. The CK6 promoter exhibits a ~twofold higher level of transgene expression compared to the Cytomegalovirus (CMV) promoter in muscle cells. In contrast, in liver cells the expression of the CK6 promoter exhibits ~42-fold lower level of transgene expression compared to CMV promoter. This highlights the importance of the employed tissue specific promoter in reducing off target effects of transgene expression on non-targeted tissue (Katwal, *et al*., 2013).

1.2 Skeletal muscle

1.2.1 Anatomy and physiology of normal skeletal muscle

Muscle can be categorized into three types: skeletal muscle, cardiac muscle and smooth muscle. Skeletal muscles control voluntary movement, while cardiac and smooth muscle are responsible for involuntary movements. In human, there are around 640 individual skeletal muscles (Randolph and Pavlath, 2015). In an adult human, skeletal muscle cells are approximate 2 to 3 cm long with a diameter of 100 µm (Alberts, *et al*., 2008). Skeletal muscle can be further categorized based on size, shape and arrangement. The main function of skeletal muscles is the control of movement, besides that skeletal muscles also play a role in heat regulation, breathing, reflexes and posture.

1.2.2 Myogenesis

The development of mesodermal precursors into myoblasts (myogenic lineage) is a strict regulated process. Subsequently, myoblasts further differentiate and fuse together to form multinucleated myotubes (Lee, *et al*., 2017). The rod-like shaped mature myofibres are formed by myofibrillogenesis. Myofibres are composed of actin (thin filaments) produce I band, myosin (thick filaments) produce A band, titin and ECM to keep the structure (Gillies and Lieber, 2011). Numerous myofibrils fuse together to form a sarcomere which is the basic unit of striated muscle (**Figure 1.2**).

Satellite cells are muscle-specific stem cells located under the basal lamina of myofibers (Ciciliot & Schiaffino 2010). In adults, satellite cells comprise about 3 – 6% of total muscle nuclei in the quiescent state. When triggered by extrinsic signals, the satellite cells will become activated and start to proliferate (Dhawan & Rando, 2005). Satellite cells undergo asymmetric divisions and most of newly generated cells eventually differentiate into myoblasts to form new myofibers, whereas the remaining satellite cells return to quiescence. Other factors that can trigger the activation of satellite cells include muscle stretch, exercise, and electrical stimulation. Studies have been performed to analyse whether normal satellite cells can be used to treat the progressive muscular disorder Duchenne Muscular Dystrophy (DMD). However, none of these studies was successful. This is due to the limited migration ability of satellite cells and reduced proliferation efficiency of the injected satellite cells. In addition, most of injected satellite cells are shortly lost after injection. Another issue is that satellite cells that were previously grown *in vitro* show a low differentiation rate when injected into the patient (Dellavalle *et al*., 2007). Moreover, satellite cells can only be administered to a local part of the human body (Briggs & Morgan, 2013).

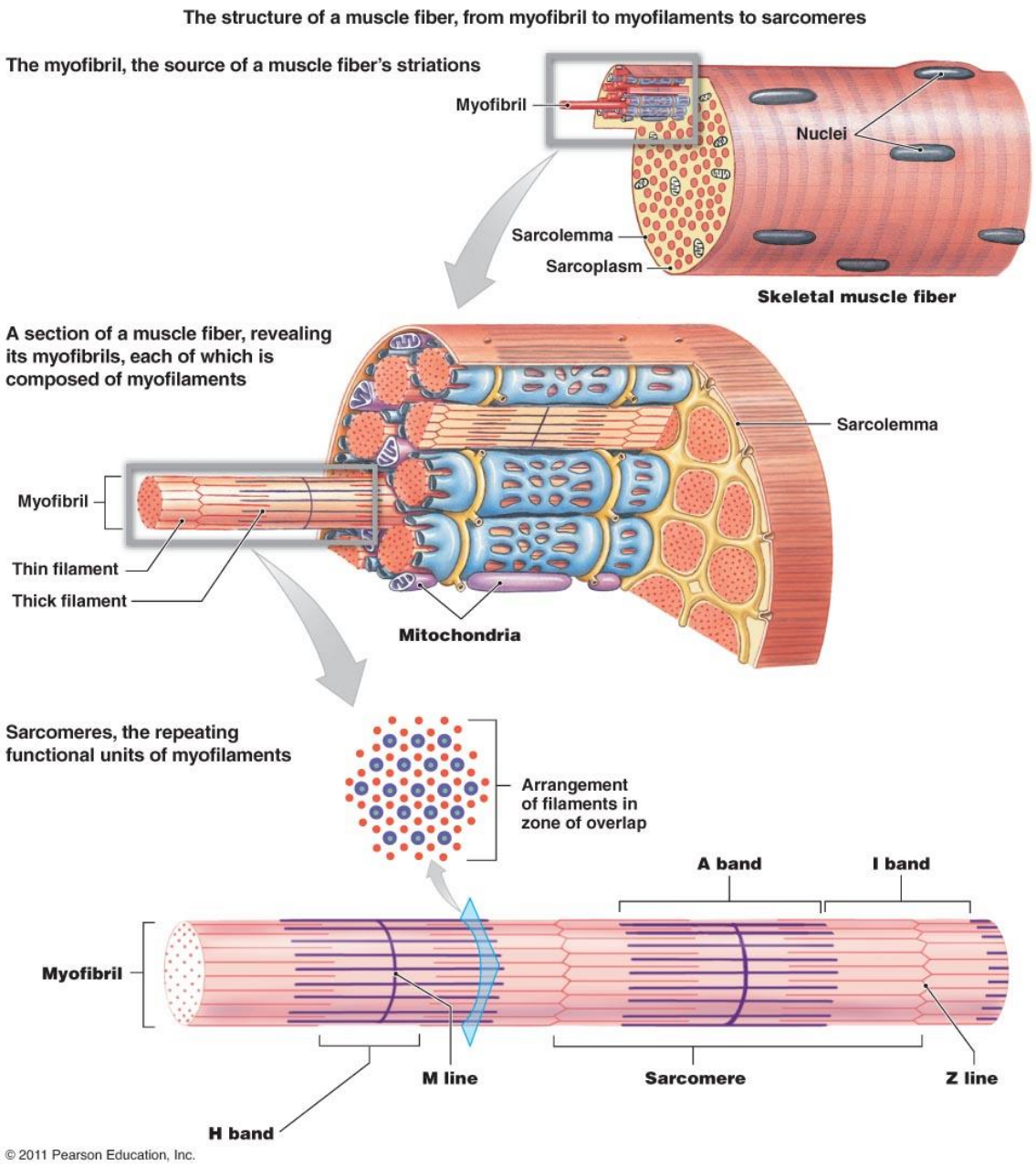

Figure 1.2 Structure of muscle fibre, from myofibril to myofilaments to sarcomeres. Numerous myofibrils form a structural unit called sarcomeres and a muscle fibre is composed of many sarcomere units (Figure taken from http://www2.highlands.edu).

1.2.3 ECM in skeletal muscle

The extracellular matrix (ECM) of skeletal muscles plays a crucial role in various biological processes, such as maintenance, repair and force transmission of skeletal muscle cells. The composition of the ECM in skeletal muscle is tightly regulated by several enzymes. Matrix metalloproteinases (MMP) are responsible for the degradation of various types of ECM components. The activity of MMPs can be inhibited by specific tissue inhibitor of matrix metalloproteinases (TIMPs). The balanced interaction between MMPs and TIMPs is crucial for muscle matrix remodelling, cell migration and myofibre formation. The ECM forms different distinct structures around skeletal muscles: endomysial (surrounding individual muscle cells), perimysial (surrounding group of muscle cells) and epimysial (surrounding the whole muscle cells) (Gillies and Lieber, 2011).

1.2.4 The composition of skeletal muscle ECM

The ECM of skeletal muscles is mainly composed of collagens, which comprise about 1 to 10 % of the total muscle mass. In adults, the main collagens found in the ECM of skeletal muscles are collagen type I and type III. However, other collagens (type IV, V, VI, XI, XII, XIV, XV and XVIII) also contribute to the development of skeletal muscles. Studies show that collagen of type I was mainly distributed in perimysial ECM, whereas collagen type III are more commonly found in endomysium and epimysium ECM (Gillies and Lieber, 2011).

1.2.5 The dystrophin-associated glycoprotein complex (DGC)

The dystrophin-associated glycoprotein complex (DGC) protein is pivotal to connect the actin cytoskeleton to the ECM of muscle cells. Thereby, this protein complex is involved in the stabilization of the skeletal muscle structure, as well as in the maintenance of the contraction function. As shown in **Figure 1.3**, the DGC comprises several different cytoplasmic (e.g. actin

filament, dystrophin, dystrobrevins and syntrophins), transmembrane (e.g. sarcospan), as well as extracellular proteins (e.g. dystroglycans and laminin). The cytoplasmic protein dystrophin is essential for the connection of the skeletal muscle ECM with actin filaments of the cytoskeleton. The ablation of dystrophin destabilizes the DGC, which leads to muscular dystrophy (Townsend, 2014).

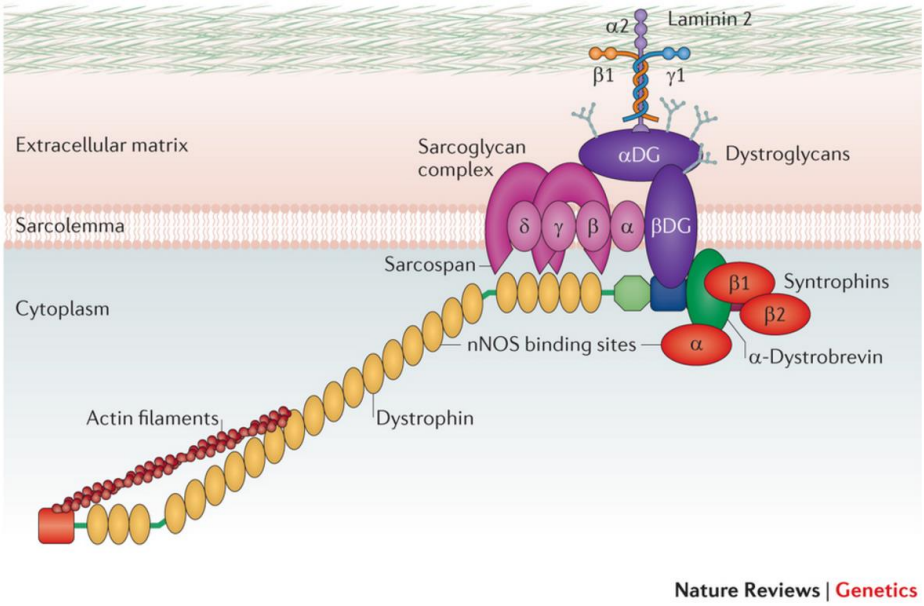

Figure 1.3 The illustration of dystrophin-glycoprotein complex (DGC). DGC combines with others components help in maintain, develop and retain normal function in muscle cells. A variety of proteins involved in DGC can be separated into three categories based on the extracellular matrix, sarcolemma and cytoplasm (Fairlough *et al*., 2013)

1.3 Muscular dystrophy (MD)

The heterogeneous genetic disorder muscular dystrophy (MD) is characterized by progressive muscle weakness and atrophy. There are about 40 different types of MD described (Muir and Chamberlain, 2009). In addition, MD occurs also during aging and can be related to the conversion of satellite cells to a fibrogenic lineage (Brack, *et al*., 2007). In patients suffering from MD, muscle fiber degeneration contributes to an excess of ECM components (Kornegay, et al., 2012a). MD can take place in cardiac muscles, in the respiratory system, as well as in the eye, skin, brain, muscle and ear (Rahimov and Kunkel, 2013). Dystrophies of muscle cells are categorised under neuromuscular (Parkinson disease and Multiple Sclerosis), muscular

dystrophies (e.g. Duchenne, Becker, facioscapulohumeral, Emery Dreifuss and limb girdle), inflammatory myopathies (e.g. polymyositis, inclusion body mitosis and dermatomyositis), congenital myopathies (e.g. Minicore myopathy, Nemaline myopathy and Central core disease), metabolic disorders (Pompe disease, McArdle disease and glycogen storage disease) and mitochondrial myopathies.

Muscular dystrophy, for example to Duchenne (DMD) or Becker muscular dystrophy (BMD), can be caused by a mutation in a protein that contributes to the formation of the DGC. In DMD, frameshift mutations lead to the absence of the dystrophin protein. In contrast to this, patients suffering from BMD exhibit mutations on the dystrophin gene allowing partial functional dystrophin protein to be produced which slows down the pathology compare to DMD. This explains why BMD is associated with milder symptoms compared to DMD (Kawecka, et al., 2015). Another form of muscular dystrophy is Limb-girdle muscular dystrophy (LGMD), which is caused by mutations in one of the four proteins that form the sarcoglycan complex. Similar to DMD and BMD, the ablation of the sarcoglyan complex causes a destabilization of the DGC (Rahimov and Kunkel, 2013).

1.3.1 Duchenne Muscular Dystrophy (DMD)

Duchenne muscular dystrophy (DMD) is an X-linked recessive genetic disorder that affects 1 in 3500 live births male worldwide (Zhou and Lu, 2010). The disorder is caused by nonsense or frameshift mutations in the gene encoding dystrophin, which results in the ablation of dystrophin in skeletal and cardiac muscle (Muntoni *et al.*, 2003). DMD is characterized by progressive weakness in limbs, cardiac and respiratory failure and premature death. The lack of dystrophin leads to a destabilization of the DGC and in consequence decreases the link between the cytoskeleton and the ECM of skeletal muscles (Gumerson and Michele, 2011; Malik *et al*., 2012; Kawecka *et al*., 2015)). The deficiency of the DGC leads to a mechanical destabilization of muscle and eventually to myofibre necrosis and muscle wasting (Matsumura *et al.*, 1993a). As a

result, a chronic inflammation occurs followed by persistent production of profibrotic cytokines, excessive synthesis and deposition of ECM proteins, and finally muscle fibrosis. Muscle fibrosis is one factor that contributes to the early death of DMD patients.

Currently, there are various strategies to ameliorate the pathology of DMD. However, none of these has the potential to stop or reverse the progression of muscular dystrophy disorders. There are several issues of replacing the dysfunctional dystrophin protein in DMD or the truncated dystrophin protein BMD patients with the full functional protein. The large size of dystrophin makes it challenging to deliver the whole coding sequence of the gene by gene therapy. In addition, the functional dystrophin gene has to be delivered to skeletal and cardiac muscles in the whole body. Moreover, DMD and BMD patients suffer from additional secondary consequences related to the disease pathology including inflammation, necrosis, oxidative stress, ischemia and fibrosis (**Figure 1.4**) (Spinazzola and Kunkel, 2016). Without treatment, DMD patients die usually in their early twenties. However, the current available interventions, such as corticosteroids treatments with anti-inflammation property and increase muscle regeneration, are able to reduce muscle loss and prolong the lifespan of DMD patients up to 40 years. On the other hand, corticosteroids treatments has several severe side effects, such as obesity, cataracts, bone fractures and behavioural changes (Hathout, *et al*., 2016).

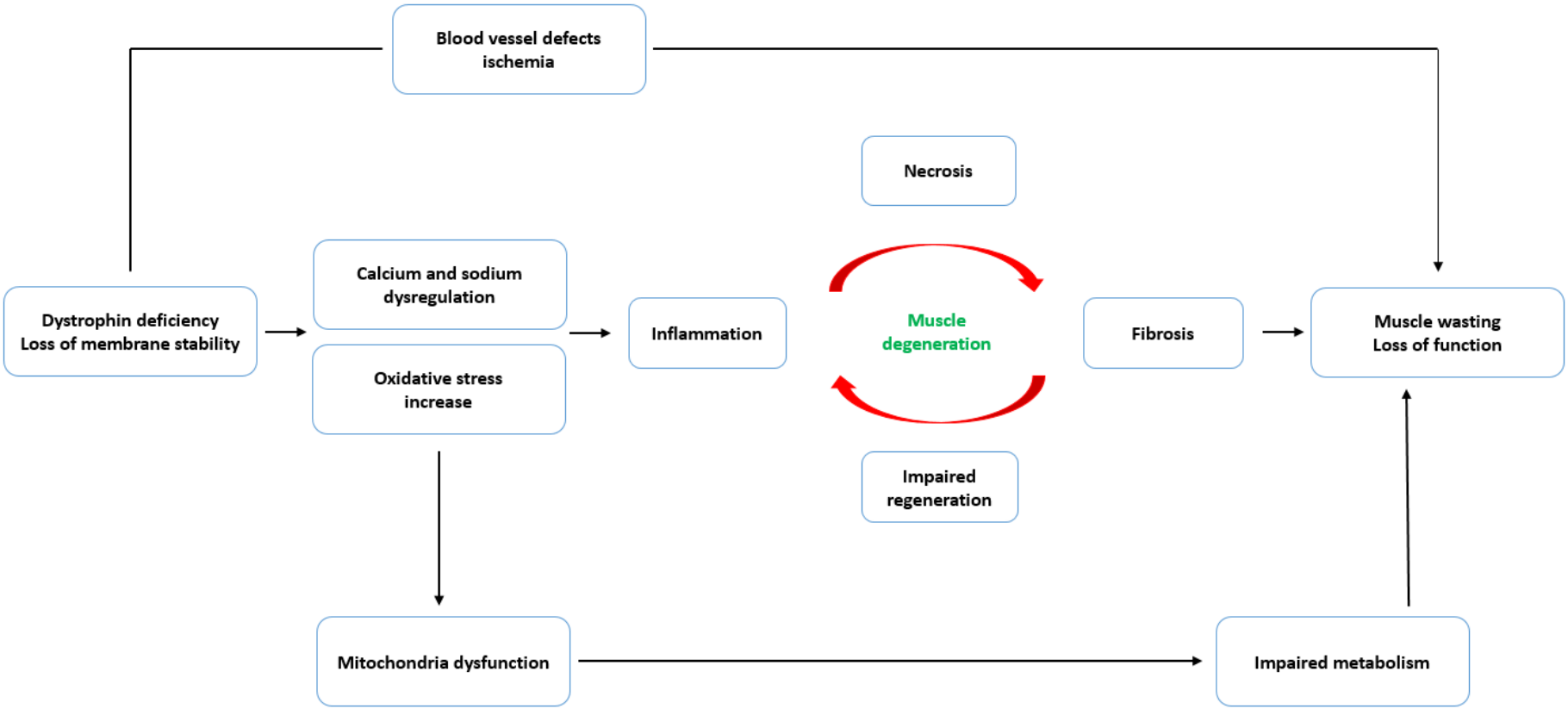

Figure 1.4 The schematic pathophysiological consequences in DMD patients. In DMD, the absence of dystrophin protein leads to loss of function of dystrophin-glycoprotein complex (DGC) cause sarcolemma prone to contraction-induced damage, which eventually increases the calcium and sodium influx into muscle cells. There are a few conditions (inflammation, necrosis, impaired regeneration and fibrosis) take place and contribute to muscle degeneration. The increase of oxidative stress which causes mitochondria dysfunction and eventually led to impaired metabolism. On the other hand, blood vessel defects and ischemia also take place. In conclusion, all the events cause by malfunction dystrophin protein contribute to muscle wasting and loss of function in DMD (Guiraud and Davies, 2017).

1.3.2 Dystrophin

1.3.2.1 Overview of the Dystrophin gene

The *DMD* gene is the largest gene in human body which consist of 2.4 Mbp (0.08% of total human genome). The gene comprises 79 exons (Kawecka *et al*., 2015) and is located at band Xp21.2 to Xp21.1 on the human X chromosome (Hoffman *et* al., 1987). There are seven different promoters that regulate the tissue-specific expression of various dystrophin isoforms (Dp427m, Dp427p, Dp427b, Dp160, Dp140, Dp116 and Dp71) (**Figure 1.5**). The isoform Dp427m is only present in skeletal and cardiac muscles. In some of the DMD cases, DMD patients and mdx mice share symptoms of a disorganised central nervous system structure, cognitive impairment and a decrease in the number of neurons due to the absence of Dp140 isoform (Dumont and Rudnicki, 2016). The Dp140 isoform dystrophin is involved in neuropsychological function responsible for fetal brain development, neuronal maturation and development (Chamove, *et al*., 2013).

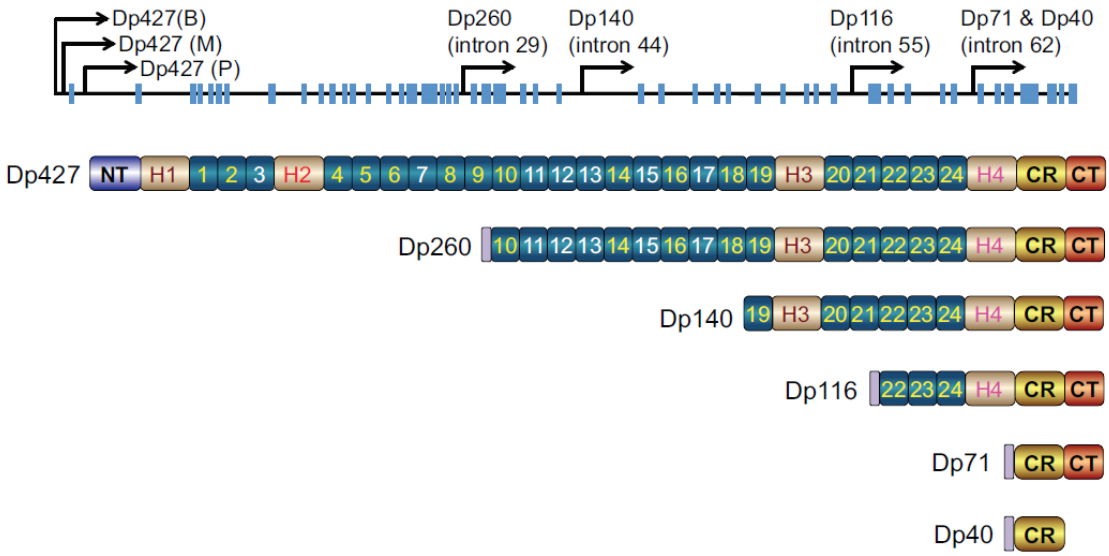

Figure 1.5 The blue vertical line represent 79 exons in the dystrophin gene. The label of natural occurring dystrophin isoforms is based on the molecular weight of dystrophin protein (Dp). Dp427 is the full length dystrophin which is produced in brain Dp427 (**B**), muscle Dp427 (**M**) and Purkinje cell Dp427 (**P**). There are other smaller isoforms which are produced from promoters within different introns; Dp260 is expressed in the retina, Dp140 in brain and kidney, Dp116 in Schwann cells. Dp71 is ubiquitously expressed in many cell types, except in muscle cells. Dp40 is expressed from the same promotor as Dp71, however Dp40 is only expressed in the brain. (McGreevy *et al*., 2015).

1.3.2.2 Structure of Dystrophin protein

Dystrophin is a huge protein that consists of 3685 amino acids and has a size of 427 kDa (**Figure 1.6**) (NCBI, 2017). Dystrophin comprises distinct protein domains: an N-terminal actin binding domain, 24 spectrin-like repeats that incorporate four hinge domains, a second actin binding domain and a neuronal nitric oxide synthase (nNOS), as well as C-terminal a cysteine-rich domain (CR) and a carboxy-terminal domain (CTD). The CTD binds to α and β syntrophin that are part of the DGC.

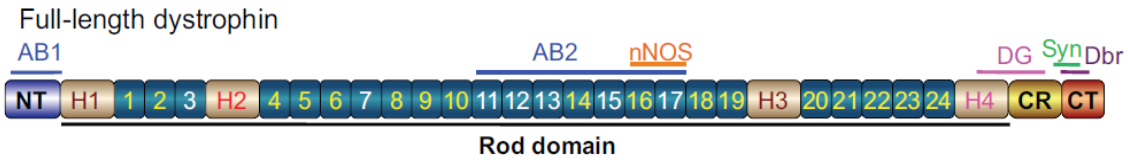

Figure 1.6 Image illustrating the full-length dystrophin protein. Full-length dystrophin content includes N-terminal domain (NT), four hinge domains (H1–H4) and a rod domain consisting of 24 spectrin-like repeats (1–24), a cysteine-rich domain (CR) and a carboxy-terminal domain (CTD). The dystrophin-associated protein binding on dystrophin are actin-binding domain 1 (AB1), actin binding domain 2 (AB2), neuronal nitric oxide synthase (nNOS), dystroglycan (DG), syntrophin (Syn) and dystrobrevin (Dbr) (McGreevy *et al*., 2015)

1.3.2.3 Mutation in Dystrophin in DMD

In humans, the *DMD* gene has the highest mutation rate compared to other genes. This is due to the large size of the gene sequence. In DMD, mutations in the Dystrophin gene are categorized into the following groups: large genomic deletions of one to several exon (>60%), duplication of one or several exons (24%), missense mutation (11%) and small in-frame deletions (4%) (Kawecka *et al*. 2015). Although mutation can happen throughout the dystrophin gene, the majority of all mutations occur in exons 45-55, whereas less mutations occur between the exons 2 and 19. Mutations in dystrophin lead either to the absence of Dystrophin (DMD) or to a truncated gene product (BMD). In BMD patients approximately half of the Dystrophin protein is absent, which contributes to the mild phenotype compared to DMD (England, *et al*., 1990).

1.3.3 Clinical and Pathological Characteristics of DMD

The progression of DMD in humans is divided into four phases, the early phase, the late childhood phase, the adolescence phase and the adulthood phase. DMD is diagnosed by measuring creatine kinase (CK) levels in the blood, genetic testing or muscle biopsy. CK is used as an indication of muscle degeneration and children suffering from DMD show 20 to 100 higher CK levels in the blood compared to children, which are not affected by DMD. The first symptoms of DMD become obvious at the age of two to three years (end of the early phase) (Bushby *et al*., 2010), with children exhibiting motor difficulties and slower movement compared to other children (Shi-Wen *et al*. 2009). Children affected by DMD struggle to stand up when lying on the floor and will use their hands as support. This is termed the Gower's manoeuvre (**Figure 1.7**).

During the late childhood phase (from 6 to 13 years) patients suffer from an extreme loss in muscle strength, which increases the risk of falling over. Furthermore, the massive reduction in muscle strength limits the walking ability of the patients so that a wheelchair is needed as support about the age of 13 years. In the third phase, adolescence phase (from 8 to 15 years) patients depend on wheelchairs and show spinal deformations. Additional symptoms include lumbar lordosis, scoliosis, kyphosis and abnormal sitting postures (Kinali *et al*., 2007). At the end of adulthood phase, at the age of around 20s to 30s years, the cardiac function of DMD patients is significantly reduced and leads to heart failure.

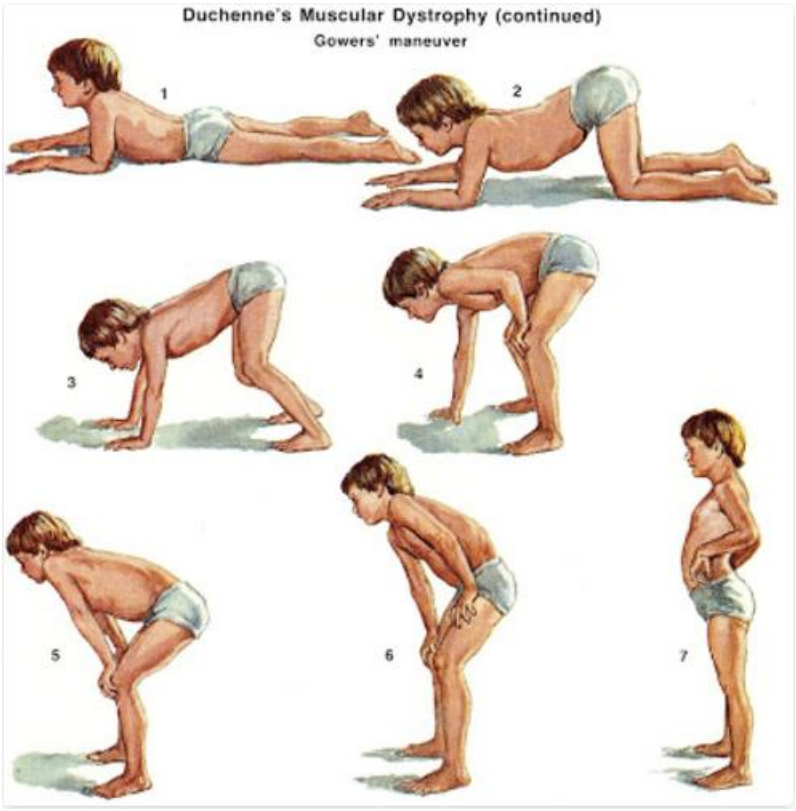

Figure 1.7 Gower`s manoeuvre of DMD. Patients DMD around 5 years old have difficulty in standing up (7) from lying on the floor (1), using the support of both hands (2 & 3) and then slowly rising by using their hands to support on the leg (4, 5 & 6) (Mihpatte, 2012).

1.3.5 Animal Model of DMD

Currently, there are around 60 animal models for DMD available (McGreevy *et al*., 2015). The most common types of DMD models that are used are in mice or dogs. These animal models allow the improvement of treatment strategies and the examination of new technologies. Gene therapy approaches mainly exploit exon skipping as a novel DMD treatment. Additionally, there have been new types of DMD animal models developed in rats (Nakmura *et al*., 2014; Larcher *et al*., 2014) and pig (Nonneman *et al*., 2012; Klymiuk *et al*., 2013). In the mdx mouse model, the pathology condition in muscle differ from the muscle fibrosis in DMD patients. However, extensive exercise aggravates the muscle fibrosis in mdx mice models and makes it more comparable to human patients (Pessina, 2014). In addition, treatment with fibrotic or laceration causes the progressive development of muscle fibrosis in mdx mice, as well as in wild type mice. A more suitable model for DMD, that shows similar muscular fibrosis compared to humans, are

the dog golden retriever muscular dystrophy (GRMD) (Kornegay *et al*., 2012b), pig (Klymiuk *et al*., 2013) and mouse (DMD^{mdx}) (Larcher *et al*., 2014). Each animal model offers advantages and disadvantages, which both have to be considered, when deciding for the appropriate model system. The DBA2 mdx model is a poor model for cardiomyopathy compared to DMD patients, however, the lower hind limb muscle weight, less myofibres, more accumulation of collagen and severe fibrosis which have much similar pathology to DMD patients (Wells, 2018). Other types of mdx mouse (Cmah mdx mouse) exhibit more severe DMD symptoms compared to mdx mouse such as a fibrosis increase in quadriceps ,gastrocnemius and diaphragm, reduction half of the lifespan, speed, peak force of diaphragm and cardiac trabeculae (Yucel, *et al*., 2018).

1.3.5.1 Mdx mouse

In 1981, the mdx mouse model, which exhibits a mutation in exon 23 of dystrophin, was discovered (Bulfield, *et al*., 1984). The mutation is a premature stop codon in exon 23, which results in a malfunctional dystrophin protein and resulting in milder symptoms compared to DMD patients. This mouse model offers several advantages, such as low maintenance cost, short gestation period and large litter size. The CK response and the muscle necrosis progression differs in the mdx mice and in human DMD patients. However, mdx mouse models and human patients both show a severe fibrosis in diaphragm. For these reasons, the mdx mouse model have been studied extensively with around 2800 studies up to date (Wells, 2018).

1.3.6 Therapeutic Approaches for DMD

There are a lot of therapeutic strategies developed to ameliorate the progression of DMD, such direct gene replacement strategy (micro-, mini-, quasi- or full version of dystrophin), mutation correction strategy (exon skipping and suppression on immature termination codon),

supplementary indirect strategy (drugs for utrophin upregulation, antibody therapies, shRNA, gene editing on myostatin) and cell therapy (myoblast or stem cell transplantation) (Kawecka, *et al*. 2015). The discovery that a truncated dystrophin from BMD patients (England *et al*., 1990) that is partially functional led to the development of mini- and micro-dystrophin constructs (**Figure 1.8**) (Gregorevic *et al*., 2006). Duan (2018) discusses that from 1997 to 2017 more than 25 variant of micro-dystrophin have been designed and tested, with different degrees of pathology reduction and force improvement.

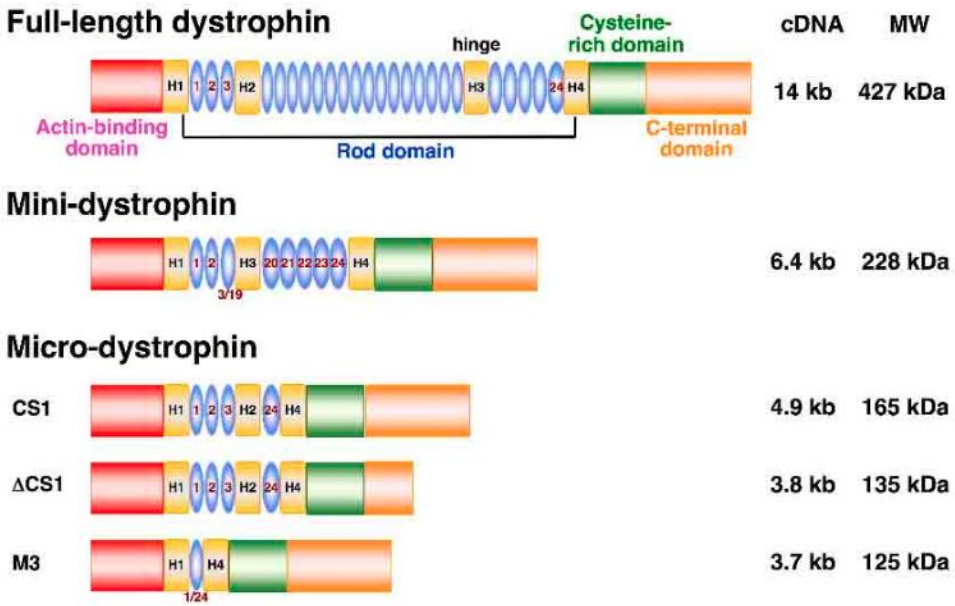

Figure 1.8 Image illustration of full-length, mini- and micro-dystrophin. Most of the rod domain is removed from full-length dystrophin to generate mini-dystrophin and micro-dystrophin. Components such as actin-binding domain, cysteine-rich domain and C-terminal domain remain in mini- or micro-dystrophin. Mini-dystrophin arose from a patient with Becker muscular dystrophy, where the in-frame deletions lead to partially functional protein. Three different micro-dystrophin cDNAs have been constructed into AAV vector, to contain four rod repeats with hinge 1, 2 and 4 (**CS1**); same components as CS1 with partially delete C-terminal domain (**delta CS1**) and one-rod repeat with hinge 1 and 4 (**M3**). (Ke, 2011)

Despite the fact short truncated *DMD* gene restoration shall not have the same effect as full length of dystrophin. In some studies, exosome offer another approach to restore full length of dystrophin transiently in vivo. The exosome is extracellular vesicle produced by a range of cell with a size >150µm. Furthermore, the exosome produced is based on the original type of

cells which offered some tissue-specificity that allowed cell to cell communication. One of the studies shown that by using exosome derived from mouse myogenic cell line (C2C12) is capable of transiently restoring the full-length dystrophin and improve cardiac function in mdx mouse heart (Su et al., 2018). Another study has shown that by using exosomes derived from cardiosphere-derived cells (clinical-stage cardiac progenitor cells) and injected into mdx mice are capable of transiently restoring the dystrophin protein in hearts but also some skeletal muscle (such as soleus limb muscle and diaphragm) (Aminzadeh et al., 2018). The exosome might offer an insight into exosome delivery with transient full length of dystrophin restoration as a therapy for DMD.

1.3.7 Clinical trials for DMD

There are a lot of ongoing, complete and terminated clinical trials available that focus on DMD. A summary of these clinical trials can be obtained on the clinical trial website (Clinical trial, 2017). These clinical trials focus on gene replacement, nonsense suppression, exon skipping (exon 53, 51, 45 and 44), muscle and stem cells therapy, anti-inflammatory drugs, antifibrotic drugs and muscle regeneration. One of these clinical trials assesses the delivery of mini-dystrophin with AAV into patients, but only a low level of dystrophin could be detected (Mendell *et al*. 2010), which might be to an immune response towards the foreign dystrophin epitope (Mendell *et al*. 2010). Recently, the most promising results were obtained from Sapenta Phase I/IIa clinical trial with AAV-micro dystrophin (Sarepta, 2018). In this study, the serum CK levels were reduced over 87 % in patients and this was accompanied by the high presence of micro-dystrophin (76.2 %). Another main focus in DMD clinical trials are antisense oligonucleotides (AON). This strategy specifically targets exon skipping on single or multiple exons to restore truncated dystrophin (Abdul-Razak *et al*. 2016). There are two exon-skipping therapies already approved ataluren targeting pre-mature stop codons and eteplirsen targeting exon 51 skippings (Verhaart and Aartsma-Rus, 2019). Although, both micro-dystrophin restoration and exon

skipping approaches aim to restore BMD like dystrophin might ameliorate DMD it did not restore the full length of dystrophin.

1.4 Wound Healing and Fibrosis in muscle

When injury take place, wound healing initiated through release of inflammatory mediators such as cytokines and growth factors by damaged cells (Tidball and Villalta, 2010). The cytokines help in processes such as proliferation and migration of the cells in the injury site. Fibroblasts are recruited to the injury site and get activated for extracellular matrix components (ECM) synthesis (Mann *et al*., 2011). ECM production plays a role in ECM remodelling, which activates satellite cell proliferation to replace the muscle cells.

1.4.1 ECM in fibrosis

Fibrosis is an uncontrollable wound-healing process that causes hardening and scar formation on tissue. This process is triggered by chronic tissue injury or inflammation. The deposition of excessive ECM proteins weaken tissue function and replaces normal parenchymal tissue with various types of fibrotic tissue. Different factors such as chemical, persistent infection, injury, radiation, allergic and autoimmune responses contribute to chronic inflammation and eventually result in fibrosis (Wynn, 2008). Some current treatments on fibrotic diseases (such as liver cirrhosis, sclerosis, cardiovascular fibrosis and idiopathic pulmonary fibrosis) focus on reducing the inflammatory response. Regulation of fibrosis pathway may not be the same as reduced inflammation, although chronic inflammation contribute to fibrosis (Wynn, 2008).

The main cell type responsible for fibrosis are Myofibroblasts, which are the primary cells involved in the production of ECM. This cell type can be generated through different ways such as activation of fibroblast, from residential mesenchymal cells, endothelial, fibrocytes (circulating fibroblast-like cells) or through epithelial cells that undergo endothelial/epithelial

transition (EMT). The activation of the myofibroblast contributes to autocrine secretion of myofibroblasts, paracrine signals from macrophages and lymphocytes, as well as to the interaction of pathogen-associated molecular patterns (PAMPs) with pattern recognition receptors on fibroblasts (Wynn, 2008). There are several factors that regulate fibrosis and might be good candidates to target for anti-fibrotic therapies: cytokines (TGF-β), renin-angiotensin-aldosterone system (ANG II), angiogenic factors (VEGF), growth factors (PDGF), chemokines (MCP-1), caspases and acute phase proteins (SAP) (Wynn, 2008). Relaxin have been prove able to reduce the TGF-β (Wang *et al*., 2016).

1.4.2 Muscle fibrosis in DMD

The pathological pathway of muscular degeneration in DMD has been studied extensively. The malfunction of dystrophin protein causes a destabilization of the DGC complex, which makes the muscle fibre more susceptible to contraction induced damage and necrosis. The decline of muscle cells, which is accompanied by muscle weakness, is caused by the replacement of muscles with fibro-adipose tissue and extracellular matrix (ECM) components (Serrano and Muñoz-Cánoves, 2010).

1.4.3 The role of relaxin in treatment of fibrosis

Relaxin is a natural suppressor of age- and disease-related fibrosis. The protein hormone has been used to target fibrosis in various tissues and organs, including skin [scleroderma (Samuel *et al*., 2005; Seibold *et al*., 2000)], lung [pulmonary fibrosis (Samuel *et al*., 2003)], kidney [renal fibrosis (McDonald *et al*., 2003; Lekgabe *et al*., 2005; Danielson *et al*., 2006)], heart [cardiac fibrosis (Samuel *et al*., 2004, 2008; Du *et al*., 2003)] and liver [hepatic fibrosis (Bani *et al*., 2001; Williams *et al*., 2001)].

In 2010, it was shown that relaxin reduces the inflammatory and fibrotic phases during muscle injury (Mu *et al*., 2010). However, it is still largely unknown how relaxin controls inflammation and fibrotic tissue formation (Li *et al*., 2004; Mu *et al*., 2010). Relaxin also plays a role in the promotion of muscle regeneration by increasing pax7 (marker of skeletal muscle differentiation) in positive satellite cells. Furthermore, relaxin represses the recruitment of neutrophils to the site of injury (Mu *et al*., 2010; Negishi *et al*., 2005). Recently, Martin, *et al*. (2018) observed that relaxin reverses inflammatory and immune signals in aged mouse hearts. Additionally, it could be demonstrated that relaxin is able to suppress several genes and signalling pathways that are involved in the inflammatory response during heart failure (Martin *et al*., 2018). In summary, it could be shown that relaxin suppresses fibrosis in various cells types.

1.5 Relaxin

Relaxin is a 6 kDa pleiotropic peptide hormone of the insulin family. It was discovered in 1926 by Fredrick Hisaw (Hisaw, 1926). Relaxin plays a role in hemodynamic changes and ligament relaxation during pregnancy and parturition (Conrad, 2011). Although relaxin and insulin display a similar structure, they bind to different receptors and trigger different cellular effects.

1.5.1 Relaxin family

Relaxin is conserved from zebrafish to humans (Wilkinson *et al.*, 2005). The three non-allelic relaxin genes in humans (h) (relaxin 1 (hRln1), relaxin 2 (hRln2) and relaxin 3 (hRln3)) are encoded by different genes. It has been shown that only higher primates and humans have RLN 1 and RLN2, while other mammals only have RLN 1 which is most similar to human RLN2 (Wilkinson *et al*., 2005). In human, hRln1 and hRln2 are located on chromosome 9p24 (NCBI, 2016). Although hRln3 was only discovered about fifteen years ago (in 2002) the phylogenetic analysis indicate that it is probably the ancestral relaxin peptide.

Despite the low sequence homology among relaxin and insulin, both of the proteins are classified into the same protein family. Both hormones, relaxin and insulin, are produced as pre-pro-hormones. The pre-pro-hormone of the relaxin/insulin family contains a signal peptide (SP) prior to B-chain at the N-terminus (B) and an A-chain at the C terminus shown in **Figure 1.9**. The A- and the B-chain are connected through a connecting chain (C). The pro-hormone is processed in the Golgi apparatus and the SP, as well as the C chain, is cleaved off. The final active heterodimer contains an A-chain (modulating the tertiary structure of B-chains) and a B-chain (binding sites) (Devarakonda and Salloum, 2018).

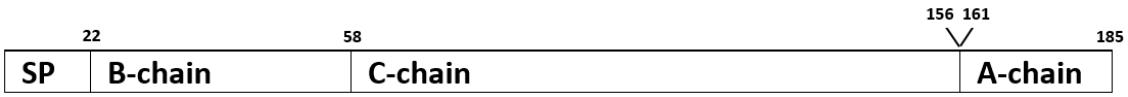

Figure 1.9 Scheme of Pre-Pro-Mouse Relaxin 1 Protein. The scheme represents the peptide structure of pre-pro-mouse relaxin 1 with 185 amino acids. The sequence represents signal peptide (**SP**), mature relaxin B-chain (**B-chain**) and A-chain (**A-chain**) and connecting peptide (**C-chain**). The number indicates amino acids location of different segment within the pre-pro-mouse relaxin 1 and the protein structure also refer as B-C-A protein structure.

1.5.2 Relaxin receptor and Cellular pathways

The main circulating relaxin in humans is hRln2 (Chan, *et* al., 2012). Relaxin binds to a family of G-protein coupled receptors (CPGR) also known as relaxin family peptide receptors (RXFPs). There are four members of RXFP, RXFP 1-4. Hsu discovered in 2002 that relaxin also binds to leucine-rich G protein coupled receptor receptors (LGR7 and LGR8), which are now termed RXFP1 and RXFP2, respectively (Hsu *et al*., 2002). Despite that relaxin protein can bind to both RXFP1 and RXFP2 receptors, some studies shown that relaxin has a higher binding affinity to RXFP1 (Debrah *et al*., 2008). In addition, the insulin like factor 3 (INSL3) also exhibits a low affinity to RXFP1. RXFP1 and RXFP2 are transmembrane receptors, that comprise seven transmembrane domains and a large extracellular domain containing leucine rich repeats (Devarakonda and Salloum, 2018).

The RXFP1 receptor belongs in the G protein-coupled receptor (GPCR) family to the subclass of leucine-rich repeat (LRR)-containing GPCRs. The RXFP1 receptor contains at the extracellular N-terminus a unique LRR domain (**Figure 1.9**). In addition, a LDL-A domain is present at the N-terminus. Aspartate and glutamate residues of the LRR domain are essential for the interaction with the B chain of the relaxin hormone. Additionally, the LDL-A domain and the extracellular loops 1 and 2 of the transmembrane domain contribute to the interaction between receptor and relaxin ligand (Kong *et al*., 2013). The binding of relaxin activates G proteins (α, β and γ), which in turn activate further signalling cascades.

Treatment of human umbilical arterial smooth muscle cells and human cardiac fibroblasts with the human recombinant relaxin 2 drug (serelaxin), causes an increase of the neuronal nitric synthase (nNOS) activity. In addition, serelaxin also causes the phosphorylation of ERK1/2, as well as cGMP signalling (Sarwar *et al*., 2015). Serelaxin also increased the vascular endothelial growth factor (VEGF) and matrix metalloproteinases (MMPs) 2 and 9. Moreover, serelaxin might be able to block TGF-β signalling through Notch1.

1.5.3 Animal model of relaxin

Knockout of relaxin in female mice causes immature mammary glands that lack milk production. In addition, knockout of relaxin in male mice delayed tissue maturation and growth in testis and prostate. Deposition of excessive collagen contributes to the pathology observed in male and female relaxin knockout mice (Samuel, *et al*., 2005a). Moreover, relaxin knockout mice exhibit various kinds of fibrosis, such as age related progressive fibrosis in lung, heart, kidney and scleroderma (Samuel, *et al*., 2003; Samuel, *et al*., 2005a; Samuel, *et al*., 2005b).

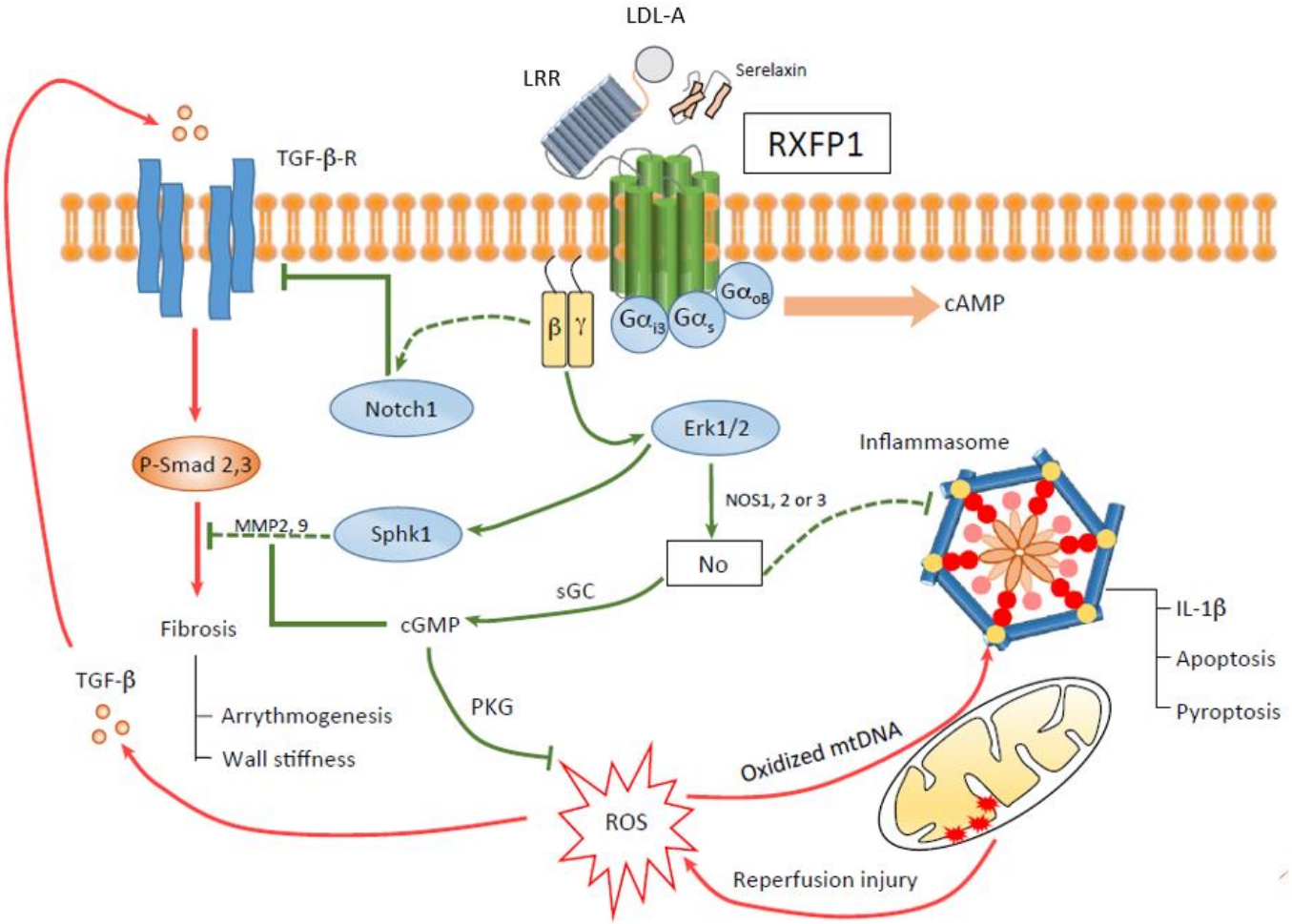

Figure 1.10 The illustration of Serelaxin interaction with RXFP1 in mammalian heart. The NO is produced by the downstream activation of β_γ subunit play a crucial protection role. Process such as cGMP production and activation of protein kinase G (PGK) reducing reactive oxygen species (ROS) and fibrosis upon injury. The uncertainty pathway (green broken line). Extracellular signal regulated kinase 1/2 (Erk1/2), mitochondrial DNA (mtDNA), nitro oxide synthase (NOS), sphingosine kinase (Sphk1), Transforming growth factor β (TGF-β), Transforming growth factor β receptor (TGF-β-R), (Image taken from Devarakonda and Salloum, 2018)

1.6 Aim and objective

This project focuses on the hypothesis that overexpression of the peptide hormone relaxin is beneficial for the treatment of fibrosis in patients suffering from muscle fibrosis. Firstly, we will examine various delivery systems of relaxin, and non-viral & viral delivery systems were designed. Subsequently, several cell lines, such as mouse muscle fibroblast cell lines (MH cells), have been transfected with the designed constructs and the expression level of relaxin was assessed by real-time quantitative PCR and by western blot analysis. In addition, further *in vitro* studies have been carried to out to analyse the effects of the increased expression of relaxin on fibrosis-related effects. This will help to assess the anti-fibrotic potential of relaxin. The future of the project is to deliver a viral vector (rAAV) that expresses relaxin in a mouse model of muscular dystrophy (mdx mouse model) and to analyse the effects of overexpressing relaxin on muscle fibrosis. Increasing the expression of the anti-fibrotic hormone relaxin might represent a novel treatment strategy for patients suffering from various types of muscular dystrophy, such as DMD or BMD

CHAPTER 2: MATERIALS & METHODS

CHAPTER 2: MATERIALS & METHODS

2.1 Standard reagents

Most of the general chemical reagents that were used in the experiment were purchased from Sigma-Aldrich and VWR (otherwise will be stated) with standard chemical purity graded as Analytical Reagents for analysis applications (AnalaR). All of the reagents (list in the table below) were dissolved in double distilled water (ddH_2O), otherwise will be stated.

Reagents	**Manufacturer**
Acetic acid	VMR
EDTA	Sigma-Aldrich
Glucose	Sigma-Aldrich
Glycerol	Sigma-Aldrich
HEPES [4-(2-hydroxyethyl)-1-piperazineethanesulfonic acid]	Sigma-Aldrich
Methanol	VMR
Magnesium sulphate ($MgSO_4$)	Sigma-Aldrich
NP-40	Fluka Biochemica
Paraformaldehyde (PFA)	Sigma-Aldrich
Sodium chloride (NaCl)	Sigma-Aldrich
Sodium dodecyl sulfate (SDS)	Sigma-Aldrich
Tris Base	Sigma-Aldrich

2.2 Plasmids

2.2.1 Transgenes Analysis

The open reading frame (ORF) of the mouse relaxin 1 gene (NCBI, NM_011272.2) was obtained from NCBI and subsequently used for primer design. Sequences of the synthetic muscle specific promoter (Spc512) were obtained from previous plasmid constructs from RHUL Dickson lab (Li, 1999) Most of the plasmid that were used for investigation were purchased online through VectorBuilder in glycerol bacterial form and stored at -80^{o}C. Other plasmids were purchased from Vector Builder in Maxi prepped form, which was eluted in TE buffer and stored at -20^{o}C freezer. An ampicillin resistance gene was included within the plasmid backbone, to allow for screening during plasmid production.

2.2.2 Relaxin Plasmids

This projects utilizes eight different plasmid constructs: pssAAV-Spc512-CO mRln1, pssAAV-Spc512-NCO mRln1, pscAAV-Spc512-CO mRln1, pscAAV-Spc512-NCO mRln1pTet On-CO mRln1, pTet On-NCO mRln1, pAAV-Tet On-CO mRln1 and pAAV-Tet On-NCO mRln1 (see table 5). The plasmids, pTet On-CO mRln1, pTet On-NCO mRln1, are conventional plasmids. In contrast to this, the plasmids pAAV-Tet On-CO mRln1 and pAAV-Tet On-NCO mRln1 can be later used for AAV constructs. Non-codon optimized variants (NCO) exhibit the wild type version of the coding sequence of the mouse relaxin 1 gene. Moreover, the online software VectorBuilder algorithm was used to construct a codon optimized (CO) sequence version of the coding sequence of the mouse relaxin 1 gene.

2.2.3 pCI-eGFP

The plasmid was kindly gifted by Dr. Susan Jarmin (RHUL Dickson lab). The plasmid comprises a Cytomegalovirus (CMV) promoter that is combined with green fluorescent protein (GFP). Additionally, a SV40 PolyA signal was included on the 3’ end.

Plasmid purchased	Details
pssAAV-Spc512-CO mRln1	A ~4.7kb construct containing muscle specific promoter (Spc512) with transgenes codon optimised mouse relaxin 1 (CO mRln1). The plasmid construct was obtained in glycerol bacterial stocks.
pssAAV-Spc512-NCO mRln1	A ~4.7kb construct containing muscle specific promoter (Spc512) with transgenes non-codon optimised mouse relaxin 1 (NCO mRln1). The plasmid construct was obtained in glycerol bacterial stocks.
pscAAV-Spc512-CO mRln1	A ~4.8kb construct containing muscle specific promoter (Spc512) with transgenes codon optimised mouse relaxin 1 (CO mRln1). The plasmid construct was obtained in glycerol bacterial stocks.
pscAAV-Spc512-NCO mRln1	A ~4.8kb construct containing muscle specific promoter (Spc512) with transgenes non-codon optimised mouse relaxin 1 (NCO mRln1). The plasmid construct was obtained in glycerol bacterial stocks.
pTet On-CO mRln1	A ~6kb construct containing tetracycline inducible system (Tet On) with transgenes codon optimised mouse relaxin 1 (CO mRln1). The plasmid construct was obtained in glycerol bacterial stocks and large amount of plasmid production (Maxiprep).
pTet On-NCO mRln1	A ~6kb construct containing tetracycline inducible system (Tet On) with transgenes non-codon optimised mouse relaxin 1 (NCO mRln1). The plasmid construct was obtained in glycerol bacterial stocks and large amount of plasmid production (Maxiprep).
pAAV-Tet On-CO mRln1	A ~7.4kb construct containing tetracycline inducible system (Tet On) with transgenes codon optimised mouse relaxin 1 (CO mRln1) and two inverted terminal repeats (ITRs). The plasmid construct was obtained in glycerol bacterial stocks and large amount of plasmid production (Maxiprep).
pAAV-Tet On-NCO mRln1	A ~7.4kb construct containing tetracycline inducible system (Tet On) with transgenes non-codon optimised mouse relaxin 1 (NCO mRln1) and two inverted terminal repeats (ITRs). The plasmid construct was obtained in glycerol bacterial stocks and large amount of plasmid production (Maxiprep).

Table 2.1 Details of plasmids used in this project

2.3 Computer Softwares and Bioinformatics Software

2.3.1 Primer design

Primers were designed using the either the IDT or the Primer3 software (http://primer3.ut.ee). All primers were designed as following: 18 – 22 bp length, melting temperature (T_m) around 55 – 60°C, GC content around 40 – 60%, primer dimer formation shall be avoided, amplicon length is around 75 - <200 nucleotide, T_m for both forward & reversed primer as close as possible. Primers were obtained from IDT.

Primer details purchase through IDT	**Primer sequence 5' – 3'**	**T_m (°C)**	**Amplicon size (bp)**
Mouse Relaxin Exon location: 1 – 2	FP: 5'-CCGTGAATATGCCCGTGAA-3' RP: 5'-AGGCTCTGCATCTTTGTTGA-3'	57 56	139
Codon Optimise mouse relaxin	FP: 5'-GAAGACCCTGCACGACAA-3' RP: 5'- TCTCCCTCTTCTTCCTGCT-3'	55 56	98
Mouse alpha actin 2 Exon location: 7 – 8	FP: 5'-GAGCTACGAACTGCCTGAC-3' RP: 5'-CTGTTATAGGTGGTTTCGTGGA-3'	56 56	129
Mouse Fibronectin 1 Exon location: 26 – 27	FP: 5'- GAGCTATCCATTTCACCTTCAGA-3' RP: 5'- TTGTTCGTAGACACTGGAGAC-3'	54 54	96
Mouse Periostin Exon location: 2 – 3	FP: 5'-CCTGTAAGAACTGGTATCAAGGT-3' RP: 5'-CCTTTCATCCCTTCCATTCTCA-3'	57 56	97
Mouse tissue inhibitor metalloproteinase 1 Exon location: 2 – 4	FP: 5'-AGACAGCCTTCTGCAACTC-3' RP: 5'-CAGCCTTGAATCCTTTTAGCATC-3'	56 57	129
Mouse tissue inhibitor metalloproteinase 2 Exon location: 3 – 4	FP: 5'-GACCTGACAAAGACATCGAGT-3' RP: 5'-GCCATCTCCTTCTGCCTTT-3'	56 56	119
Mouse Matrix metalloproteinases 9 Exon location: 8 – 9	FP: 5'-GACATAGACGGCATCCAGTATC -3' RP: 5'-GTGGGAGGTATAGTGGGACA -3'	56 53	125
Mouse Procollagen 1 Exon location: 1 – 2	FP: 5'-CGCAAAGAGTCTACATGTCTAGG-3' RP: 5'-CATTGTGTATGCAGCTGACTTC -3'	56 56	134
Mouse Rplp0 Exon location: 5 – 6	FP: 5'-TTATAACCCTGAAGTGCTCGA-3' RP: 5'-CGCTTGTACCCATTGATGATG-3'	52 56	147

Table 2.2 Details of primer used in this project. Primer sets (forward and reverse primer) used for amplification specific sizes fragment of mouse gene were purchased through IDT. **FP**, forward primer; **RP**, reverse primer; **Tm**, melting temperature of primer.

2.3.3 SnapGene Software

SnapGene software was used for illustration nucleotide and sequence visualization.

2.3.4 GraphPad Prism Software

The GraphPad Prism software was used to plot the graph.

2.3.5 FlowJo Software (BD Falcon)

FlowJo software was used to analyze flow cytometry data. The percentage of dead and live cells were determined. In addition, the level of GFP expression of single cells was assessed.

2.3.6 ImageJ Software

Microscopy images of wound scratch assays were analysed with Image analysis ImageJ**.** The area of wound closure was highlighted and recorded in GraphPad Prism software for graph design and statistical analysis.

2.4 Bacterial Cultures

2.4.1 Materials

- **LB agar powder** (Sigma)
- **Glycerol** (Sigma): 80% Glycerol stock was prepared by added 40ml of glycerol made up to 50ml with ddH_2O.
- **LB powder** (Sigma)
- **Ampicillin** (Sigma): prepared as 1000X stock in ddH_2O at 50mg/ml concentration, filtered through the 0.22µm filter (Falcon) and stored in -20°C freezer.
- **LB broth**: 20g of LB powder was made up to 1000ml with ddH_2O, autoclaved and stored at RT.
- **LB agar**: 7g of LB agar powder was made up to 200ml with ddH_2O. The LB agar mixture was autoclaved and used straight away or stored in 60°C. The LB agar mixture was allowed to cool down until the mixture bottle become warm and can be felt by hand. All the following work was carried out beside Bunsen burner, where ampicillin was added into the LB agar mixture. Once the LB agar mixture with ampicillin was mixed well, approximate 25ml of the mixture was poured into 100mm petri dish. Once the LB agar has solidified, the LB agar plates used for bacterial culture or stored at 4°C (not longer than 30 days).
- **LB SOC media**: 100µl of 1M $MgSO_4$ and 20µl of 1M glucose (0.22µm filtered) made up to 10ml with LB broth.
- **SCS110 (E.coli) competent cells** (Agilent)

2.4.2 Heat Shock Transformation plasmid into Bacteria

The commercial competent cells SCS110 were purchased from Invitrogen and Agilent. The TOP10 competent cell is suitable for high-efficiency cloning and plasmid propagation, which is stable for high-copy-number plasmid replication. SCS110 competent cells are suitable to prepare plasmid DNA free of Dam or Dcm methylation, which resulted in DNA that can be digested with methylation-sensitive restriction enzymes. The competent cell was thawed on ice and plasmid DNA with concentration ranging 400 – 600ng was added to 50µl bacterial competent cells (SCS110). The competent cells with plasmid DNA mixture were mixed gently and incubated at 4°C on ice for 30 minutes. Heat shock was performed at 42°C for 30 seconds in laboratory water bath and allowed to recover at 4°C on ice for 10 minutes. 250µl of antibiotic-free LB media was added to the bacterial suspension and incubated at 32°C (pAAV-based plasmid) or 37°C (conventional plasmid) for 1 hour shaking at 200 rpms, prior to plating in LB agar with antibiotics and screening for positive transformants.

2.4.3 Screening for Transformants

The bacterial suspension was split into 100µl and 200µl into two separate LB agar plates, in an attempt to obtain the suitable amount of bacterial densities. The LB agar plates were placed inverted to avoid contamination and incubated overnight at 32°C (pAAV-based plasmid) or 37°C (conventional plasmid) with ampicillin antibody selection. On the next day, checking was done to see whether any bacterial colonies grew on LB agar plates or not. If the bacterial were grew in appropriate densities (overgrowth was avoided), each individual bacterial colony was picked by using sterile pipette tips and inoculated 5ml LB broth with ampicillin.

2.4.4 Production of Bacterial Cultures

After overnight incubation of bacterial suspension in the incubator at 32°C (pAAV-based plasmid) or 37°C (conventional plasmid), checking was done to make sure the bacterial colonies were grown in appropriate densities (Overgrowth of bacterial was avoided). All the following work was carried out near Bunsen burner, one colony was picked by using pipette tip and growth with 5ml LB broth with ampicillin in the bijou bottle. Once the LB broth was inoculated, it was incubated at 32°C (pAAV-based plasmid) or 37°C (conventional plasmid) in the incubator with shaking at 200 rpms. The post incubation of bacterial suspension can be used either for larger bacterial culture production for Maxiprep preparation or Miniprep plasmid DNA extraction.

2.4.5 Long-term Glycerol Bacterial Storage

Long-term glycerol bacterial storage was produced by mixing 750µl of the bacterial suspension together with 250µl of 80% sterile glycerol stock, and stored at -80°C freezer.

2.4.6 Bacterial stocks

The long-term glycerol bacterial stock is used to create single bacterial colonies.

A sterile plastic loop was used to scrape the top of the frozen bacteria stocks without unthaw glycerol bacteria. Single colonies of the glycerol bacterial stock, which were grown on a LB plate supplemented with ampicillin. Plates were incubated overnight at a suitable temperature at 32^{o}C (pAAV-based plasmid) or 37^{o}C (conventional plasmid) overnight.

2.4.7 Amplification and Purification of Plasmid DNA

- **QIAprep Spin Miniprep Kit** (Qiagen)
- **EndoFree Plasmid Maxi Kit** (Qiagen)

Mini-Prep was performed with Qiagen Mini-Prep kit to extract the small amount of plasmid DNA from the 5ml bacterial culture in LB broth for identity check through restriction-digest mapping. Maxi Prep required 500µl of bacterial suspension to inoculate in 250ml of LB broth with ampicillin for a large amount of plasmid DNA extraction with Qiagen Maxi-Prep kit. Both Mini and Maxi prep was carried out according to manufacturer's instructions. The concentration of plasmid DNA was determined by using the spectrophotometer. A variety yield of plasmid DNA was extracted based on the amount of starting bacterial culture (5ml for miniprep and 250ml for maxiprep) and a range of concentration of plasmid DNA (>20µg plasmid DNA for miniprep and >10mg plasmid DNA for maxiprep). The plasmid DNA will be stored at -20^{o}C freezer or used for further analysis (restriction digest mapping, sub-cloning and transfection).

2.5 Nucleic acid manipulation

2.5.1 Materials

- **Restriction enzymes and buffers** (NEB)
- **50X TAE buffer**: 242g Tris Base, 57.1ml Glacial Acetic Acid, 100ml of 0.5M EDTA pH 8.0 were made up to 1000ml with ddH_2O. The 1x TAE buffer diluted from 20ml 50X TAE buffer with 980ml ddH_2O and stored in room temperature.
- **UltraPure Agarose powder** (Bioline)
- **1000x SYBR Safe DNA gel stain** (Invitrogen)
- **Gel Loading Dye, Purple** (NEB)
- **DNA molecular weight markers: Hyperladders I &V** (Bioline)
- **Nanodrop Spectrophotometer** (ThermoFisher)
- **Digital imaging system** (Vilber)

2.5.2 Determination of Nucleic Acid Concentration through Optical Density

The determination of nucleic acid concentration and purity through measuring the absorbance of a sample at the wavelength of 260nm and 280nm. The different form of nucleic acid (RNA, single-stranded DNA, double-stranded DNA), all absorb at wavelength 260nm. The reading at 260nm/280nm ratio value used to access nucleic acid purity with a ratio ~1.8 for DNA and ~2.0 for RNA. The ratio lower below this point indicate contamination might be occurred due present of other components (protein, reagent or compound) absorb at 280nm. The secondary measurement reading at 260nm/230nm ratio value used to determine purity of the nucleic acid with a ratio ranging from 2.0 – 2.2, lower beyond this value indicate contamination (EDTA, phenol, carbohydrates) may cause absorbance at wavelength 230nm. Nanodrop spectrophotometer was used to determine the concentration and purity of nucleic acid. Once the blank (1µl of ddH_2O) and reagent blank (1µl of buffer dissolved nucleic acid) was set, 1µl of each sample was applied to the spectrophotometer.

2.5.3 Endonuclease Restriction Digest

The identity of the plasmid was identified through endonuclease restriction enzyme digest mapping. The restriction digest targeted site within the plasmid was identified with SnapGene Software and details of the restriction enzyme were checked on NEB website (http://nebcloner.neb.com/#!/redigest). The restriction enzyme mapping was performed through single, double or multiple digests with a variety of restriction enzyme. Once the restriction enzyme needed to be used was decided, 1µg plasmid DNA was applied in each reaction. The restriction digest reaction is made of 1x CutSmart Buffer, restriction enzyme (~10 units to 1µg of plasmid DNA), 1µg plasmid DNA and makeup to total 20µl with ddH_2O. The reaction was set up as manufacturer recommended in table below. The restriction digest product was either analysed through agarose gel electrophoresis.

NEB enzyme	NEB buffer	Restriction digest condition
AhdI	CutSmart® Buffer 100%	37°C for 1 hour, heat inactivation at 65°C for 20 min
BamHI-HF	CutSmart® Buffer 100%	37°C for 1 hour, No heat inactivation
EagI-HF	CutSmart® Buffer 100%	37°C for 1 hour, heat inactivation at 65°C for 20 min
EcoRI-HF	CutSmart® Buffer 100%	37°C for 1 hour, heat inactivation at 65°C for 20 min
KpnI-HF	CutSmart® Buffer 100%	37°C for 1 hour, No heat inactivation
MscI	CutSmart® Buffer 100%	37°C for 1 hour, heat inactivation at 80°C for 20 min
NaeI	CutSmart® Buffer 100%	37°C for 1 hour, No heat inactivation
NcoI-HF	CutSmart® Buffer 100%	37°C for 1 hour, heat inactivation at 80°C for 20 min
NdeI	CutSmart® Buffer 100%	37°C for 1 hour, heat inactivation at 65°C for 20 min
NotI-HF	CutSmart® Buffer 100%	37°C for 1 hour, heat inactivation at 65°C for 20 min
PvuI-HF	CutSmart® Buffer 100%	37°C for 1 hour, No heat inactivation
SpeI-HF	CutSmart® Buffer 100%	37°C for 1 hour, heat inactivation at 80°C for 20 min
SmaI	CutSmart® Buffer 100%	37°C for 1 hour, heat inactivation at 65°C for 20 min

Table 2.3 List of restriction endonuclease enzyme used in this project

2.5.4 Analysis Restriction Digest Plasmid with Horizontal Agarose Gel Electrophoresis

Restriction digest profile of plasmid DNA will be analyzed through agarose gel electrophoresis. Either 1% or 3.5% of agarose gel (mass of agarose powder in a total volume of 1X TAE buffer) was set up according to anticipated size fragment of restriction digest plasmid. The agarose mixture was microwave till completely dissolved (avoid overheating), it was cool down to lower temperature. 0.01% of 1000x SYBR Safe DNA gel stain (enable visualization under UV light) was added to the agarose mixture and mixed well prior to set up on gel tray together with the comb. Once the gel has solidified, it is placed into the gel tank filled with 1X TAE buffer and the comb was removed gently. 2µl of gel loading dye was added to 10µl of samples (Section 2.5.3). Approximate 12 µl of samples and DNA molecular weight markers (first and last wells) was loaded into each well on the agarose gel. The gel was then electrophoresed at ~65V for 1 hour (adjusted if necessary based on the run of DNA molecular weight marker and gel loading dye). Electrophoresis allowed quality control verification of the plasmid size determination with a variety of restriction digest, by direct comparison to DNA molecular weight marker. The results obtained were recorded by the image captured with digital imaging system (Vilber).

2.6 Tissue Cultures

2.6.1 General Tissue Culture Reagents

- **Sterile PBS**: 10 Phosphate-buffered salines (PBS) tablet (Oxoid) was dissolved in 1000ml of ddH_2O. The PBS solution was autoclaved at 110^oC for 1 hours, the PBS solution was stored at room temperature (RT) once it is cool down.
- **Dulbecco`s modified Eagle`s medium (DMEM), high glucose, GlutaMAX™ Supplement, pyruvate** (Gibco)
- **Fetal Bovine Serum (FBS)** (Gibco): FBS will be heat-inactivated at 56^oC for 30 minutes, once the FBS was cooldown and stored at -20^oC freezer.
- **10x Trypsin** (Sigma): 0.5% trypsin in sterile PBS was prepared in Class II Lamina flow hood and stored at 4^oC fridge.
- **1% penicillin-streptomycin (PIS)** (ThermoFisher)
- **Tissue Grade DMSO** (Sigma)
- **Trypan Blue solution** (Sigma)
- **Hemocytometer (Neubauer Chamber)**
- **Sterile Plastic Stripettes, 5ml, 15ml, 25ml and 50ml Pipettes** (Corning)
- **T175cm^3, T125cm^3 and Tissue Culture Flask** (Corning)
- **15ml and 50ml Falcon Tube** (Corning)
- **Mr. Frosty™, Freezing Container** (Thermo)
- **Cryogenic tube vial** (Nunc)

2.6.2 Cell Lines

- **C2C12 (ATCC)** – Cells were obtained from ATCC. These cells were expanded and stored in liquid nitrogen. All the experiment were carried out with C2C12 cells passage <30 cycles.
- **MH (ATCC)** – Cells were obtained from ATCC. These cells were expanded and stored in liquid nitrogen. All the experiment were carried out with C2C12 cells passage <30 cycles.

2.6.3 Cell Culture Growth Media

Growth media was prepared according to manufacturer's instructions.

2.6.3.1 Growth Media for Culturing Mouse Myoblast (C2C12)

- **10% FBS DMEM with 1% Penicillin-Streptomycin (PIS)**: 50ml heat-inactivated FBS and 1% PIS was added into 500ml. The preparation was carried out in Class II Lamina flow hood and stored at 4^{o}C fridge. The 10% FBS DMEM was pre-heated to 37^{o}C for 15 minutes at water bath prior to use.

2.6.3.2 Growth Media for Culturing Mouse Muscle Fibroblast (MH)

- **10% FBS DMEM**: 50ml heat-inactivated FBS was added into 500ml. The preparation was carried out in Class II Lamina flow hood and stored at 4^{o}C fridge. The 10% FBS DMEM was pre-heated at 37^{o}C for 15 minutes at water bath prior to use.

2.6.4 Thawing Cells

Pre-warm growth media (based on different cell type) was prepared before thawing cells. The cells were taken from liquid nitrogen, incubated at 37^{o}C water bath to thaw in approximate 2 minutes. The 1ml thawed cells was mixed with 9ml growth media in the 50ml falcon tube and centrifuged (Beckmann centrifuge) at 1000 rpms, 200g for 5 minutes in RT. The supernatant was aspirated, and cell pellet re-suspended in a small amount (~3ml) DMEM media. All of the cells were transferred into T125cm^{3} tissue culture flask that contained 15 ml of growth media. The cells were closely observed under the light microscope once per day to make sure the cell densities are not over confluence before further passage.

2.6.5 Counting of live Cells with Haemocytometer (Neubauer Chamber)

Cells were detached using trypsin. After more than 95 % of cells were detached, fresh media was added. Following this, cells were stained with Trypan blue (0.4%) solution. Trypan blue staining is only taken up by dead cells. For this reason, dead cells appear dark under the microscope. A mixture was prepared containing 5µl 0.4% trypan blue solution and 5µl of the cell solution and subsequently the number of viable cells was assessed with a haemocytometer (Neubauer chamber). The Neubauer chamber was placed under the light microscope with 10X

magnification. The counting system only included the viable cells located within the middle square (highlight in the circle in **Figure 2.1A**) and count according to as left and the upper line of middle square (shown in **Figure 2.1B**). The total number of viable cells is calculated by the formula (**Figure 2.1C**), by comparing the cell count with standard cell count.

A

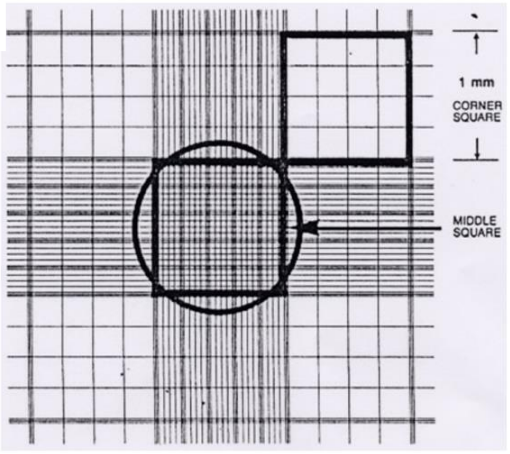

B

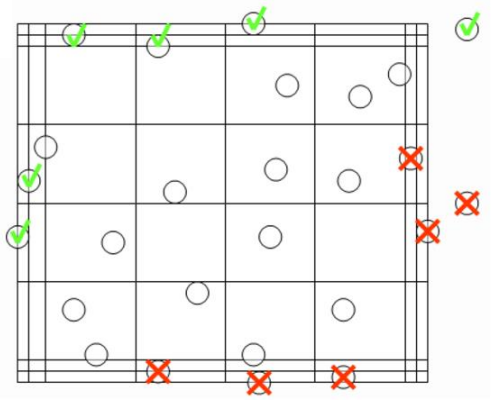

C Total cell count = Viable cell count in middle square x 2
Standard cell count: 50 Cells Count = 5 x 10^5 Cells/ml

Figure 2.1 Haemocytometer and Cell counting system (A) Visualise appearance of haemocytometer under the microscope. (B) Counting system within the middle square of haemocytometer under the microscope. (C) The formula of total cell count compared to standard cells count.

2.6.6 Culturing and Maintenance Cell Lines

Cell lines were grown and maintained at 37°C and 5% CO_2 with suitable types of growth media (Section 2.6.2). When the cell growth up to ~60 – 80% confluence, cells were passaged to avoid overgrowth or differentiation. The old media in tissue culture flask was aspirated and flask washed with 1X sterile PBS. Cells were detached using trypsin. Once 95% of the cells are detached, it was diluted in 15ml growth media transferred into 50ml Falcon tube and centrifuged at 1000 rpms for 5 minutes at RT.

2.6.7 Cryopreservation of cells

The sub-confluent cell cultures were treated with trypsin and re-suspended in 3ml growth media. Cell count was accessed the viability and number of cells using a haemocytometer (Section 2.6.3). 900µl of re-suspended cell culture (5 x 10^5 cells) was top up to total volume of 1ml with 100µl DMSO in cryotubes (appropriate labelled). The cryotube was placed in Mr. Frosty™, freezing container at -80°C freezer overnight and transferred into liquid nitrogen tank for long-term storage on the next day.

2.7 Transient Transfection Protocols

2.7.1 Preparation of Cells for Transfection in 6 Well Plate

Cells were plated into 6 well plate with suitable cells density by haemocytometer (Section 2.6.3), in order to get up to ~80% confluence prior transfection on the next day (adjusted if necessary based on the confluence of cell growth through observation under the light microscope). Cell densities needed to be placed into the 6 well plate was approximately 2 x 10^5 cells.

2.7.2 Comparison of the Efficiency of Different Transfection Reagent

The optimization of transgene delivery into cells was investigated using 1000ng pCi-eGFP. Different types of transfection reagents and various ratios of reagent to plasmid DNA were analysed.

2.7.2.1 Transfection Reagents and Ratios

The ratio of transfection reagent to plasmid DNA was prepared in accordance with manufacturer instruction.

Cell line	Transfection Reagent	Ratio Used (transfection reagent volume (µl): DNA mass (µg)
C2C12	**Viafect**	3:1, 4:1 and 5:1
	Lipofectamine p3000	0.8:1, 1.2:1 and 1.6:1
	PEI	2:1, 3:1 and 4:1
MH	**Viafect**	3:1, 4:1 and 5:1
	Lipofectamine p3000	2:1, 3:1 and 4:1
	PEI	2:1, 3:1 and 4:1

2.7.3 Transient Transfection with Viafect

- **Transfection Reagent Viafect** (Promega)
- **Dulbecco`s modified Eagle`s medium (DMEM), high glucose, GlutaMAX™ Supplement, pyruvate** (Gibco): The serum-free DMEM used to set up transient transfection mixture consist of plasmid DNA and transfection reagent.

Viafect transfection reagent is a cationic delivery agent in aqueous solution with high efficiency and low toxicity. Viafect was allowed to reach RT before adding to DNA to form a complex. The Viafect DNA complex mixture was produced by added Viafect with DNA and made up to 200µl total volume with serum-free growth media into Eppendorf tube as shown in the table below. The Viafect DNA complex was allowed to incubate in RT for 15min prior to transfection. During the 15 min interval, the growth media in 6 well plate with ~80% confluence cells were replaced with new growth media. After 15 min, 200µl of Viafect DNA complex was added to each well in 6 well plate through dropwise circular motion and shaking the plate gently to ensure maximize the cell coverage. Cells were transfected for 24 hours (total RNA extraction) and 48 hours (total RNA extraction and protein extraction).

Plate size	The volume of Cells in Media (per well)	Total Volume of Transfection Complex (per well)	Amount of pDNA (per well)	Amount of Viafect Transfection Reagent (per well) for various Viafect Transfection Reagent: DNA ratio		
				1:3	1:4	1:5
6-well plate	2ml	200µl	2.5µg	7.5µl	10µl	12.5µl

2.7.4 Transient Transfection with Lipofectamine® 3000

- **Transfection Reagent Lipofectamine® 3000** (Invitrogen)
- **Dulbecco`s modified Eagle`s medium (DMEM), high glucose, GlutaMAX™ Supplement, pyruvate** (Gibco): The serum-free DMEM used to set up transient transfection mixture consist of plasmid DNA and transfection reagent.

Lipofectamine® 3000 transfection reagent offers high transfection efficiency with lipid nanoparticle in eukaryotic cells. The Mixture 1 (Serum free DMEM and Lipofectamine® 3000) and mixture 2 (Serum free, 2500 ng of pDNA and Lipofectamine® P3000 reagent) was prepared as shown in table below were incubated for 5 minutes in room temperature (RT). Both of the mixture 1 and 2 were mixed together and incubated for 15 minutes in RT to form pDNA-lipid complex. The 250µl of transfection mixture pDNA-lipid complex was added directly to the cells in culture medium on each well in 6 well plate.

	Mixture 1		Mixture 2		
Reagent	DMEM (µl)	Lipofectamine ® 3000 (µl)	DMEM (µl)	pDNA (µl)	P3000 (µl)
-	Top up to 437.5	35	Top up to 437.5	-	14
2:1		17.5		8.75	14
3:1		26.25		8.75	14
4:1		35		8.75	14

2.7.5 Transient Transfection with Polyetheylenime (PEI)

- **Transfection Reagent Polyetheylenime (PEI)** (Invitrogen)
- **Dulbecco`s modified Eagle`s medium (DMEM), high glucose, GlutaMAX™ Supplement, pyruvate** (Gibco): The serum-free DMEM used to set up transient transfection mixture consist of plasmid DNA and transfection reagent.

Polyetheylenime (PEI) is a stable cation polymer allowing positively charged DNA to condense such that can bind to the anionic surfaces of the cell (Longo, et al. 2013). As a result, the DNA is transferred into the cytoplasm through endocytosis of pDNA:PEI complex. Three different ratio of PEI were tested with the same amount of 2500ng pDNA shown in table below to investigate the effect of different concentration of PEI on transfection efficiency. The pDNA:PEI complex was prepared as shown in table below and incubated 15 minutes in RT. The 200µl of transfection mixture pDNA-PEI complex was added directly to the cells in culture medium on each well in 6 well plate.

Plate size	**The volume of Cells in Media (per well)**	**Total Volume of Transfection Complex (per well)**	**Amount of pDNA (per well)**	**Amount of PEI Transfection Reagent (per well) for various Viafect Transfection Reagent: DNA ratio**		
				1:2	1:3	1:4
6-well plate	2ml	Top up to 200µl	2.5µg	5µl	7.5µl	10µl

2.8 Flow Cytometry

2.8.1.1 Materials

- **4% Paraformaldehyde (PFA)** (Sigma)
- **FACs Buffer**: 500ml Sterile PBS, 2ml of 0.5 EDTA and 5ml 10% NaN_3
- **FACs Bends** (BD Falcon)
- **5ml round bottom snap cap FACs Tubes** (BD Falcon)
- **FACs Canto II** (BD Biosciences)
- **Clean and Rise Solutions** (BD Falcon)

2.8.2 Harvest GFP Expression in Cell Cultures

Flow cytometry was used to investigate and determine the cell that is expressing Green Fluorescent Protein (GFP) through GFP tagged pCI-GFP plasmid (Section 2.2.3). The two types of cells (MH cells and C2C12 cells) were seeded at 1 x 10^5 cells/ 6 well plate prior to transient transfection protocol (Section 2.7.3) with pCI-GFP plasmid. Post 48 hours transfection, the cells were harvested in FACs buffer into FACs tubes.

2.8.3 GFP detection and analysis

For the purposes of flow cytometry analysis, the control cells without the GFP protein expression will be used as a control to compare with the cells that are transfect with the pCI-GFP plasmid. The efficiency of the transfection was performed with the counting of GFP expression verified from the proportion of expressing cells in the transfection efficiency experiment. The efficiency of the transfection efficiency was analysed through FlowJo software (section 2.3.5) and expressed in the percentage of positive live cells with GFP expression over total cells within the gated region.

2.9 Total RNA Extraction

- **RNeasy mini kit** (Qiagen)

The RNeasy mini kit was used for total RNA extraction according to manufacturer's instruction. The DNase was applied during the RNA extraction to eliminate DNA. RNA was eluted in 30µl of RNase free water. The concentration of total RNA was determined by using the spectrophotometer (Section 2.5.2). The total RNA will be stored in -80^{o}C freezer or used for further analysis (cDNA construction and RT-qPCR).

2.10 Polymerase Chain Reaction (PCR) and Reverse transcription PCR (RT-PCR)

2.10.1 Materials

- **Go Taq G2 Flex (**Promega)
- **Primers** (IDT)
- **dNTP mix 100mM** (Bioline)
- **2x Red mastermix** (GeneSys ltd): Ready use PCR Mastermix made up with Tris-HCI pH8.5, 4mM $MgCl_2$, 0.2% Tween 20®, 0.4mM dNTPs, 0.2units/µl Taq DNA polymerase and inert red dye & stabilizer.
- **ProFlex 3 x 32 wells PCR System** (ThermoFisher)
- **LightCycler 480 plate-based real-time PCR instrument** (Roche)

2.10.2 First strand cDNA Construction for RT-qPCR

- **Oligo-p(dT)$_{15}$ (Oligo dT)** (Promega)
- **Random Primer (**Invitrogen)
- **GoScript Reverse Transcriptase Kit** (Promega)
- **Oligo dT** (Promega, C1101)
- **Random Primer** (Sigma, 48190011)
- **DEPC treat water** (Ambion)
- **ProFlex 3 x 32 wells PCR System** (ThermoFisher)

The total RNA (Section 2.9) extracted from in vitro tissue culture was used as RNA template for cDNA construction. Approximate 1000ng of total RNA was mixed with 50µM of Oligo dT and 300µg Random primer made up to the total volume of 10µl with DEPC treated water and incubated at 70^{o}C for 2 minutes in PCR machine (ProFlex PCR system). This initiation incubation step was to ensure total RNA and non-specific primers are denatured and secondary

structures were eliminated. The cDNA construction was performed according to the manufacturer's instruction. The mixture of 4µl of reaction buffer, 2µl of 25mM $MgCl_2$, 2µl of 2mM dNTP, 1µl of reverse transcriptase enzyme, 6µl of ddH_2O was mixed with the 10 µl initial incubation mixture to form a total volume of 25 µl. The next step was incubated at 25°C for 5 mins, followed by 42°C for 60 mins, then 70 ^{0}C for 15 mins in ProFlex PCR system. The cDNA was stored at -20°C or further used for RT-qPCR.

2.10.3 RT-qPCR

- **Sybr Green Master** (Roche)
- **RT-qPCR primer assay** (IDT)
- **DEPC-treated water** (Ambion)
- **LightCycler 481 II Instrument** (Roche)

2.10.3.1 RT-qPCR mastermix preparation

The 1µl cDNA construction (section 2.10.2) was used as a template. The cDNA was diluted in 1:50 with DEPC water contain with each samples. The appropriate positive samples were chose for a series dilution (1:10, 1:100, 1:1000, 1:10000, 1:100000) with DEPC water as standard. On each RT-qPCR reaction, the samples was prepared as shown in table below.

Reagent	Amount needed
Dilute cDNA	4 µl
20x RT-qPCR primer assay	0.5 µl
Sybr Green Master	5 µl
DEPC-treated water	Top up to 10 µl
Total	10 µl

2.10.3.2 RT-qPCR set up

Each of the specific target forward and reverse primer set were designed and described in section (2.3.1). The initiation denaturing at 95°C, follow by 35 cycles of standard amplification cycles conditions were set at 95°C for 15 seconds, 60°C for 15 seconds and 70°C for 15 seconds.

2.10.3.3 RT-qPCR analysis

The RT-qPCR housekeeping control *GADPH* gene, which is an enzyme involve in glycolysis break down of glucose to produce energy within the cell. The mRNA level expression of different target genes and normalized with mRNA level expression housekeeping genes were compared by using GraphPad software (section 2.3.4) and expressed in fold of changes of targeted genes mRNA expression level within the cells before and after transfection of relaxin plasmid.

2.11 Wound scratch assay

2.11.1 Materials

- **MH [mocha] Mouse Muscle fibroblast** (ATCC CRL-2709)
- **Fetal bovine serum (FBS)** (Gibco)
- **Dulbecco`s modified Eagle`s medium (DMEM), high glucose, GlutaMAX™ Supplement, pyruvate** (Gibco)
- **Sterile PBS**: 10 Phosphate-buffered salines (PBS) tablet (Oxoid) was dissolved in 1000ml of ddH_2O. The PBS solution was autoclaved at 110^oC for 1 hours, the PBS solution was stored at room temperature (RT) once it is cool down.
- **Recombinant human Transforming growth factor β (TGF-β) protein** (Abcam, ab50036)
- **Recombinant murine Interferon-γ** (Preprotech, 315-05)
- **Tetracycline hydrochloride** (Sigma, T7660-5G)
- **Transfection Reagent Viafect** (Promega)
- **35mm high Ibidi µ dishes** (Ibidi)
- **Zeiss Axio Observer D1 Microscope** (Zeiss)

2.11.2 Wound scratch assay dishes labelling

After the Ibidi plate was labelled as illustrated in Figure 11 the wound scratch was induced close to the 3 label dots in the inner part of the dishes. The labelling allows microscopy images to be taken over a time course of three days.

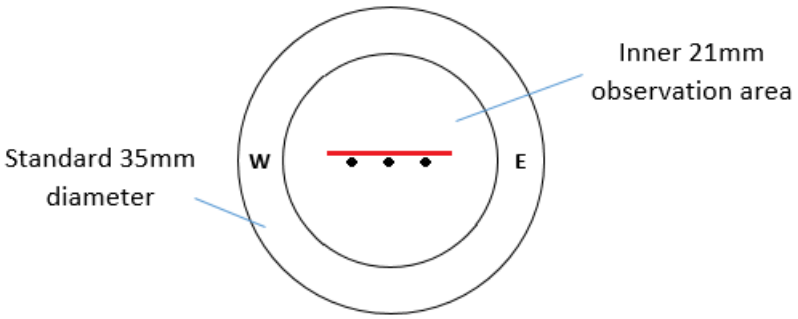

Figure 2.2 The illustration shows the bottom labelling ibidi dishes. The label of 3 dots (left, right and middle) near middle of the inner part of the dishes. The west (W) and east (E) was label on the standard outer part of the dishes. The wound scratch (red line) was done near to the 3 label dots on the middle of inner dishes.

2.11.3 Seeding Cells

MH cells were harvested by using trypsin treatment and suspended in 10% FBS DMEM. 1.2 x 10^5 of MH cells (in 400µl 10% FBS DMEM) were plated into each pre-coated collagen I 35mm high ibidi µ dishes (Ibidi) and incubated for 1 hour at 37°C with 5% CO_2. After 1 hour, 1.6ml 10% FBS DMEM was added into the ibidi dish and the dish was incubated overnight at 37°C with 5% CO_2. On the next day, the cells were grown up to approximate 80% confluency and the media was replaced by 1ml 0.5% FBS DMEM (to reduce the proliferation rate of MH cells). After an incubation time of at least 16 hours the cells reached 95% confluence.

2.11.4 Wound Scratch

When the cells reached 95% confluence, a linear wound scratch was induced with a p20 pipette tip. The cells were then washed twice with 1x PBS to clear floating debris and 1 ml 0.5% FBS media was added into the dishes. Various treatments, such as 40ng/ml TGF-β protein (Abcam, ab50036), 200ng/ml interferon γ (Preprotech, 315-05), 20µl 100ng/µl tetracycline hydrochloride (Sigma, T7660-5G), were used.

2.11.5 Transfection

Once the wound scratch was induced, a transfection was performed according to section 2.7.3.

2.11.6 Microscopy imaging on wound scratch

Brightfield microscopy images were taken with low resolution (2.5x) and high resolution (10x) using a Zeiss microscopy (Zeiss, Axio Observer D1). Images were taken immediately after wound scratching (T0), after 24 (T24) and 48 hours post transfection (T48).

2.11.7 Wound closure assessment

The area of wound closure was measured by using Image J software (https://imagej.nih.gov/ij/). The mean percentage of the wound closure was calculated by comparing to wound area T0 to T48.

2.12 Isolation of mouse organs and protein extraction

2.12.1 Materials

- **Dissection knife**
- **PAPBNI RIPA buffer**: NaCl 0.15M, HEPES 0.5M, NP-40 1%, Sodium Deoxycholate (SOC) 0.5%, SDS 10%, EDTA 0.01M, Protease inhibitor tablet 1 in 50ml (Roche). The PAPBNI RIPA Buffer was aliquoted into the bijou bottle with 5ml each and stored at -20^{o}C freezer.
- **QIAgen Tissue Lyser**

2.12.2 Dissection of mouse tissue from mouse

The animal work is done according to UK animal (Scientific Procedures) Act, 1986. The C57BL/10 mice were bred in and maintained with standard 12 hours in light or dark cycle with free access to food and water in our animal facility. The dissection was performed by Dr Ngoc Lu Nyugen to obtain mouse kidney, prostate, testis and vas deferens. The mouse tissue samples were kept in -80^{o}C freezer.

2.12.3 Protein extraction from frozen mouse tissue samples

Approximately 10 – 20 mg of the frozen mouse tissue samples was cut with dissection knife and weighed. The samples were transferred into Eppendorf tube with 1 Tungsten Carbide bead (3mm) and 100 µl ice cold RIPA buffer. Each sample was homogenised at 25 Hz for 2 minutes on QIAgen Tissue Lyser in 4^{o}C. The tube was then centrifuged at 14,000 rpm for 10 minutes at 4^{o}C, followed by decanting of the supernatant into fresh pre-chilled Eppendorf tube on ice. The protein samples were quantified or stored at -20^{o}C.

2.13 Protein extraction and quantification

2.13.1 Materials

- **Sterile PBS**: 10 Phosphate-buffered salines (PBS) tablet (Oxoid) was dissolved in 1000ml of ddH_2O. The PBS solution was autoclaved at 110^{o}C for 1 hours, the PBS solution was stored at room temperature (RT) once it is cool down.
- **PAPBNI RIPA buffer**: NaCl 0.15M, HEPES 0.5M, NP-40 1%, Sodium Deoxycholate (SOC) 0.5%, SDS 10%, EDTA 0.01M, Protease inhibitor tablet 1 in 50ml (Roche). The PAPBNI RIPA Buffer was aliquoted into the bijou bottle with 5ml each and stored at -20^{o}C freezer.
- **Benchtop microcentrifuge** (Eppendorf)
- **DC Assay protein kit**: Reagent A, S & B (BioRad)
- **2µg BSA standard** (Invitrogen)
- **96 well plate** (Corning)
- **96 well plate reader** (Genbank)
- **Methanol** (VMR)
- **Chloroform** (Sigma)
- **Centrifuge 5810R** (Eppendorf)

2.13.2 Protein Extraction

C2C12 cells were cultured in 6 wells plate up to 80% confluence. The transfection mixture was prepared with 2.5µg of non-codon optimized relaxin plasmid, transfection reagent Viafect (Promega) and top up to 200µl serum-free DMEM. The ratio of transfection reagent to pTRE-CO/NCO mRln1 plasmid is 3:1 (Optimised ratio Viafect with the plasmid for transfection, data not show). 1ml of the supernatant was transferred into 1.5ml Eppendorf tube and protein was precipitated from supernatant, while protein extraction from cell lysate was performed with cells adhered on the plate.

2.13.2.1 Protein Extraction from Cell Lysate

Cells were washed with 500µl ice-cold PBS. PBS was aspirated and 100µl of PABPN1 RIPA buffer was added. The plate was held at 45^{o} angle and cells were scrapped down by using bent 200µl pipette tips. The mixture contains PABPN1 RIPA buffer and cell mixture was transferred into pre-chilled 1.5ml Eppendorf tube on ice with an appropriate label. The mixture was incubated on ice for 15 minutes and vortexed each minute. The protein lysates mixture was centrifuged at 13,000 rpm for 15 minutes at 4^{o}C to pellet down the cell debris. The supernatant dissolved in PABPN1 RIPA buffer was transferred to another pre-chilled and labelled 1.5ml Eppendorf tube and stored at -20^{o}C freezer.

2.13.2.2 Protein Precipitation through Supernatant with Methanol/Chloroform Methods

This method involves using methanol, chloroform and water to precipitate protein. The ratio of protein:methanol:chloroform:water is 1:4:1:3. The protein will be precipitated and form a layer in between of top aqueous layer of methanol contain soluble compound (e.g. nucleic acids, salt, detergents and reducing agents) and bottom layer consists of chloroform containing lipids. 1ml of growth media was used as starting material together with 4 volume water (4ml), 1

volume chloroform(1ml) and 3 volume water (3ml) in 15ml falcon tube. The Falcon tube was centrifuged at 5000 rpms at 4^{o}C for 10 minutes, followed by removing the top water/methanol mixture (disturbing on the visible cloudy white layer contain protein shall be avoided). Another 3 volume (3ml) of methanol was added and vortex well before proceeding to another final centrifuge spin at 5000 rpms at 4^{o}C for 15 minutes. The supernatant was removed and carefully transferred the protein pellet into 1.5ml Eppendorf tube. The protein pellet was air dry (avoid the protein over dry) at RT and resuspended in approximate 100µl PABPN1 RIPA buffer. The protein is now ready for protein quantification or storage at -20^{o}C freezer.

2.13.3 Protein Quantification

A standard series dilution contains BSA standard and PABPN1 RIPA buffer with 0 - 2µg range of concentration as shown in the table below:

Concentration (µg)	2	1.8	1.5	1.2	1	0.8	0.6	0.4	0.2	0
PABPN1 RIPA buffer (µl)	0	4	10	16	20	24	28	32	36	40
BSA standard (µl)	40	36	30	24	20	16	12	8	4	0

5µl of protein sample and 0.5 µl of each concentration of the standard series dilution was transferred into 96 well plate. All conditions were prepared in triplicates. All the following experiment was carried out in fume hood by using reagents in DC assay protein kit. 25µl of mixture reagent A and S (20µl reagent S was added to each 1ml of reagents A) was added to each sample on 96 well plate. Next, 200µl of reagent B was applied and the resultant mixture is agitated (observation of the color changes from yellowish into blue once reagent B was added). The 96 well plate was incubated at room temperature for 15 minutes. The colorimetric analysis was performed through 96 well plate reader (Genbank) at 750nm. A standard curve was calculated and subsequent to this sample protein concentrations were determined.

2.14 Western Blot

2.14.1 Materials

- **NuPage® 10% Bis-Tris precast gels, 1.0mm, 15 well** (ThermoFisher)
- **NuPage® 20X MES SDS Running Buffer** (ThermoFisher)
- **NuPage® 10X Reducing Agent** (ThermoFisher)
- **NuPage® 4x LDS Sample Buffer** (ThermoFisher)
- **NuPage® Antioxidant** (ThermoFisher)
- **NuPage® 20X Transfer Buffer** (ThermoFisher)
- **Novex® Sharp Pre-Stained Protein Standard** (ThermoFisher, LC4800)
- **XCell SureLock™ Mini-Cell Electrophoresis System** (ThermoFisher)
- **X-Cell II™ Blot Module** (ThermoFisher)
- ***E.coli* positive control whole cell lysate** (Abcam ab5395)
- **Absolute Methanol** (VMR)
- **Amersham Protran Premium 0.2uM Nitrocellulose blotting membrane** (GE Healthcare)
- **Tween 20 Detergent** (Sigma)
- **Marvel Milk Powder**
- **Ponceau S Stain** (SigmaAldrich P7170-1L)
- **Filter paper**
- **Odyssey CLx** (LI-COR)

2.14.2 Antibodies

2.14.2.1 Primary Antibodies

Antibody name	Raised in	Dilution factor used	Expect binds to
HA tag (Sigma, SAB4200080-200UL)	**Rabbit**	**1:5000**	**HA tag peptide sequence**
Mouse relaxin 1/Human relaxin 2 (Abcam, ab183505)	**Rabbit**	**1:2500**	**Mouse relaxin 1**
Vinculin (Sigma SAB4200080-200UL)	**Mouse**	**1:10000**	**Mouse vinculin**

2.14.2.2 Secondary Antibodies

Antibody name	Dilution factor used	Expect binds to
IRDye® 680RD Goat anti-Mouse IgG (H+L) [LI-COR P/N 925-68070]	**1:10000**	**Mouse antibody**
IRDye® 800CW Goat anti-Rabbit IgG (H+L)), 0.1mg [LI-COR P/N925-32211]	**1:10000**	**Rabbit antibody**

2.14.3 Sample Preparation

Sample preparation was performed according to the table below (Taken from NuPage Technical guide 2010) with total protein extracted from the cell lysate and precipitate from supernatant:

Reagent	Reduced	Non-reduced Sample	Reduced
Sample	x µl	x µl	x µl
NuPage® 10X Reducing Agent	1 µl	-	2.5 µl
NuPage® 4x LDS Sample Buffer	2.5 µl	2.5 µl	6.25 µl
ddH_2O	To 6.5 µl	To 7.5 µl	To 16.25 µl
Total Volume	10 µl	10 µl	25 µl

(2x) master stock was prepared according to the table above contains: various amount of protein sample (40 µg – 120 µg) (Suggested 15µl sample on each well in NuPage® 10% Bis-Tris precast gels, 1.0mm, 15 well or 25 µl sample on each well in NuPage® 4 – 12 % Bis-Tris precast gels, 1.0mm, 10 well) in Eppendorf tube. In reduced condition, the reduced sample was prepared by NuPage® 10X Reducing Agent. All protein samples were heated at 70^{o}C for 10 minutes. The Novex® Sharp Pre-Stained Protein Standard was loaded into both wells at the end of the NuPage Bis-Tris precast gel and another well with positive control (E.coli positive control whole cell lysate or mouse tissue samples).

2.14.4 SDS-PAGE Gel set up and Electrophoresis

The setup conditions of electrophoresis were followed as the manufacturer (ThermoFisher) recommended. NuPage® 1X MES SDS Running Buffer was prepared by mixing 50ml of NuPage® 20X MES SDS Running Buffer with 950ml ddH_2O. A NuPage® Bis-Tris precast gels, 1.0mm, 15 well was used to resolve recombinant relaxin hormone with HA tag. The comb was removed gently and wells were washed with ddH_2O as initiation step to prepare the gel. Next, the white tape on the bottom part of the precast gel was removed. The precast gel was placed vertical (far from the gel tension wedge) on XCell SureLock™ Mini-Cell Electrophoresis

System together with plastic buffer dam (near the gel tension lock). The gel tension lock was lock up and filled with 200ml 1X MES SDS Running Buffer (the running buffer shall cover the well of the gel). Double checked to make sure there was no leaking of the running buffer from upper buffer chamber into the lower buffer chamber. 500µl of the NuPage® Antioxidant was added into the upper buffer chamber. 600ml of 1X MES SDS Running Buffer was filled into lower buffer chamber prior to starting electrophoresis. The gel electrophoresis was set to run at 200V for around 40 minutes. In order to make sure was not overrun, the smallest standard protein on protein ladder was located around 90% end on the bottom of the gel before stopping electrophoresis stop.

2.14.5 Opening Precast Gel Cassettes and Transferring protein to membranes

The opening precast gel cassettes and transferring protein to the membrane was followed as the manufacturer (ThermoFisher) recommended. The precast gel was removed from the upper buffer chamber, gel knife was placed in the groove between cassette halves and lever the knife gently to avoid excessive pressure on the gel. The top plate was removed and allowed the gel to come off by gentle shaking in the container with 1X transfer buffer (prepared as shown in the table below).

Reagent	Reduced Sample	Non-reduced Sample
NuPage® Transfer Buffer (20X)	50 ml	50 ml
NuPage® Antioxidant	1 ml	-
Methanol	100 ml	100 ml
ddH_2O	849 ml	850 ml
Total Volume	1000 ml	1000 ml

Once the gel was detached from the lower plate, the transferring set up as shown in **Figure 2.3** (Adapted from NuPage Technical guide 2010) in X-Cell II™ Blot Module. For one gel transferring, 4 blotting pad, 2 filter paper and 0.2µM nitrocellulose blotting membrane size similar to the gel were pre-soaked in transfer buffer. All trapped air bubbles was removed by using roller on the surface of blotting pad and filter paper. Extra care has taken to minimize the

air bubble trapped in between the gel and transfer membrane. Blot module was filled to 200ml of transfer buffer and make sure the buffer does not leak. The lower buffer chamber was filled with 600ml ddH_2O, placed the lid and run at 70V for 90 minutes.

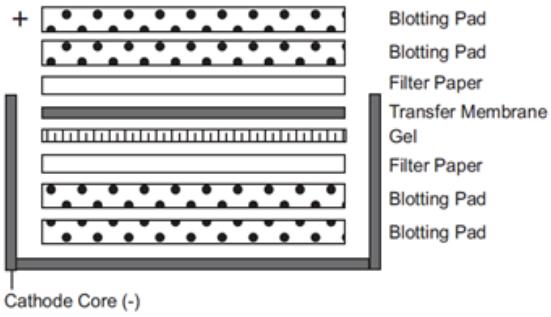

Figure 2.3 The Illustration of One Gel transferring process during western blot. Two blotting pads were placed at the bottom (cathode core) Blot module (X Cell II^{TM} Blot Module). This was followed by filter paper, gel and transfer membrane. Then the roller was used to remove air bubble trap in between gel and transfer membrane. Then another layer of filter paper was added and finally two blotting pads were added on the top. The anode core was placed on the top of the X Cell II^{TM} Blot Module, which is ready for Western blot transferring process.

2.14.6 Post-Transfer Nitrocellulose Membrane (NCB) Checks and Blocking

Following 90 minutes transfer, the membrane was stained with 1X Ponceau S solution for 5 minutes on weighing boat shaking on the shaker at 120 rpms. The stains will bind to all of the protein that is present in the membrane, the image was captured. The Ponceau S stains membrane was washed by using 0.1% PBS-Tween 20 (PBS-T) at 5 minutes intervals until no stains were visible.

The nitrocellulose membrane was then blocked with different types of blocking buffer (5% (w/v) Marvel milk in, 3% BSA in 0.2% PBS-Tween 20 or 3% BSA in 0.1% PBS-Triton X-100) for 1 hour in RT and shaking on the shaker at 120 rpms. The blocking step was to prevent non-specific binding of antibody on the membrane. Once the membrane was blocked, it is incubated in 4^{o}C overnight shaking on the shaker at 70 rpms with specific primary antibodies (Section 2.12.2.1) in 5% Marvel milk 0.2% PBS-T.

2.14.7 Visualization of the Nitrocellulose membrane (NCB): The Odyssey Method

After the overnight primary antibody incubation, the NCB was then subject to 4 washes for 10 minutes with 0.1% PBS-T in RT and shaking on the shaker at 120 rpms. The membrane was incubated with secondary antibody (Section 2.12.2.2) in 5% Marvel milk 0.2% PBS-T for 1 hour in RT, shaking on the shaker at 120 rpms. The post incubation of membrane in secondary antibody, further 4 times washes for 10 minutes in RT and shaking on the shaker at 120 rpms. Throughout the secondary antibodies incubation and post-incubation membrane washes, the membrane was kept in the dark. The detection of fluorescence was done at 680nm (Housekeeping protein shown in the red fluorescence band) and 800nm (Targeting protein shown in the green fluorescence band) through Odyssey CLx (LI-COR).

CHAPTER 3: STUDIES ON THE RELAXIN PLASMID DESIGN AND PLASMID VERIFICATIONS

CHAPTER 3: STUDIES ON THE RELAXIN PLASMID DESIGN AND PLASMID VERIFICATIONS

3.1 Introduction

Relaxin is a small (~6 kDa) pleiotropic hormone belonging to the insulin-like growth factor family; which plays an important role in female sex organs during pregnancy (Bathgate *et al*., 2003). In addition, relaxin inhibits the TGF-β induced transition of fibroblast to myofibroblast (Mookerjee *et al*., 2009), mediates Notch-1 inhibition of TGF-β/Smas3 signalling (Sassoli *et al*., 2013) and induces MMP-9 and MMP13 expression (Ahmad *et al*., 2012). Relaxin supresses several types of disease-related fibrosis, such as pulmonary fibrosis (Samuel *et al*., 2003), renal fibrosis (Danielson *et al*., 2006), hepatic fibrosis (Williams *et al*., 2001), cardiac fibrosis (Samuel *et al*., 2008) and scleroderma (Samuel *et al*., 2005). In skeletal muscle, relaxin has been shown to be involved in MMP regulation which suppress inflammation, tissue remodelling and fibrosis (Formigli *et al*., 2005) and promotes also the mobilization of satellite cells (Mu *et al*., 2010). Adenoviral-mediated delivery of relaxin reversed cardiac fibrosis through reduction in interstitial collagen content (Bathgate *et al*., 2008) and upregulation of the expression of MMP in keloid fibroblasts (Lee *et al*., 2012). In this project, we are interested in the potential effect of mouse relaxin 1 (mRln1) upregulation to reduce fibrotic condition *in vitro* studies with mRln1 expressing plasmid.

The reporter system based on the fluorescent protein allows visualization of the protein in living cells. In this thesis, a Green Fluorescence Protein (GFP) reporter system is adapted for detecting the efficiency of transfection through GFP expression *in vitro*. GFP was first isolated from the jellyfish *Aequorea victoria* (Ormö *et al*., 1996), where the protein exhibits green fluorescence when exposed to blue or ultraviolet range light (Tsien, 1998). The mutant GFP also known as enhanced GFP (eGFP) have mutations (F64L, S65T) within the chromophore region of the eGFP protein to increase the fluorescence when excited at 488nm (Cormack *et al*., 1996). The eGFP exhibits ~30 fold brighter fluorescence intensity compare to wild type GFP in *in vitro* transfection investigation (Cormack *et al*., 1996). An advantage of GFP reporter systems is that

they allow a direct visualization without the use of secondary proteins or cofactors. Some of the applications of the GFP protein are as a reporter gene for fluorescence microscopy or live imaging, fluorescence-activated cell sorting, fusion tag protein, co-transfection as a control for transfection efficiency in *in vitro*, reporter gene as transgene biodistribution *in vivo* (Kumar and Pal, 2016; Gangadaran *et al*., 2017).

Plasmid DNA is a circular, double stranded form of extra-chromosomal DNA that replicates independent compared to nuclear DNA, it is normally present in bacteria (Lodish, 2000); plasmids are commonly found in bacteria and often carry genes beneficial to the organism survival (Thomas *et al*., 2008). In biotechnology, plasmids are used as bacterial cloning vectors. Some genes in the original bacterial plasmid have been replaced with transgenes for specific biological research purposes, such as tissue specific promoters and genes of interest from mammalian cells for biological research (Gill *et al*., 2009). The plasmid DNA eventually undergoes gene silence over a period of time due to the CpG methylation in promoter or histone modification in mammalian (How *et al*., 2016). The sustainability of long-term transgene expression is highly dependent on the promoter and others elements (polyadenylated tails contribute to mRNA stability, Kozak sequence for translation initiation) (Gill *et al*., 2009). Plasmids including viral vector elements (e.g. inverted terminal repeat are needed in adeno-associated viral vector production) allow the production of viral vectors that favour long-term transgene expression which can be used for gene therapy (Naso *et al*., 2017). In this chapter different plasmid constructs and their level of transgene expression *in vitro* is investigated.

In mammalian expression vectors, promoter/enhancer elements are necessary to promote transgene expression. Currently, there are a few different types of promoter that are commonly used in mammalian expression system, such as viral promoters from cytomegalovirus (CMV), promoters from “native” human genes that exhibit high and tissue-specific transgene expression, as well as inducible promoters and synthetic promoters. The CMV promoter (~800bp) exhibits a ubiquitous and high level of transgene expression (Gray *et al*., 2011). In gene therapy,

the CMV promoter offers a strong constitutive transgene expression *in vivo* that will decline gradually over a period of time to DNA methylation (Doerfler, 2011). The CBh promoter (~800bp) is an improved version of the CMV promoter consisting of the CMV enhancer, chicken β-actin promoter and a hybrid intron (hybrid between chicken β-actin and intron of mice minute virus) (Gray *et al*., 2011). In this project, we designed plasmids with gene expression driven by a CBh promoter with a tetracycline inducible transcriptional activation system to control our transgene expression.

Tetracycline inducible transcriptional activation systems allow the regulation of transgene transcription through the presence (Tet-On) or absence (Tet-Off) of antibiotic tetracycline or its derivations (Kallunki *et al*., 2019). This system originated from gram-negative bacteria where it is responsible for tetracycline antibiotic resistance (Rodríguez-García *et al*., 2005). The presence of tetracycline activates the expression of the membrane protein TetA, which regulates the efflux of the antibiotic. In the absence of tetracycline the expression of TetA is repressed through binding of the protein TetR to the tetracycline operator tetO (Oeth *et al*., 2000). The protein TetR recognizes the Tetracycline Response Element (TRE) that comprises a 7 repeats of a length of 19 nucleotides. This system was developed to have a rapid and controlled transgene expression through the presence of tetracycline in mammalian HeLa cell system (Gossen and Bujard, 1992).

The Tet-On system was further developed with a reverse Tet repressor (rTetR) through random mutagenesis of TetR at 4 different amino acids positions (E71K, D95N, L101S and G102D). The Tet-On system allow for transgenes expression in the presence of tetracycline, in contrast absence of tetracycline repress transgenes expression. During the absence of tetracycline, the TetR fused with KRAB silencing domain bind to the tetO to suppress transgene expression (T Das *et al*., 2016). The rTetR fused to the C-terminal of VP16 (transcriptional domain from Herpes Simplex virus) and became the first generation of reverse tetracycline-controlled transactivator (rtTA) allow transgene expression to be turn on in the presence of tetracycline

(Gossen *et al*., 1995). Improvements led to the development of the second generation of rtTA also known as rtTA Advanced; rtTA Advanced consists of mutations on 5 amino acid positions (S12G, E19G A56P, D148E and H179R), which offer higher sensitivity to tetracycline and reduce leaky activity in the absence of tetracycline compare to rtTA (T Das *et al*., 2016). In this project, we utilised the Tet-On system to control our transgenes expression driven by the presence of antibiotic.

In DMD gene therapy, cardiac and skeletal muscle tissue-specific promoters allow specific transgenes to be expressed only in these cells to avoid off-target transgene expression across other types of cells (Rudeck *et al*., 2016). The muscle-specific synthetic promoter Spc512 offers high specificity on gene expression in muscle and cardiac cells compare to natural myogenic promoter (Darghia *et al*., 2004). The Spc512 is constructed with random assembling of multiple copies of 4 elements: upstream regulatory region of muscle-specific genes (MEF-1), promoter/enhancer regions of the myosin light chain 3 gene (MEF-2), serum response element (SRE) and transcription enhancer factor-1 (TEF-1) (Darghia *et al*., 2004). We are interested in utilising the Spc512 promoter to achieve high level of transgenes expression in skeletal muscle.

Temporary exogenous transgene expression delivery into the nucleus can be achieved through plasmid DNA transfection in cultured mammalian cells. The transgene is transcribed and translated into a specific functional protein, which is stable over a certain period of time. Exogenous transgene expression in gene therapy have various purposes based on the types of research or therapeutic effects (Naldini, 2015). We aimed for a high level of secreted hormone production in skeletal muscle. We hoped to improve the translation process through codon optimization, where we designed a codon-optimised mRln1 construct through online bioinformatics software. We focused on designing various plasmid constructs with either codon optimised mRln1 or native mRln1.

Introduction of nucleic acids into eukaryote cells through non-viral methods is known as transfection. This process involves transferring the negatively charged nucleic acid into cells

through the negatively charged membrane. There are a range of methods (chemical, biological and physical) that have been developed to introduce nucleic acids into the cells. Cationic polymers bind to negatively charged genetic materials that form a complex prior to being taken up by a cell via endocytosis (Midoux *et al.,* 2008). On the other hand, lipofection involves a positively charged liposome (phospholipid bilayer vesicle) to aggregate with negatively charged nucleic acids that merges with the cell membrane (Felgner *et al*., 1987). In this project, we focused on a comparison of three different types of transfection reagents that are chemical based transfection. We utilised transfection to achieve transgene expression *in vitro* studies.

In this chapter, we designed plasmids to express mouse relaxin 1 variants and characterised all plasmids constructs and their functional elements, including promoters (Spc512, CBh), tetracycline inducible activating system (Tet On), presence or absence of inverted terminal repeat (ITR) sequences, and origins of replication through restriction digest. Next, we optimised the transfection efficiency through a GFP reporter system into mouse myogenic cell line (C2C12) and mouse myogenic fibroblast cell line (MH). These preliminary *in vitro* transfection efficiency studies will be applied to mouse relaxin 1 expressing plasmid in the two following chapters.

3.2 Results

3.2.1 Plasmid construct design

All plasmid vectors that were constructed for this thesis are described in Section 2.2.

3.2.1.1 Reporter gene design and validation

Details of the reporter plasmid pCI-eGFP used in this thesis are shown in figure 3.1. The pCI-eGFP plasmid was a kind gift provided by Dickson Lab. The reporter plasmid pCI-eGFP expresses the gene eGFP under control of the promoter CMV.

3.2.1.2. Design and validation of plasmids expressing mRln1 driven by Spc512 (AAV based plasmid)

All plasmid constructs that contain mouse relaxin 1 (*mRln1*) were designed and synthesised by VectorBuilder. AAV based (contain inverted terminal repeat which allow for AAV viral vector production) plasmids that express mouse relaxin 1 (mRln1) under the control of synthetic muscle-specific (Spc512) promoter were designed. The 558 bp ORF of native *mRln1* was obtained from NCBI (NM011272.2) (native *mRln1*) and the sequence-optimised version of *mRln1* (CO mRln1) was generated through VectorBuilder Codon Optimization online software. Two types of AAV based plasmids were designed; single-stranded AAVs (ssAAV) were named pssAAV-Spc512-CO mRln1 (illustrated in figure 3.2A) and pssAAV-Spc512-NCO mRln1 (illustrated in figure 3.3A) and self-complementary AAVs (scAAV) were named pscAAV-Spc512-CO mRln1 (illustrated in figure 3.4A) and pscAAV-Spc512-NCO mRln1 (illustrated in figure 3.5A). The expression of mRln1 (CO mRln1 or NCO mRln1) cDNAs are driven by Spc512 promoter.

3.2.1.3 Design and validation of plasmids expressing mRln1 driven by a Tet On system (conventional & AAV based plasmid)

All plasmid constructs with mRln1 were designed and purchased online through VectorBuilder. Plasmids were designed with CO mRln1 or NCO mRln1 driven by a tetracycline inducible transcriptional activating system (Tet-On). Two of the conventional plasmids (plasmid that does not allow AAV viral vector production) that express mRln1 include a HA tag (HA) located C terminal of mRln1 driven by Tet-On system are pTet On-CO mRln1/HA (illustrated in figure 3.6A) and pTet On-NCO mRln1/HA (illustrated in figure 3.7A). The second set of the single-stranded AAV based plasmids (pssAAV) are pssAAV-Tet On-CO mRln1 (illustrated in figure 3.8A) and pssAAV-Tet On-NCO mRln1 (illustrated in figure 3.9A).

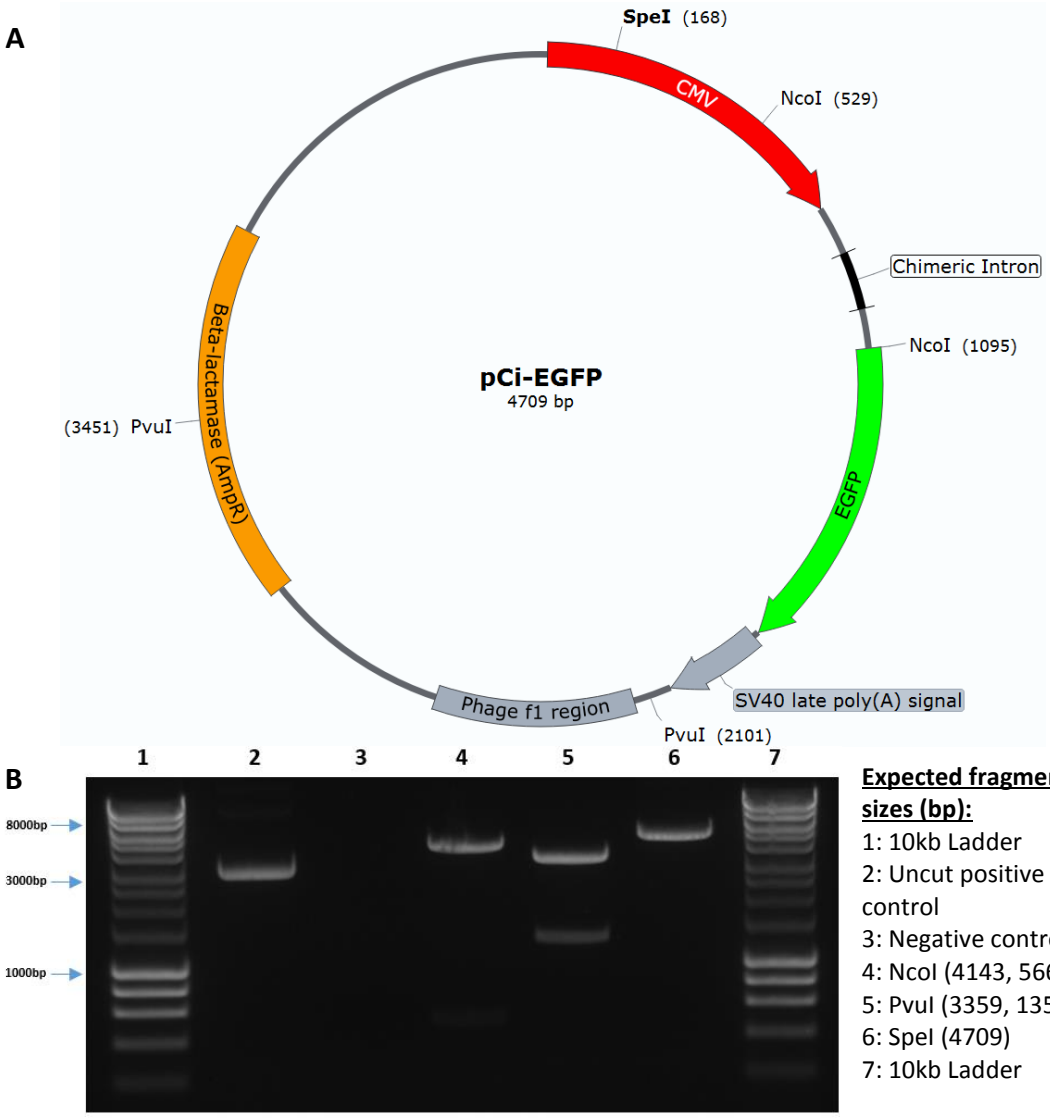

Figure 3.1 Design and characterisation of pCi-eGFP. **A.** Map of the reporter plasmid pCi-eGFP, which contains a DNA sequence for enhanced Green Fluorescence Protein (eGFP). The plasmid was obtained from Dickson Lab. Restriction digestion was set up with 1000ng of plasmid DNA digested with one unit of restriction enzyme for one hour as manufacturer suggested. **B.** Detailed restriction endonuclease analysis of pCi-eGFP was used to verify the plasmid construct and digests run on a 1% (w/v) agarose TAE gel. The reporter plasmid pCi-GFP was digested with different restriction enzymes, including NcoI (lane 4), PvuI (lane 5) and SpeI (lane 6) with expected fragment sizes produced. A positive (uncut plasmid) was included to be able to differentiate between digested and undigested plasmids. In addition, a negative control (no plasmid) was used to indicate the absence of contamination.

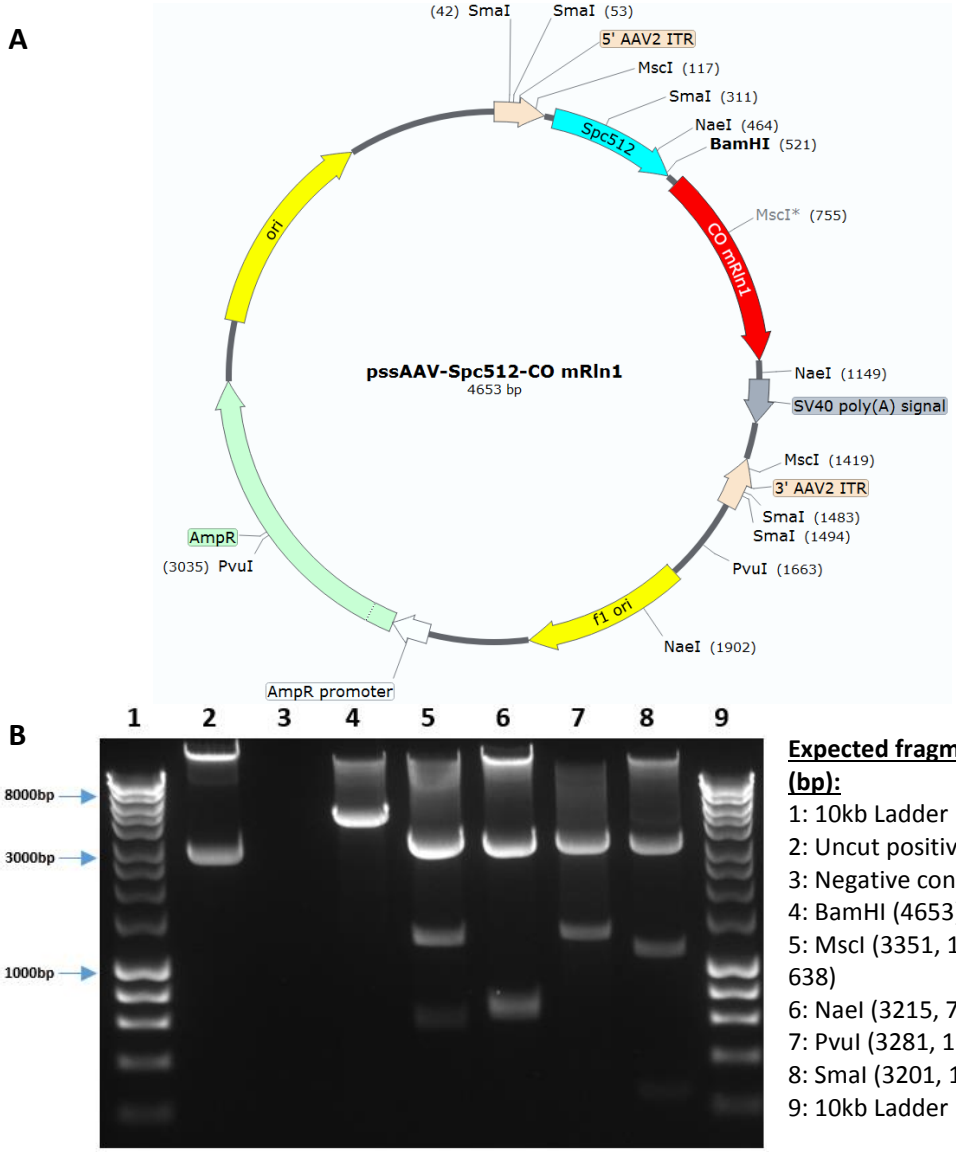

Expected fragment sizes (bp):

1: 10kb Ladder
2: Uncut positive control
3: Negative control
4: BamHI (4653)
5: MscI (3351, 1302, 664, 638)
6: NaeI (3215, 753, 685)
7: PvuI (3281, 1372)
8: SmaI (3201, 1172, 258)
9: 10kb Ladder

Figure 3.2 Design and characterisation of pssAAV-Spc512-CO mRln1 vectors. **A.** Functional map of pssAAV-Spc512-CO mRln1. The plasmid was designed online and ordered through VectorBuilder in bacterial glycerol stocks. The specific restriction digest site is located in the map and methylation site (*) for certain restriction enzyme. Restriction digestion was set up with 1000ng of plasmid DNA digested with one unit of restriction enzyme for one hour as manufacturer suggested **B.** Detailed restriction endonuclease analysis of pssAAV-Spc512-CO mRln1 was used to verify the plasmid construct and digests run on a 1% (w/v) agarose TAE gel. The pssAAV-Spc512-CO mRln1 is analysed respectively with different restriction enzyme BamHI (lane 4), MscI (lane 5), NaeI (lane 6), PvuI (lane 7) and SmaI (lane 8) with expected fragment sizes. A positive (uncut plasmid) was included to be able to differentiate between digested and undigested plasmids. In addition, a negative control (no plasmid) was used to indicate the absence of contamination.

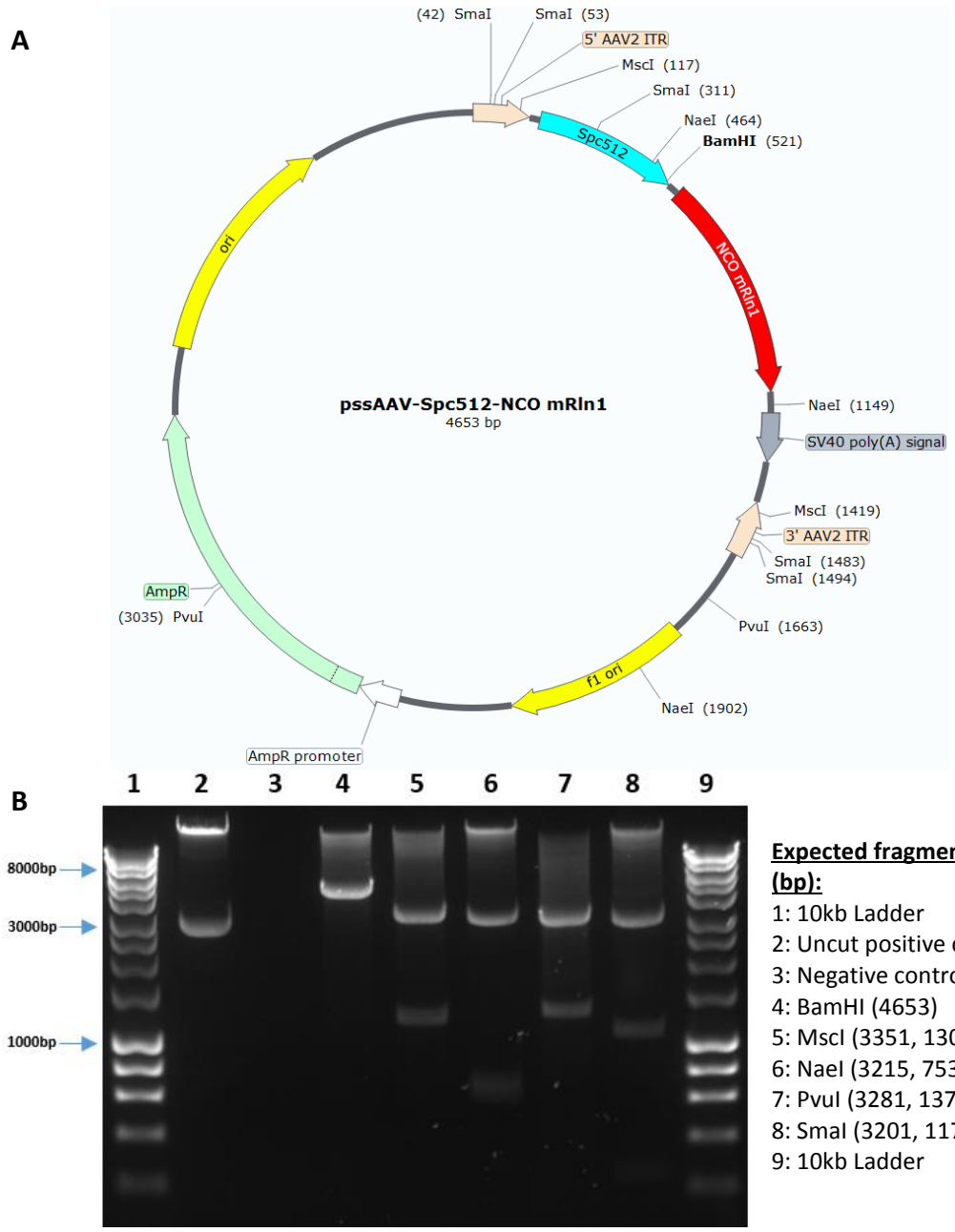

Expected fragment sizes (bp):

1: 10kb Ladder
2: Uncut positive control
3: Negative control
4: BamHI (4653)
5: MscI (3351, 1302)
6: NaeI (3215, 753, 685)
7: PvuI (3281, 1372)
8: SmaI (3201, 1172, 258)
9: 10kb Ladder

Figure 3.3 Design and characterisation of pssAAV-Spc512-NCO mRln1 vectors. **A.** Functional map of pssAAV-Spc512-NCO mRln1. The plasmid was designed online and ordered through VectorBuilder in bacterial glycerol stocks. The specific restriction digest site is located in the map. Restriction digestion was set up with 1000ng of plasmid DNA digested with one unit of restriction enzyme for one hour as manufacturer suggested **B.** Detailed restriction endonuclease analysis of pssAAV-Spc512-NCO mRln1 was used to verify the plasmid construct and digests run on a 1% (w/v) agarose TAE gel. The pssAAV-Spc512-NCO mRln1 is analysed respectively with different restriction enzyme BamHI (lane 4), MscI (lane 5), NaeI (lane 6), PvuI (lane 7) and SmaI (lane 8) with expected fragment sizes. A positive (uncut plasmid) was included to be able to differentiate between digested and undigested plasmids. In addition, a negative control (no plasmid) was used to indicate the absence of contamination.

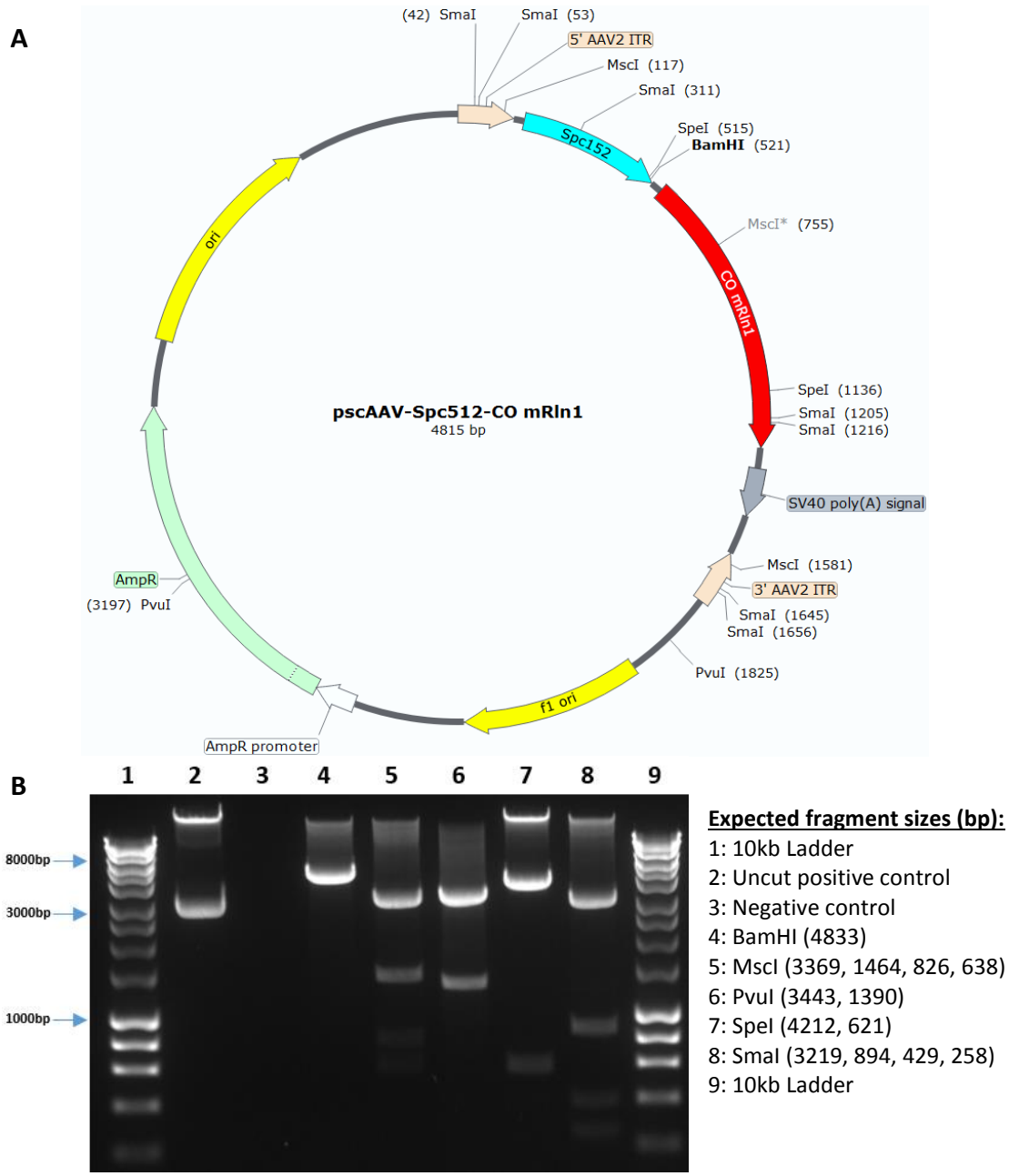

Expected fragment sizes (bp):

1: 10kb Ladder
2: Uncut positive control
3: Negative control
4: BamHI (4833)
5: MscI (3369, 1464, 826, 638)
6: PvuI (3443, 1390)
7: SpeI (4212, 621)
8: SmaI (3219, 894, 429, 258)
9: 10kb Ladder

Figure 3.4 Design and characterisation of pscAAV-Spc512-CO mRln1 vectors. **A.** Functional map of pscAAV-Spc512-CO mRln1. The plasmid was designed online and ordered through VectorBuilder in bacterial glycerol stocks. The specific restriction digest site is located in the map and methylation site (*) for certain restriction enzyme. Restriction digestion was set up with 1000ng of plasmid DNA digested with one unit of restriction enzyme for one hour as manufacturer suggested **B.** Detailed restriction endonuclease analysis of pscAAV-Spc512-CO mRln1 was used to verify the plasmid construct and digests run on a 1% (w/v) agarose TAE gel. The pscAAV-Spc512-CO mRln1 is analysed respectively with different restriction enzyme BamHI (lane 4), MscI (lane 5), NaeI (lane 6), PvuI (lane 7) and SmaI (lane 8) with expected fragment sizes. A positive (uncut plasmid) was included to be able to differentiate between digested and undigested plasmids. In addition, a negative control (no plasmid) was used to indicate the absence of contamination.

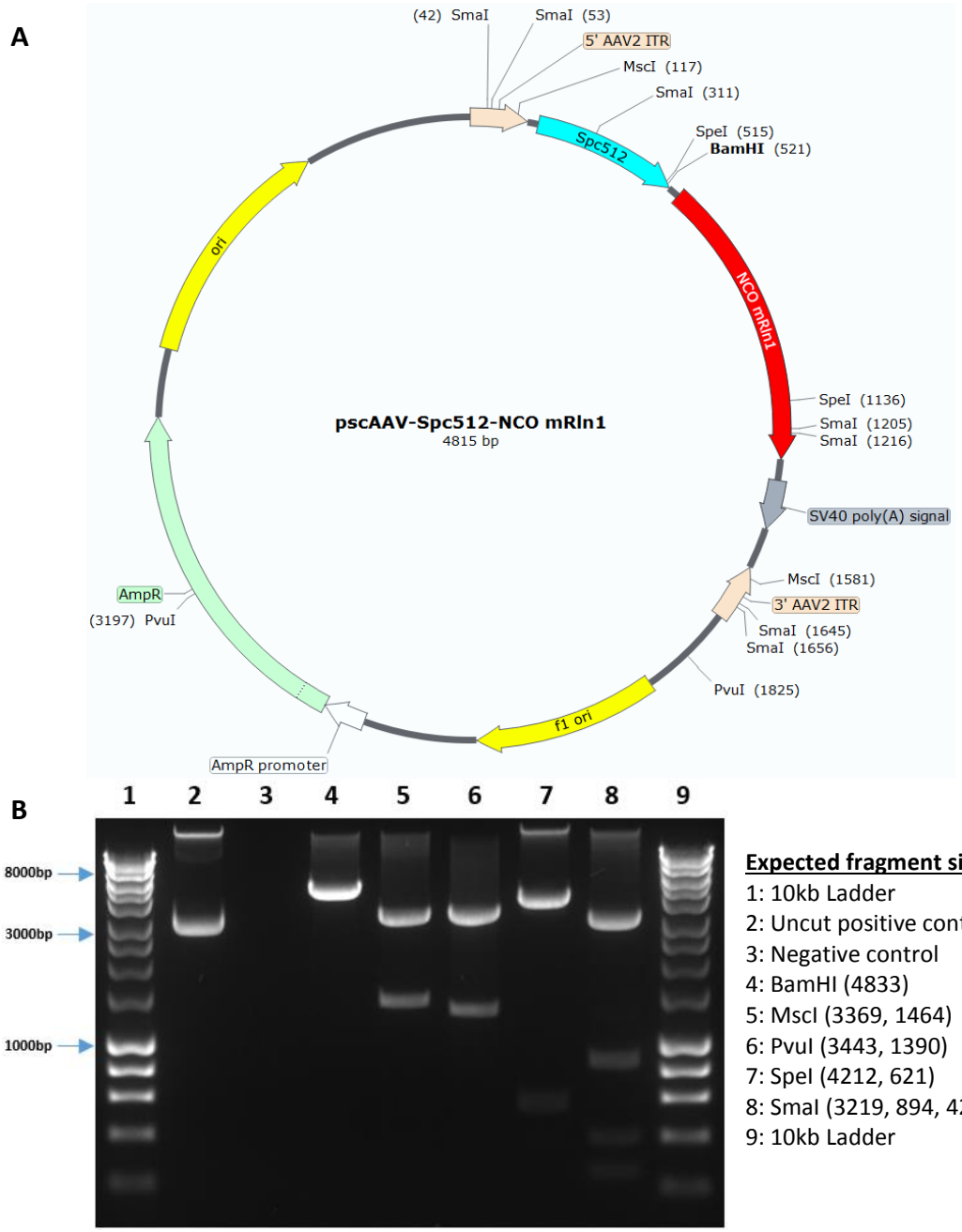

Expected fragment sizes (bp):

1: 10kb Ladder
2: Uncut positive control
3: Negative control
4: BamHI (4833)
5: MscI (3369, 1464)
6: PvuI (3443, 1390)
7: SpeI (4212, 621)
8: SmaI (3219, 894, 429, 258)
9: 10kb Ladder

Figure 3.5 Design and characterisation of pscAAV-Spc512-NCO mRln1 vectors. **A.** Functional map of pscAAV-Spc512-NCO mRln1. The plasmid was designed online and ordered through VectorBuilder in bacterial glycerol stocks. The specific restriction site is located in the map. Restriction digestion was set up with 1000ng of plasmid DNA digested with one unit of restriction enzyme for one hour as manufacturer suggested **B.** Detailed restriction endonuclease analysis of pscAAV-Spc512-NCO mRln1 was used to verify the plasmid construct and digests run on a 1% (w/v) agarose TAE gel. The pscAAV-Spc512-NCO mRln1 is analysed respectively with different restriction enzyme BamHI (lane 4), MscI (lane 5), PvuI (lane 6), SpeI (lane 7) and SmaI (lane 8). A positive (uncut plasmid) was included to be able to differentiate between digested and undigested plasmids. In addition, a negative control (no plasmid) was used to indicate the absence of contamination.

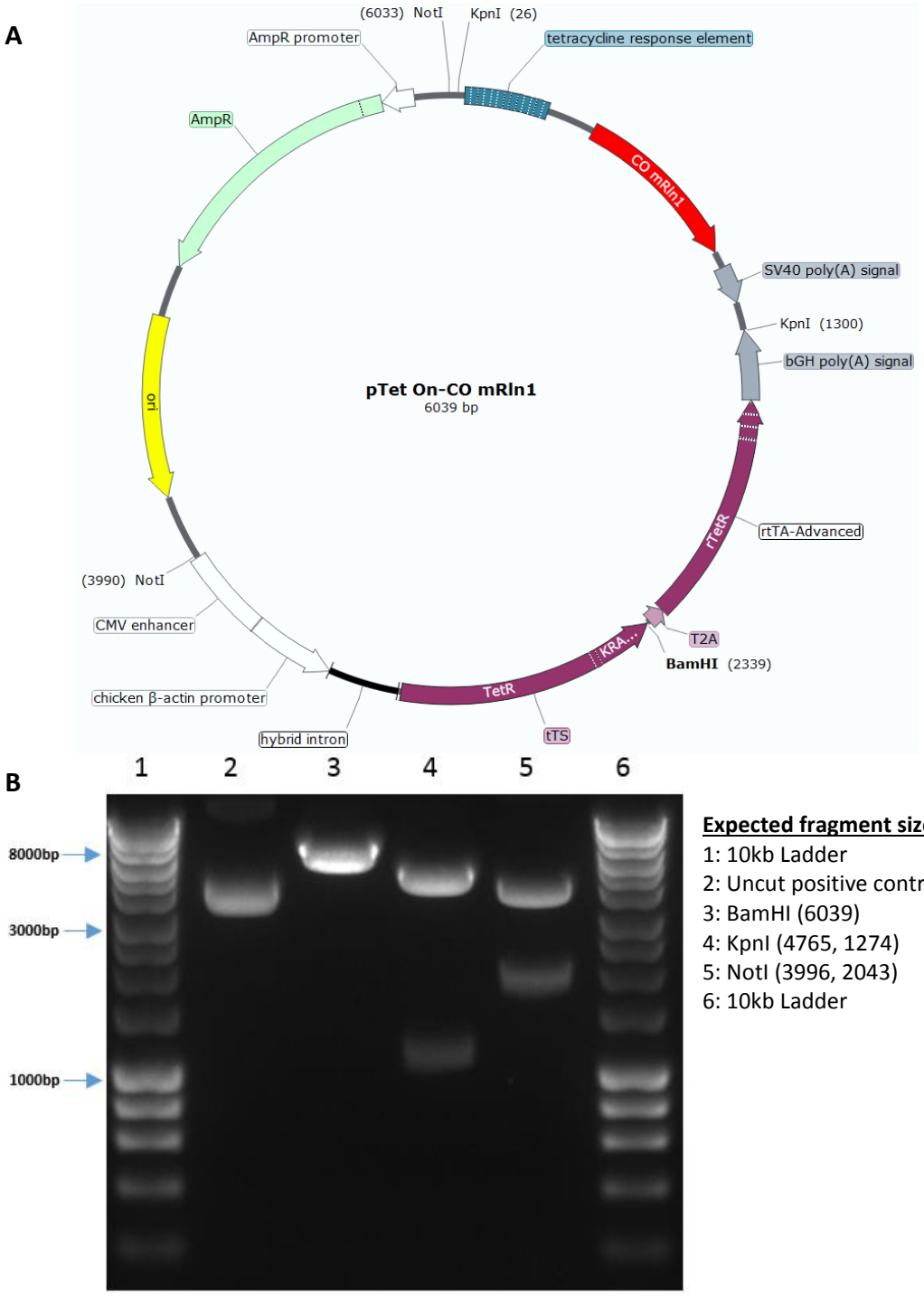

Expected fragment sizes (bp):

1: 10kb Ladder
2: Uncut positive control
3: BamHI (6039)
4: KpnI (4765, 1274)
5: NotI (3996, 2043)
6: 10kb Ladder

Figure 3.6 Design and characterisation of pTet On-CO mRln1 vectors. **A.** Functional map of pTet On-CO mRln1. The plasmid was designed online and ordered through VectorBuilder in bacterial glycerol stocks. The specific restriction site is located in the map. Restriction digestion was set up with 1000ng of plasmid DNA digested with one unit of restriction enzyme for one hour as manufacturer suggested **B.** Detailed restriction endonuclease analysis of pTet On-CO mRln1 was used to verify the plasmid construct and digests run on a 1% (w/v) agarose TAE gel. The pTet On-CO mRln1 is analysed respectively with different restriction enzyme BamHI (lane 3), KpnI (lane 4) and NotI (lane 5). A positive (uncut plasmid) was included to be able to differentiate between digested and undigested plasmids.

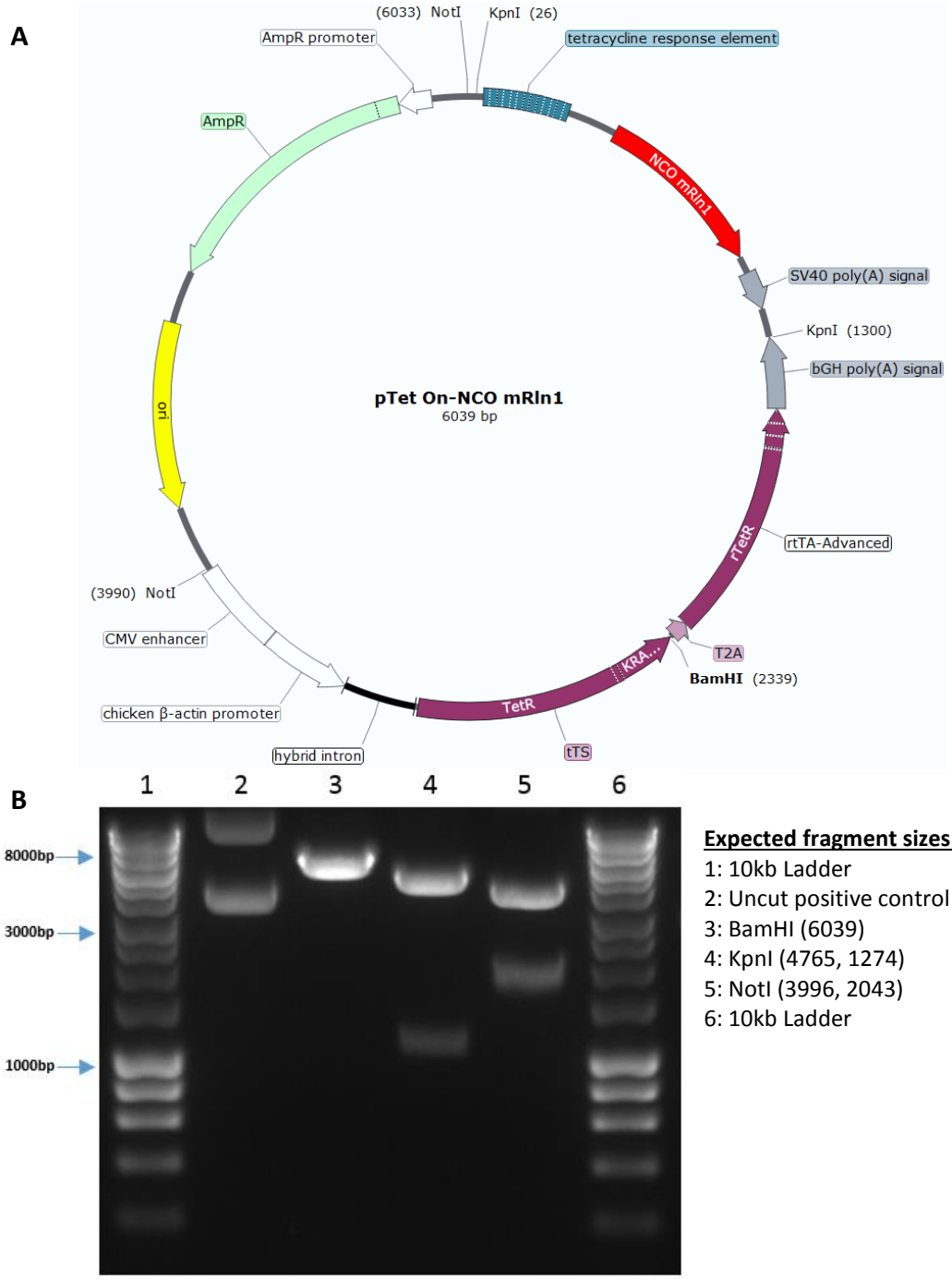

Expected fragment sizes (bp):

1: 10kb Ladder
2: Uncut positive control
3: BamHI (6039)
4: KpnI (4765, 1274)
5: NotI (3996, 2043)
6: 10kb Ladder

Figure 3.7 Design and characterisation of pTet On-NCO mRln1 vectors. **A.** Functional map of pTet On-NCO mRln1. The plasmid was designed online and ordered through VectorBuilder in bacterial glycerol stocks. The specific restriction site is located in the map. Restriction digestion was set up with 1000ng of plasmid DNA digested with one unit of restriction enzyme for one hour as manufacturer suggested **B.** Detailed restriction endonuclease analysis of pTet On-NCO mRln1 was used to verify the plasmid construct and digests run on a 1% (w/v) agarose TAE gel. The pTet On-NCO mRln1 is analysed respectively with different restriction enzyme BamHI (lane 3), KpnI (lane 4) and NotI (lane 5). A positive (uncut plasmid) was included to be able to differentiate between digested and undigested plasmids.

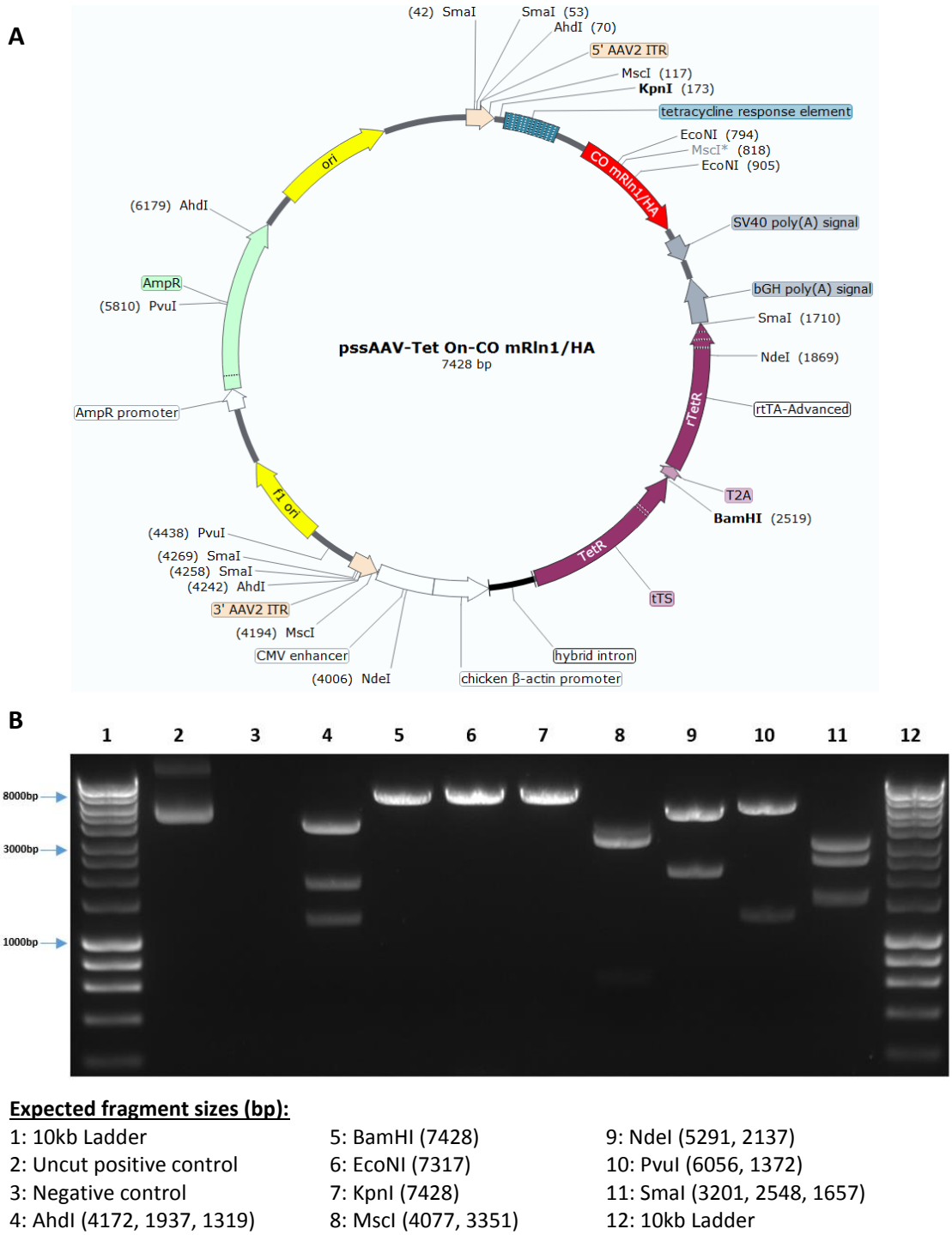

Expected fragment sizes (bp):

1: 10kb Ladder	5: BamHI (7428)	9: NdeI (5291, 2137)
2: Uncut positive control	6: EcoNI (7317)	10: PvuI (6056, 1372)
3: Negative control	7: KpnI (7428)	11: SmaI (3201, 2548, 1657)
4: AhdI (4172, 1937, 1319)	8: MscI (4077, 3351)	12: 10kb Ladder

Figure 3.8 Design and characterisation of pssAAV-Tet On-CO mRln1/HA vectors. **A.** Functional map of pssAAV-Tet On-CO/HA mRln1. The plasmid was designed online and ordered through VectorBuilder in bacterial glycerol stocks. The specific restriction site is located in the map. Restriction digestion was set up with 1000ng of plasmid DNA digested with one unit of restriction enzyme for one hour as manufacturer suggested. **B.** Detailed restriction endonuclease analysis of pssAAV-Tet On-CO mRln1 mRln1/HA was used to verify the plasmid construct and digests run on a 1% (w/v) agarose TAE gel. The pssAAV-Tet On-CO mRln1/HA is analysed respectively with different restriction enzyme AhdI (lane 3) BamHI (lane 4), EcoNI (lane 5), KpnI (lane7), MscI (lane 8), NdeI (lane 9), PvuI (lane 10) and SmaI (lane 11). A positive (uncut plasmid) was included to be able to differentiate between digested and undigested plasmids. In addition, a negative control (no plasmid) was used to indicate the absence of contamination.

A

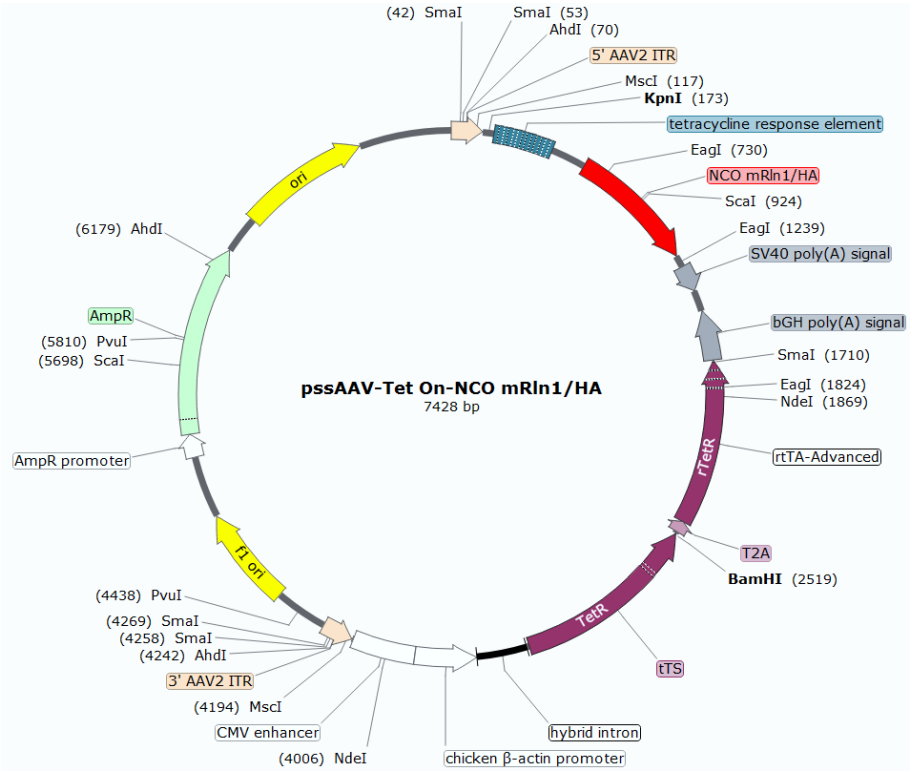

B

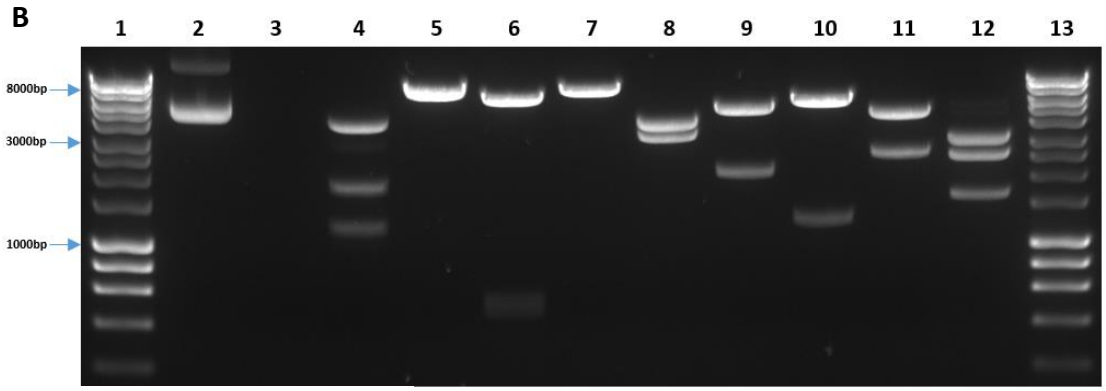

Expected fragment sizes (bp):

1: 10kb Ladder
2: Uncut positive control
3: Negative control
4: AhdI (4172, 1937, 1319)
5: BamHI (7428)
6: EagI (6334, 585, 509)
7: KpnI (7428)
8: MscI (4077, 3351)
9: NdeI (5291, 2137)
10: PvuI (6056, 1372)
11: ScaI (4774, 2654)
12: SmaI (3201, 2548, 1657)
13: 10kb Ladder

Figure 3.9 Design and characterisation of pssAAV-Tet On-NCO mRln1/HA vectors. **A.** Functional map of pssAAV-Tet On-NCO/HA mRln1. The plasmid was designed online and ordered through VectorBuilder in bacterial glycerol stocks. The specific restriction site is located in the map. Restriction digestion was set up with 1000ng of plasmid DNA digested with one unit of restriction enzyme for one hour as manufacturer suggested. **B.** Detailed restriction endonuclease analysis of pssAAV-Tet On-NCO mRln1/HA was used to verify the plasmid construct and digests run on a 1% (w/v) agarose TAE gel. The pssAAV-Tet On-NCO mRln1/HA is analysed respectively with different restriction enzyme AhdI (lane 3) BamHI (lane 4), EcoNI (lane 5), KpnI (lane7), MscI (lane 8), NdeI (lane 9), PvuI (lane 10) and SmaI (lane 11). A positive (uncut plasmid) was included to be able to differentiate between digested and undigested plasmids. In addition, a negative control (no plasmid) was used to indicate the absence of contamination.

3.2.2 Comparison between codon optimised and native mouse relaxin 1

We utilize codon optimization of the nucleotide sequence and hoped it might increase the translation efficiency compare to native nucleotide sequence. The native mouse relaxin 1 (mRln1) nucleotide sequence was obtained from NCBI (NCBI, NM011272.2). The codon optimised sequence was generated with the mouse relaxin 1 amino acids sequence obtained from Uniprot (Uniprot, P47932) and the codon optimised mRln1 (CO mRln1) sequence was generated with online Vectorbuilder codon optimization software (VectorBuilder). Both of the CO mRln1 and mRln1 nucleotide sequence was compared by using online Clustal multiple sequence alignment by MUSCLE 3.8 (EMBL, MUSCLE). The result suggested there are only 39.45% codon from mRln1 remain the same as CO mRln1, while the other 60.55% codons replaced the low frequency rare codon to higher frequency codon (**Figure 3.10**).

The rare codon analysis was performed with online bioinformatics GenScript rare codon analysis tool (GenScript). In the Vectorbuilder codon optimization (CO) mouse relaxin 1 (mRln1) there was an increase in Codon Adaptation Index (**CAI**) and GC content, while there was a reduced Codon Frequency Distribution (**CFD**) compared to the native mRln1. The ideal CAI would be between 0.8 and 1.0; the CAI for native mRln1 is 0.71, there was therefore an increase in CAI in the CO mRln1 to 1.0, suggesting the CO mRln1 had a higher chance of being expressed at a higher level compared to native mRln1. Next the GC content increased from 51.76% in native mRln1 to 66.03% in CO plasmid. The increase in the GC content lead to a reduction of CFD which indicated a low percentage frequency of rare codons have been replaced with higher frequency codons that are translated into the same amino acid. Lastly, both of the negative Cis-regulatory elements (CIS) element and negative repeat elements are not present in both of the native mRln1 and CO mRln1. In summary, an increase of the GC content and the replacement of rare codons allows codon replacement which is vital for codon optimization.

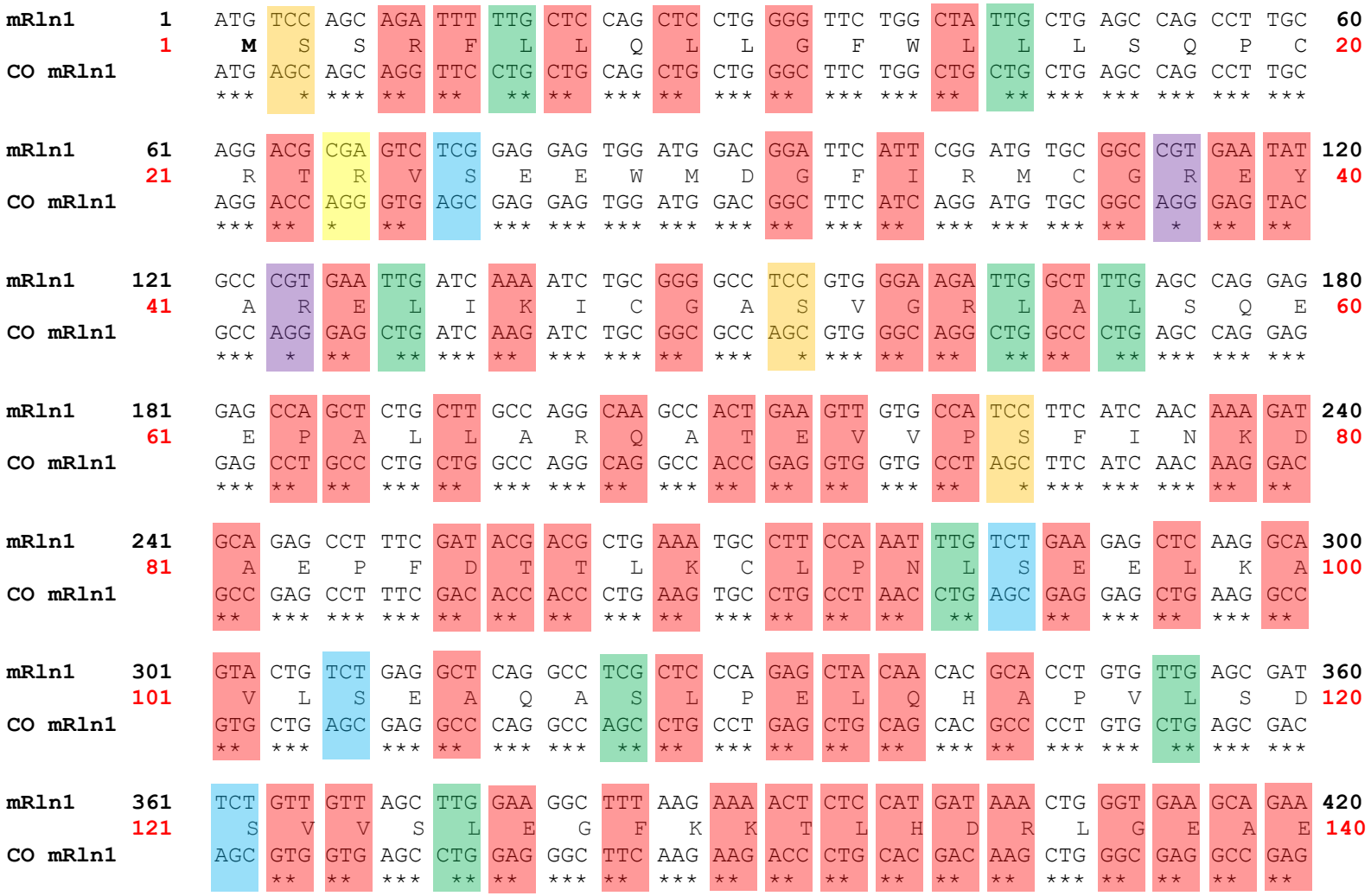
mRln1 1 ATG TCC AGC AGA TTT TTG CTC CAG CTC CTG GGG TTC TGG CTA TTG CTG AGC CAG CCT TGC 60
1 M S S R F L L Q L L G F W L L L S Q P C 20
CO mRln1 ATG AGC AGC AGG TTC CTG CTG CAG CTG CTG GGC TTC TGG CTG CTG CTG AGC CAG CCT TGC
mRln1 61 AGG ACG CGA GTC TCG GAG GAG TGG ATG GAC GGA TTC ATT CGG ATG TGC GGC CGT GAA TAT 120
21 R T R V S E E W M D G F I R M C G R E Y 40
CO mRln1 AGG ACC AGG GTG AGC GAG GAG TGG ATG GAC GGC TTC ATC AGG ATG TGC GGC AGG GAG TAC
mRln1 121 GCC CGT GAA TTG ATC AAA ATC TGC GGG GCC TCC GTG GGA AGA TTG GCT TTG AGC CAG GAG 180
41 A R E L I K I C G A S V G R L A L S Q E 60
CO mRln1 GCC AGG GAG CTG ATC AAG ATC TGC GGC GCC AGC GTG GGC AGG CTG GCC CTG AGC CAG GAG
mRln1 181 GAG CCA GCT CTG CTT GCC AGG CAA GCC ACT GAA GTT GTG CCA TCC TTC ATC AAC AAA GAT 240
61 E P A L L A R Q A T E V V P S F I N K D 80
CO mRln1 GAG CCT GCC CTG CTG GCC AGG CAG GCC ACC GAG GTG GTG CCT AGC TTC ATC AAC AAG GAC
mRln1 241 GCA GAG CCT TTC GAT ACG ACG CTG AAA TGC CTT CCA AAT TTG TCT GAA GAG CTC AAG GCA 300
81 A E P F D T T L K C L P N L S E E L K A 100
CO mRln1 GCC GAG CCT TTC GAC ACC ACC CTG AAG TGC CTG CCT AAC CTG AGC GAG GAG CTG AAG GCC
mRln1 301 GTA CTG TCT GAG GCT CAG GCC TCG CTC CCA GAG CTA CAA CAC GCA CCT GTG TTG AGC GAT 360
101 V L S E A Q A S L P E L Q H A P V L S D 120
CO mRln1 GTG CTG AGC GAG GCC CAG GCC AGC CTG CCT GAG CTG CAG CAC GCC CCT GTG CTG AGC GAC
mRln1 361 TCT GTT GTT AGC TTG GAA GGC TTT AAG AAA ACT CTC CAT GAT AAA CTG GGT GAA GCA GAA 420
121 S V V S L E G F K K T L H D R L G E A E 140
CO mRln1 AGC GTG GTG AGC CTG GAG GGC TTC AAG AAG ACC CTG CAC GAC AAG CTG GGC GAG GCC GAG

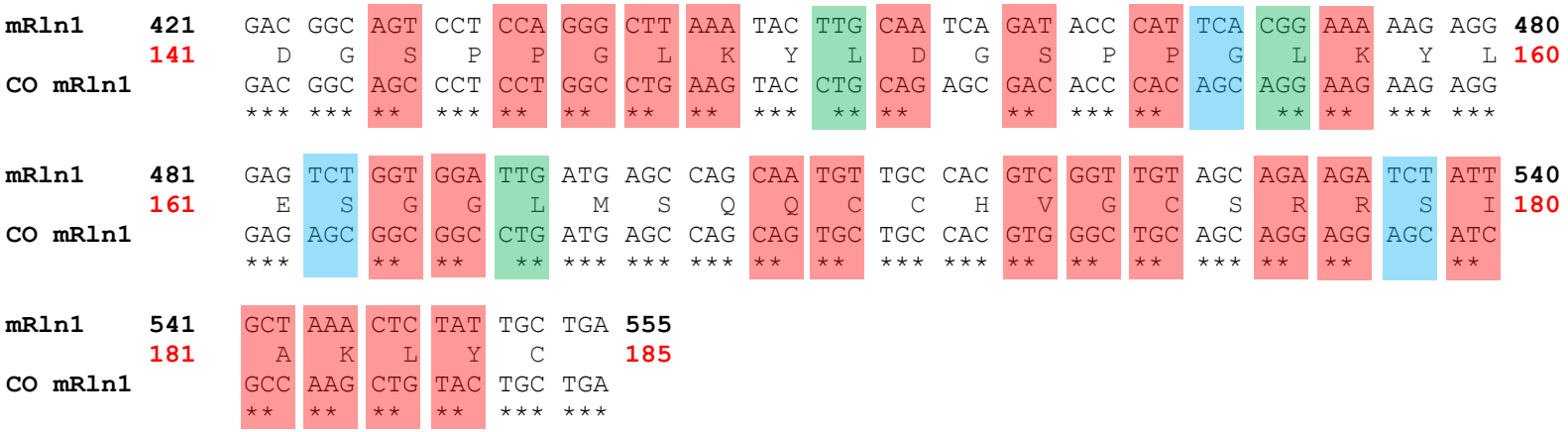

Codon details	Colour	Percentage (aa/full length aa)
Nucleotide one and two are identical	Red	45.4% (84aa/185 aa)
Nucleotide two and three are identical	Green	6.48% (12aa/185aa)
No nucleotides are identical	Blue	3.78% (7aa/185aa)
Only nucleotide one is identical	Yellow	0.005% (1aa/185aa)
Only nucleotide two is identical	Purple	0.01% (2aa/185aa)
Only nucleotide three is identical	Orange	0.01% (3aa/185aa)
Nucleotides remain unchanged	No Highlight	39.45% (73aa/185aa)

Figure 3.10 Comparison between codon optimise and native mouse relaxin 1. The native mouse relaxin 1 (**mRln1**) nucleotide sequence are obtained from NCBI (NCBI, NM011272.2). The mRln1 amino acids sequence was obtained from Uniprot (Uniport, P49732) and the amino acids sequence was used to generated codon optimise mRln1 (**CO mRln1**) sequence with online VectorBuilder codon optimization software. The comparison between CO mRln1 and mRln1 was performed with NCBI blastn. Amino acid (aa)

	native mRln1	VB CO mRln1
CAI	0.71	1.0
GC content	51.76%	66.03%
CFD	4%	0%
Negative CIS element	0	0
Negative repeat elements	0	0

Table 3.1 Rare codon analysis comparison between codon optimised mouse relaxin 1 and native mouse relaxin 1. The rare codon analysis was performed through GenScript online rare codon analysis to compare between the native mouse relaxin 1 (**native mRln1**) and codon optimised mouse relaxin 1 (**CO mRln1**) generate from VectorBuilder (**VB**). The native mRln1 amino acid sequence was used to generate CO mRln1 through the VectorBuilder online codon optimization (**VB CO mRln1**). The codon optimization prediction analysis on Codon Adaptation Index (**CAI**) and GC content, Codon Frequency Distribution (**CFD**).

3.2.3 Optimising transgene expression efficiency in C2C12 and MH cells with a GFP reporter system

The mouse myogenic (C2C12) and mouse myogenic fibroblasts (MH) cell line was transiently transfected with the GFP reporter plasmid (pCi-eGFP). The GFP fluorescence intensity was measured by flow cytometry analysis (**Figure 3.11**) and fluorescence microscopy imaging for C2C12 (**Figure 3.12**) and MH (**Figure 3.13**). Three different types of chemical transfection reagents with various ratios were investigated: Liposomal based (Lipofectamine P3000, Invitrogen), Polyethylenimine (PEI) and non-liposomal polymer (Viafect, Promega). Transfected cell viability was assessed 48 hours post-transfection with flow cytometry analysis, at which MH viability is around 65% to 80% and C2C12 viability around 90%. It is vital to investigate how the presence of transfection reagent and plasmid DNA can be used without affecting the cell viability to maximise transfection efficiency and minimise cell viability before proceed to transfection experiment.

The transfection efficiency was measured and the eGFP fluorescence in the cells (C2C12 and MH) are analysed by fluorescence microscopy and flow cytometry. Our investigation focused on comparing three different types of transfection reagents (Lipofectamine p3000, PEI and Viafect) and was performed to determine the optimum ratio of the transfection reagent (µl):one ratio plasmid DNA (1000ng) which gave the best transfection. The eGFP fluorescence

intensity detected with flow cytometry in C2C12 and MH cell were represent as mean±standard error of mean (**Figure 3.11**). In C2C12, Viafect have the highest percentage of eGFP fluorescence in live cell where the ratio 3:1 (86.63 ± 4.45 %), 4:1 (78.30 ± 10.00 %) and 5:1 (86.93 ± 5.30 %). While the Lipofectamine p3000 with a ratio 0.8:1 (41.63 ± 6.73 %), 1.2:1 (53.80 ± 3.06 %) and 1.6:1 (61.73 ± 4.61 %). The PEI with a ratio 2:1 (12.37 ± 0.75 %), 3:1 (18.80 ± 1.76 %) and 4:1 (26.20 ± 0.53 %). The percentage of eGFP fluorescence in positive live control samples untreated samples mock (1.48 ± 0.43 %), presense of plasmid only (1.56 ± 0.34 %), presence of Lipofectamine P3000 (1.91 ± 0.24 %), presence of PEI (15.6 ± 1.57 %) and Viafect (1.957 ± 0.07 %). Most of the control have very low percentage of eGFP fluorescence except PEI. The eGFP fluorescence imaging in C2C12 cell was capture by fluorescence microscope (**Figure 3.12**). The cell viability of C2C12 cells with plasmid transfection of three different types of transfection reagents: Viafect (~80%), PEI (~80%) and Lipofectamine p3000 (~70%) were examined. Meanwhile, the presence of transfection reagents only is considered with similar cell viability compared to plasmid transfection which suggests that plasmid transfection does not cause harm to C2C12 cell viability.

In MH cell, Viafect have highest percentage of eGFP fluorescence in live cell where with a ratio 3:1 (35.23 ± 1.86 %), 4:1 (50.2 ± 2.81 %) and 5:1 (46.37 ± 1.56 %). While the Lipofectamine p3000 with a ratio 2:1 (19.70 ± 0.30 %), 3:1 (19.93 ± 0.83 %) and 4:1 (21.57 ± 1.33 %). The PEI with a ratio 2:1 (0.15 ± 0.03 %), 3:1 (1.94 ± 0.18 %) and 4:1 (2.32 ± 2.29%). The percentage of eGFP fluorescence in positive live control samples untreated samples mock (0.12 ± 0.03 %), presense of plasmid only (0.07 ± 0.39 %), presence of Lipofectamine P3000 (0.41 ± 0.13 %), presence of PEI (0.05 ± 0.46 %) and Viafect (0.16 ± 0.05 %). Most of the control have near to 0% of eGFP fluorescence. The eGFP fluorescence imaging in MH cell was capture by fluorescence microscope (**Figure 3.13**). The cell viability of MH cells with plasmid transfection of three different types of transfection reagents is ~90%, which is similar with transfection reagent only.

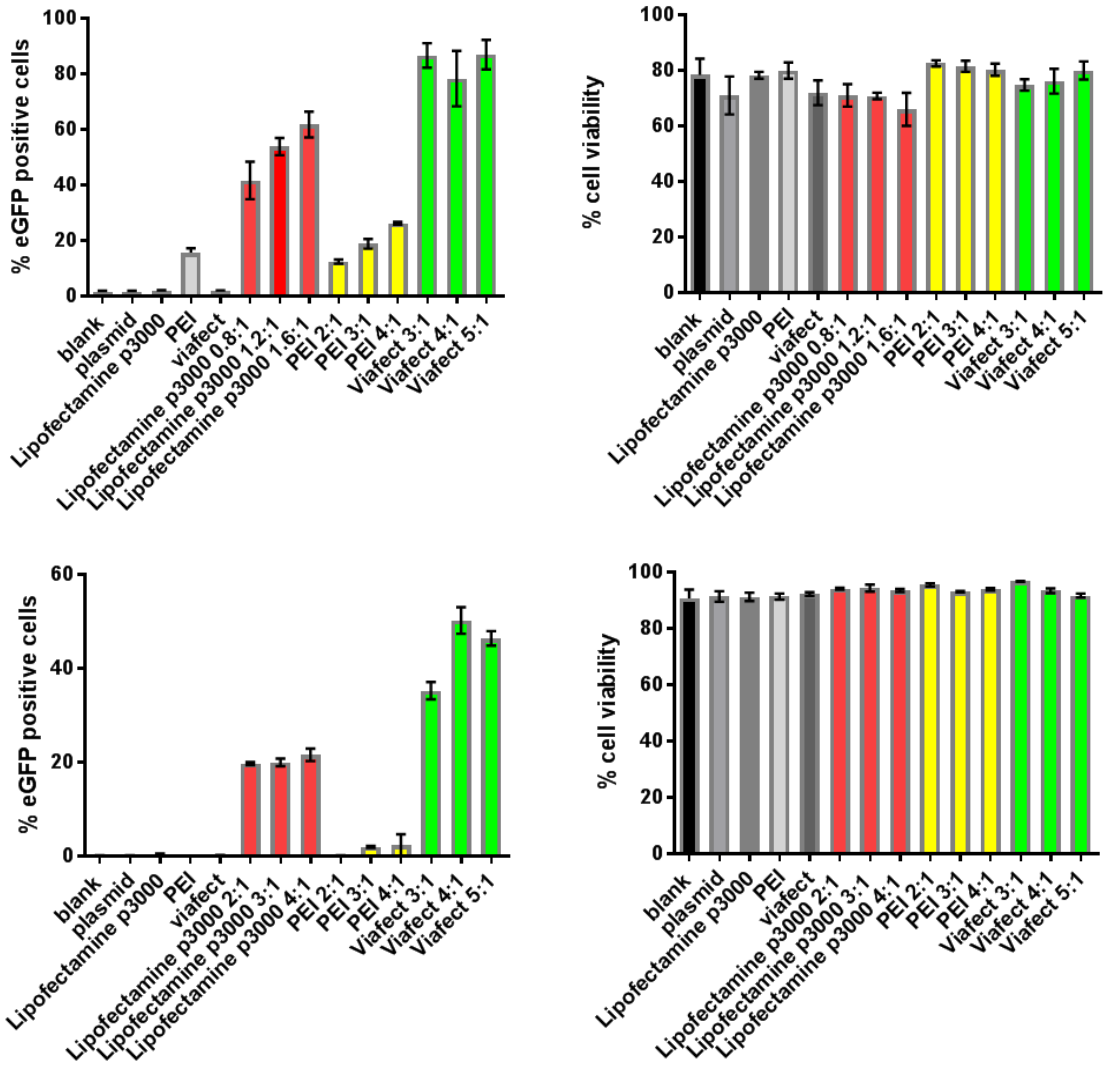

Figure 3.11 Comparative transfection efficiency with various transfection reagents (Lipofectamine p3000, PEI and Viafect) in C2C12 and MH cells. The C2C12 cell (top) and MH cell (bottom) cells was transfection with plasmid pCi-GFP via transfection reagents for 48 hours. The flow cytometry analysis of transfection efficiency expressed as percentage of green fluorescent protein in positive live (Left) and cell viability (Right). The ratio of transfection reagent to plasmid used for transfection as indicate Lipofectamine p3000 (0.8:1, 1.2:1 & 1.6:1), PEI (2:1, 3:1 & 4:1) and Viafect (3:1, 4:1 & 5:1) with one unit plasmid DNA in C2C12 cells, while Lipofectamine p3000 (2:1, 3:1 & 4:1), PEI (2:1, 3:1 & 4:1) and Viafect (3:1, 4:1 & 5:1) with one unit plasmid DNA in MH cells. Graph show the mean ± standard error of mean, 3 technical repeats. Results will be analysed by using FlowJo V10 software and result were plotted by using Graph Pad Prism 7.

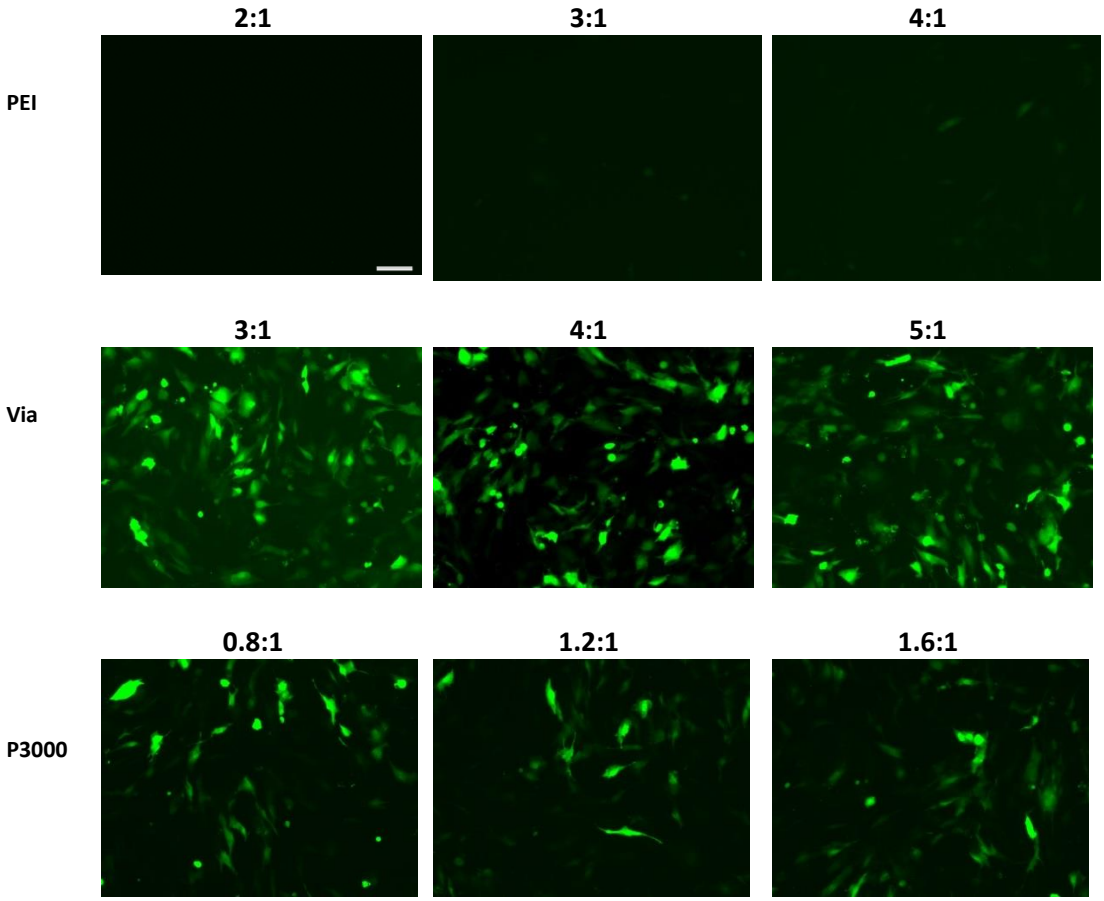

Figure 3.12 Fluorescence microscopy images with various transfection reagents in C2C12 cell. The pCi-eGFP plasmid (1000ng/well of 6-well plate) was transfected into mouse muscle-derived fibroblasts (MH) cell with standard transfection protocol by using three different transfection reagents: PEI (**PEI**, upper panel) PEI:pDNA (µl/ng) at a ratio of 2:1, 3:1 and 4:1, Viafect (**Via,** middle panel) Viafect:pDNA (µl/ng) at a ratio of 3:1, 4:1 and 5:1 and Lipofectamine p3000 (**P3000**, lower panel) lipofectamine p3000:pDNA at a ratio of 0.8:1, 1.2:1 and 1.6:1 respectively. The cells were visualized by Zeiss Axio Observer D1 fluorescence microscope 48 hours after transfection. Scale bars 100µm

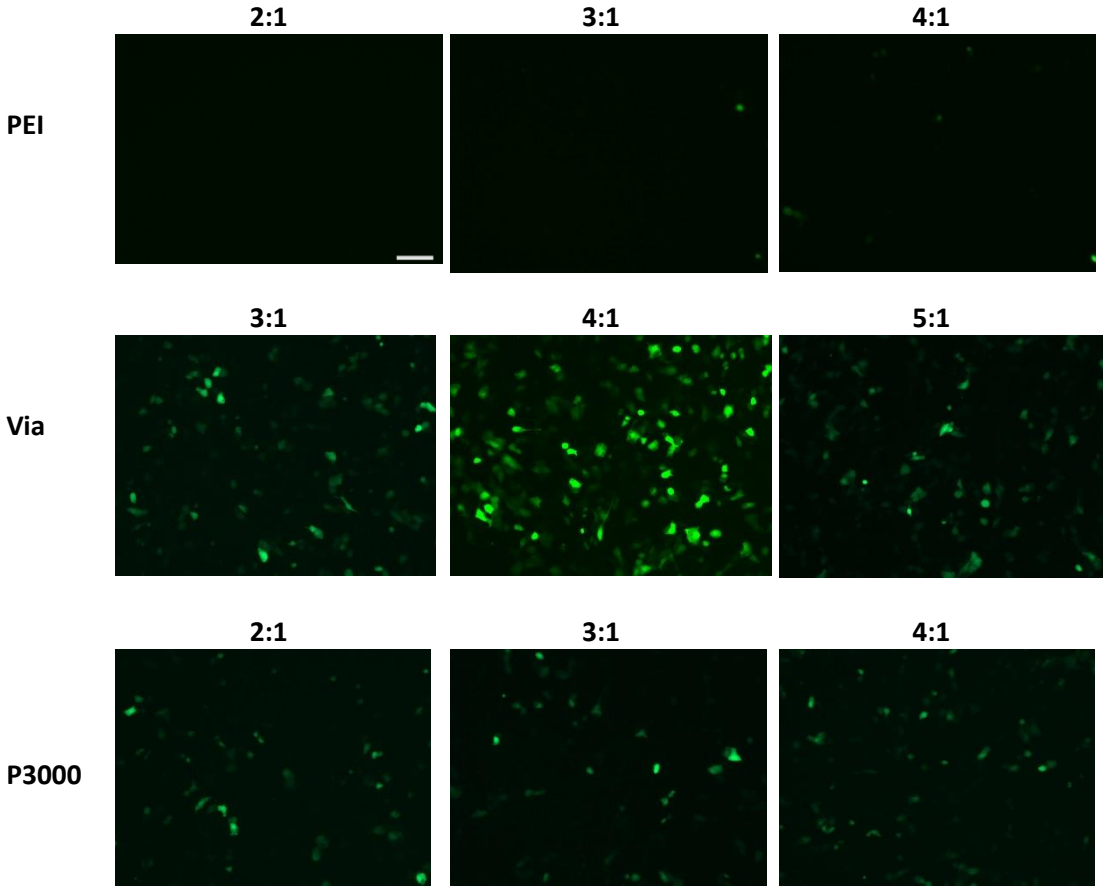

Figure 3.13 Fluorescence microscopy images with various transfection reagents in MH cell. The pCi-eGFP plasmid (1000ng/well of 6-well plate) was transfected into mouse muscle-derived fibroblasts (MH) cell with standard transfection protocol by using three different tranfection reagents: PEI (**PEI**, upper panel) PEI:pDNA (µl/ng) at a ratio of 2:1, 3:1 and 4:1, Viafect (**Via**, middle panel) Viafect:pDNA (µl/ng) at a ratio of 3:1, 4:1 and 5:1 and Lipofectamine p3000 (**P3000**, lower panel) lipofectamine p3000:pDNA at a ratio of 2:1, 3:1 and 4:1 respectively. The cells were visualized by Zeiss Axio Observer D1 fluorescence microscope 48 hours after transfection. Scale bars 100µm.

3.2.4 Bioinformatics analysis of mouse relaxin 1 and human relaxin 2

A comparison was done between the mouse relaxin 1 (mRln1) amino acids sequence (Uniprot, P47932) and human relaxin 2 (hRln2) amino acids sequence (Uniprot, P04090) was obtained through Uniprot. We are particular interest to mouse relaxin 1 isoform as the protein sequence is a homologous protein to human relaxin 2 isoform. Our result indicate that the full-length (pre-pro relaxin) with 185 amino acids have 48.09% similarity in the amino acid sequence between mRln1 and hRln2, while the mature relaxin comparison between mRln1 and hRln2 for B-chain is 44.83% and A-chain is 37.5% respectively (**Figure 3.14**). We further compared the B-C-A protein structure between mRln1 and hRln2 (**Figure 3.15**), where both of the protein have similar structure of relaxin B chain (B), connecting peptide (C) and relaxin A chain (A) to form a B-C-A protein structure. The only different is the present prohormone convertase 2 targeting site in hRln2 but not mRln1.

Full length relaxin (pre-pro-relaxin)

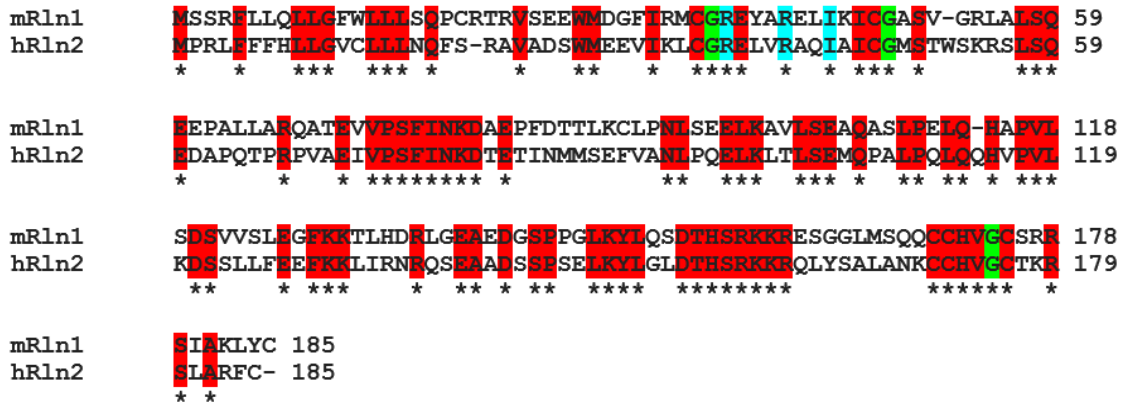

Relaxin B-chain

Relaxin A chain

Details	Similarity
Full-length mRln1 versus full-length hRln2	48.09%
mRln1 B-chain versus hRln2 B-chain	44.83%
mRln1 A-chain versus hRln2 A-chain	37.5%

Figure 3.14 Comparison amino acid sequence between mRln1 and hRln2. The full-length amino acid sequence mouse relaxin 1 (**mRln1**) (Uniprot, P47932) and human relaxin 2 (**hRln2**) (Uniprot, P04090) was obtained through Uniprot and amino acid sequence align was performed through online bioinformatics software Clustal Omega (EMBL). The conserved residues involve relaxin binding to relaxin receptor are R, R and I in B-chain (Blue highlight), glycine residues that is vital for relaxin secondary structure (Green highlight) and the same group of amino acid between mRln1 and hRln2 (Red highlight and star). The amino acids similarity comparison between amino acids sequence of full-length mRln1 versus full length hRln2, mRln1 B-chain versus hRln2 B-chain and mRln1 A-chain versus hRln2 A-chain are shown in table.

A

```
          10         20         30         40         50
MSSRFLLQLL GFWLLLSQPC RTRVSEEWMD GFIRMCGREY ARELIKICGA
          60         70         80         90         100
SVGRLALSQE EPALLARQAT EVVPSFINKD AEPFDTTLKC LPNLSEELKA
          110        120        130        140        150
VLSEAQASLP ELQHAPVLSD SVVSLEGFKK TLHDRLGEAE DGSPPGLKYL
          160        170        180
QSDTHSRKKR ESGGLMSQQC CHVGCSRRSI AKLYC
```

B

```
          10         20         30         40         50
MPRLFFFHLL GVCLLLNQFS RAVADSWMEE VIKLCGRELV RAQIAICGMS
          60         70         80         90         100
TWSKRSLSQE DAPQTPRPVA EIVPSFINKD TETINMMSEF VANLPQELKL
          110        120        130        140        150
TLSEMQPALP QLQQHVPVLK DSSLLFEEFK KLIRNRQSEA ADSSPSELKY
          160        170        180
LGLDTHSRKK RQLYSALANK CCHVGCTKRS LARFC
```

	Signal peptide	B-chain	C-chain	A-chain	Disulfide bond between interchain	Disulfide bond between intrachain
mRln1	1-22	23-57	58-156	161-185	36-171 and 48-185	170-175
hRln2	1-24	25-53	56-157	162-185	35-172 and 47-185	171-176

Figure 3.15 Comparison protein structure between mRln 1 and hRln2. The amino acids sequence of mouse relaxin 1 (**mRln1**) (Uniprot, P47932) (**A.**) and human relaxin 2 (**hRln2**) (Uniprot, P04090) (**B**.) are obtained through Uniprot, both protein are makeup of 185 amino acids. The detailed structure of Relaxin and the length of the amino acid chains are recorded in the table. The relaxin protein structure consists of relaxin B-chain (B), connecting peptide (C) and relaxin A-chain (A) shown as B-C-A protein structure. The pre-pro mRln1 and pre-pro hRln2 details was illustrated where signal peptide (without highlight), followed by B-chain (Yellow highlight), pro-peptide (Purple highlight) and A-chain (Blue highlight). The mature relaxin was consist of B-chain and A-chain connecting with 3 disulfide bond: two form interchain between B-chain and A-chain (Green and Red highlight) and one intrachain form between A-chain (Purple highlight). The prohormone convertase targeting by furin (ubiquitous prohormone convertase) targeting site RKKR (Grey highlight) on both relaxin, while prohormone convertase 2 targeting site KR (Dark green highlight). The details position of the amino acids present with both mRln1 and hRln2 is shown in table.

3.3 DISCUSSION

3.3.1 Plasmid construct design and characterisation

In this chapter we describe the design full length design of mouse relaxin 1 cDNAs in conventional or AAV–based plasmid vectors. All of the plasmids have been characterised and all functional elements are present within the plasmids. All plasmids have been analysed through various restriction digests. Restriction enzymes were used that focus on crucial elements such as promoter, codon optimised/non-codon optimised mouse relaxin 1 and inverted terminal repeat (ITR).

3.3.2 Comparison between codon optimised and native mouse relaxin 1

Codon optimization is a methods with bioinformatics software prediction aim for higher protein expression compare to the native gene nucleotide sequence. The high protein expression is related to the CAI value that is near 1.0, where the ideal CAI >0.8 value for better protein expression in the specific organism (mouse in our project). The Genscript online rare codon analysis suggested the CAI of CO mRln1 (1.0) have increased compared to native mRln1 (0.71). Next, the GC content is increase for CO mRln1 (14.28%) compare to NCO mRln1, where the GC content is ideal within a range of 30% to 70%. The rare codon analysis CFD value indicate the CO mRln1 (0%) are reduced compare to native mRln1 (4%), where the lower percentage indicate the low percentage of rare codons can increase the translation efficiency. Finally, the native mRln1 and CO mRln1 does not have negative Cis-regulatory elements (CIS) elements which negatively regulate gene expression or negative repeat elements (direct or inverted repeats) can affect the gene synthesis or expression. Despite the fact that there are many studies indicating higher protein expression can be achieved with codon optimization, it is not a guarantee and has to be verified through experiment.

3.3.3 Assessment of GFP fluorescence and detection by flow cytometry analysis in mouse myogenic cell line (C2C12) and mouse myogenic fibroblast cell line (MH).

Commercial companies have developed a range of products to allow DNA transfection into specific cell types. Many studies have compared transfection efficiency in different specific type of cell lines to maximise transfection efficiency. One study found that in transfections of C2C2 cells where the GFP plasmid:transfection reagent Fugene HD (a lipid-based transfection reagent) had a ratio 3:10, there was around a 60% to 70% transfection efficiency with 10% of cell death (Balcı *et al*., 2009). Although more nucleic acid can contribute to the transgene expression, conversely the high level of transfection reagent or exogenous nucleic acid may contribute to toxicity and reduce cell viability (Masotti *et al*., 2009). Therefore, it is vital to optimise the transfection conditions to analyse which reagent and with optimum ratio to plasmid shows the highest transfection efficiency.

In this study, we evaluated a range of commercially available non-viral transfection reagents in single layered adherent cell lines (C2C12 and MH) with the pCi-eGFP reporter plasmid. The assessment of GFP fluorescence and cell viability were compared with non-transfected control cell line. Three different types of transfection reagents were used: Lipofectamine P3000 (cationic liposome), PEI (cationic polymer) and Viafect (cationic lipid mixture with neutral lipid L-dioleoyl phosphatidylethanolamine). We focused on the parameters of the ratio of transfection reagents to the same amount of plasmid DNA. The GFP fluorescence intensity was detected 48 post-transfection through flow cytometry.

We show that the Viafect/plasmid DNA ratio of 3:1 and 5:1 lead to a high transfection efficiency with ~90% GFP positive C2C12 cells and ~ 50% MH cells that were transfected with a Viafect/plasmid DNA ratio of 4:1 were GFP positive. In both types of cells, no signs of increasing toxicity were observed in the conditions that caused the highest transfection efficiency. It must be addressed that in C2C12, the ratio of the transfection reagent Lipofectamine P3000 to plasmid DNA (0.8:1, 1.2:1 or 1.6:1) used in the investigation differed from the recommendations

of the manufacturers, (2:1, 3:1 or 4:1). It is therefore possible that the use of the recommended plasmid DNA ratios might have increased the transfection efficiency. However, in the ratio of 1.6:1 a slight reduction in cell viability was observed and further increasing the ratio might have negative toxic effects. The highest transfection efficiencies were obtained with the Viafect transfection reagent. The Viafect transfection reagent in MH cells showed a 2 to 2.5 fold higher efficiency compared to Lipofectamine P3000. From the three transfection reagents tested PEI showed at the highest ratio (4:1) the lowest transfection efficiency, only ~25 % of the C2C12 cells and ~5% of the MH cells were GFP positive. For these reasons, it was decided to use the transfection reagent Viafect for all further experiments.

Transfection efficiency can be affected by various factors such as cell types, cell density during transfection, cell toxicity and amount of nucleic acid. Cell density can affect transfection as when cell density is too high it can inhibit cell growth, in contrast too low of a cell density led to a low transfection efficiency. We carried out our transfection when the cell density was around 90% confluent, because a 90-95% cell confluency is normally associated with high transfection efficiency (Dably *et al*., 2004). One question that remained was whether cells present in the culture dishes are not the same confluence when the experiment was carried out. Another transfection method nucleofection also enable nucleic acids to be transferred into cells by using voltage and reagents should also be consider in the transfection efficiency investigation with GFP plasmid. One study of nucleofection by LONZA found that their protocol can achieve ~80% transfection efficiency and ~70% cell viability (LONZA, 2013), which both are lower compared to our results with transfection reagent Viafect.

The optimization transfection efficiency investigation is a valid method to examine with much more appropriate GFP plasmids. This is because the GFP plasmids that we are using is driven by CMV promoter which is not the same as the promoter (Spc512 and CBh) in our designed mRln1 expressing plasmid. We suggested the GFP should be driven by Spc512 or pTet On-eGFP for much closer transfection efficiency evaluation to plasmid express mRln1.

Our *in vitro* investigation with mRln1 expressing plasmid might offer certain degree of similarity compared to AAV viral vector expressing mRln1, as either the plasmid or AAV viral vector offer delivery method of mouse relaxin 1 into mammalian cell. Therefore, it is important to investigate on how the mRln1 plasmid express and translate in *in vitro* as a proof to express mRln1 protein and secreted before going to next stage *in vivo* investigation with AAV viral vector.

3.2.4 Bioinformatics analysis of mouse relaxin 1 and human relaxin 2 analysis

Both of the relaxin protein mRln1 are equivalent to hRln2 only consist of 48.09% similar in the amino acids sequence. In **Figure 3.14**, have shown that the conserved amino acids sequence R, R, I are present in both mRln1 and hRln2 which bind to relaxin family peptide receptor 1 (RXFP1) (Bathgate *et al*., 2003). The relaxin protein has glycine residues within B-chain and A-chain play a role in secondary structure. Despite the fact that both mouse relaxin 1 and human relaxin 2 have similar protein structure consist of 185 amino acids, hRln2 have a prohormone convertase targeting site KR by prohormone convertase 2 but not present in mRln1. There are no information on which category types of prohormone convertase are targeting at specific cleavage targeting amino acid sequence (LS) in mRln1 (**Figure 3.15A**). Our next interest would be investigate the effect of mouse relaxin 1 on fibrosis.

Chapter 4: ANALYSIS *mRln1* TRANSCRIPT LEVEL AND PROTEIN EXPRESSION *in vitro*

CHAPTER 4 ANALYSIS *mRln1* TRANSCRIPT LEVEL AND PROTEIN EXPRESSION *in vitro*

4.1 Introduction

Measuring gene expression plays an important role in biological sciences research. This can be achieved in two ways: either by quantifying how much mRNA is transcribed, by determining the level of expressed protein or both. In gene augmentation therapy, high translation efficiency allows reduction the amount of viral vectors needed to achieve the same level of transgene expression and minimizes the immunotoxicity to the host (Anguela and High, 2019). In this chapter, we investigate the transfected mouse muscle-derived fibroblast cell line (MH) or mouse myogenic cell line (C2C12) with either conventional based plasmid (p) or adeno associated viral vector (AAV) based plasmid where single-stranded AAV (pssAAV) or self-complementary AAV (pscAAV) with either muscle tissue-specific promoter (Spc512) or improved version of CMV promoter (CBh) with tetracycline inducible transcriptional activation system (Tet On) driven to express codon optimised mouse relaxin 1 (CO mRln1) or native mouse relaxin 1 (NCO mRln1). Here are the lists of plasmids: pssAAV-Spc512-CO mRln1, pssAAV-Spc512-NCO mRln1, pscAAV-Spc512-CO mRln1, pscAAV-Spc512-NCO mRln1, pTet On-CO mRln1, pTet On-NCO mRln1, pssAAV-Tet On-CO mRln1 and pssAAV-Tet On-NCO mRln1 that we are going to used investigate how these plasmid effect on mRln1 transcript level and protein expression with different plasmid constructs expressing mouse relaxin 1 in C2C12 and MH cell.

In different organisms, there are variations between the codons that code for the same amino acids (Athey *et al*., 2017). The replacement of rare codons to higher frequency codon to code for the same amino acid also known as codon usage bias may contribute improvement to the translation efficiency of a protein – this process is codon optimization. The codon usage bias contribute to favourable translational selection to the relative tRNA abundances and aim to increase the translation efficiency and accuracy (Plotkin and Kudla, 2011). In contrast, some study have shown there are no or weak effect of codon bias to the gene expression (Kudla *et al*., 2009). In this project, we designed the plasmid with codon optimised version of mRln1 (CO

mRln1) or native mRln1 (NCO mRln1) version and compared the efficiency of expression of both construct via mRNA and protein level.

Since the development of Polymerase chain reaction (PCR) in 1983, it has been a common molecular biology technique used to amplify specific DNA segment through a set of oligonucleotide primer match 5' and 3' end (Mullis *et al*., 1986). Reverse transcription Polymerase Chain Reaction (RT-PCR) is a variation PCR method that combines reverse transcription of cellular mRNA into complement DNA (cDNA) and subsequent PCR amplification (Lodish *et* al., 2007). RT-PCR is widely applied to investigate the level of specific amount of mRNA. The combination of quantitative PCR (qPCR) with RT-PCR known as RT-qPCR allow monitoring of transcription of cDNA construct with mRNA. In qPCR, the visualizing of PCR amplification process utilizes DNA binding dyes (such as Sybr green or Taqman) that bind to double stranded DNA emit fluorescence. The two steps RT-qPCR involve two steps where the reverse transcription was used on the first part experiment involving construction of cDNA followed by the second part experiment with PCR separately (Wong and Medrano, 2005). The RT-qPCR analysis was done based on quantitation cycle (Cq) value. The Cq values are inverse to the amount of DNA copy present in the samples, as the lower Cq number contain more amount of copy of DNA is present in the samples. In this chapter, we exploited two step RT-qPCR to assess the level of m*Rln1* expression in C2C12 and MH cells transfected with mRln1 expression plasmids.

The mRln1 protein can be detected with mRln1 targeting antibody within the cells (prepro- or propeptide form) or as secreted hormone (mature form) in medium of cultured cells *in vitro* or in the plasma of *in vivo* models. The secreted hormone contains a signal peptide sequence located at the N-terminus of the pre-pro peptide, which facilitates secretion. In parallel, incorporation of the epitope tag together with mRln1 could facilitate detection. Epitope tagging involves synthesizing the recombinant protein with an epitope tag to facilitate protein isolation, purification, tracking and detection. The epitope tag is engineered on either the C- or N-terminus of recombinant proteins normally without affecting the bioactivity of the protein

(Brizzard., 2008). Human influenza A hemagglutinin (HA) tag is one of the common epitope tag reporter systems have been widely used; it consists of HA amino acids sequence 98 – 106 (YPYDVPDYA) from the virus (Schembri *et al*., 2007). We have designed the plasmid with HA tag located on the C-terminus of m*Rln1* before the stop codon and investigated the mRln1 protein with HA tag detection with western blot.

Western blotting is a common technique used to separate and detect specific proteins. This technique involves: i) separation of the protein based on the size through sodium dodecylsulfate-polyacrylamide gel electrophoresis (SDS-PAGE), ii) transfer of all the separated proteins from the gel to a membrane, iii) visualization of the specific protein via primary and secondary antibodies on the membrane (Lodish 2007 p. 98 -99). In this chapter, we particularly focus on the mRln1 protein detection through western blot using antibodies targeting HA tag or mRln1 protein.

In this chapter, we are particularly interested in investigation two objective where the first is to detect the level of *mRln1* expression after the cell transfected with various mRln1 expressing plasmids with PCR. Second, we focus on using the highest *mRln1* expressing plasmids to study on how the mRln1 protein is express after transfection with mRln1 expressing plasmids. We utilize western blot with either human relaxin 2 antibody (react to mouse relaxin 1, mouse relaxin 1 and human relaxin 2) to detect mRln1 or antibody target HA tag to detect mRln1 with HA tag.

4.2 RESULTS

4.2.1 Gradient PCR optimization to analysis of *mRln1* expression

Gradient PCR was set up to look for optimum annealing temperature on two different sets of primers, one targeting codon optimized mRln1 (CO mRln1) and the other non-codon optimized mRln1 (NCO mRln1). The C2C12 cells were transfected with the same amount (1000 ng) plasmid DNA pTet On-CO mRln1 or pTet On-NCO mRln1 plasmid driven by Tet On system (Tet On) with 40 ng/ml tetracycline present for 24 hours prior to total RNA extraction, followed by cDNA construction. The cDNA construct was used as a template for gradient PCR over a range of annealing temperature (54^{o}C to 61^{o}C) with CO mRln1 primer for samples transfected with pTet On-CO mRln1 or NCO primer for samples transfected with pTet On-NCO mRln1. In **Figure 4.1A,** the illustration show the primers targeting CO mRln1 amplicon size are 98 bp or NCO mRln1 amplicon size are 139 bp. The result indicate amplicon (**Figure 4.1B**) size produced with CO mRln1 primer are around 100 bp with the optimal amplification at around 55^{o}C to 56^{o}C, while the amplicon (**Figure 4.1C**) size produce with NCO mRln1 primer are around 139bp with highest amount at around 55^{o}C to 57^{o}C. The gel image indicates that the gradient PCR is efficient and has no non-specific binding to create a secondary off-target PCR product.

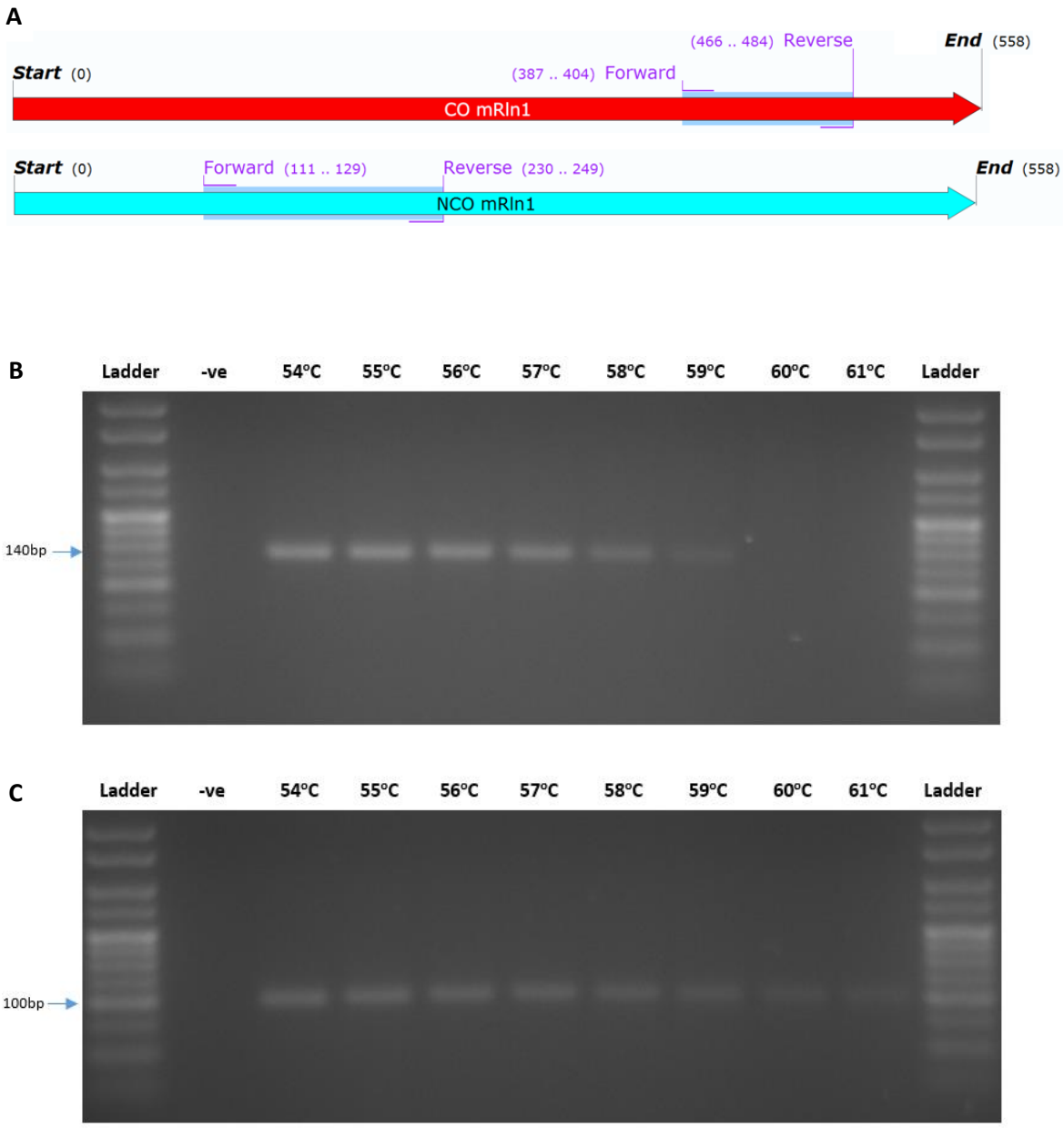

Figure 4.1 Gel Image indicate a gradient PCR. An illustration (**A.**) of the primer set to target CO mRln1 (Red bar) and NCO mRln1 (Blue bar) and the amplicons are highlighted in purple with Forward and Reverse primer. 600 ng of total RNA was extracted from C2C12 cells transfected with either pTet On-CO mRln1 or pTet On-NCO mRln1 plasmid for 24 hours followed by cDNA construction. The constructed cDNA was used as a template for PCR, which 30 PCR cycles was performed with a range of gradient annealing temperature (54°C to 61°C) with either CO mRln1 (**B.**) or NCO mRln1 (**C.**) specific primers. The analysis of the amplicon was performed with separation of products on 3.5% (w/v) agarose TAE gel electrophoresed for 65V for 60 minutes and 70V for 40 minutes. The **Ladder** is a 25bp ladder (500bp to 25bp) and the negative control (**-ve**) was a control without cDNA template.

4.2.2 Detection of *mRln1* transcripts in C2C12 or MH cell line by RT-qPCR analysis

We investigated the expression level of mRln1 mRNA transcripts in C2C12 or MH cells transfected with various plasmids (pssAAV-Spc512-CO mRln1, pssAAV-Spc512-NCO mRln1, pscAAV-Spc512-CO mRln1, pscAAV-Spc512-NCO mRln1, pTet On-CO mRln1, pTet On-NCO mRln1). Subsequently, the total RNA was extracted, cDNA was synthesized and reverse transcription (RT)-quantitative (q) PCRs were performed. The mRNA level of mRln1 was analysed in RNA samples from C2C12 cells transfected with same amount (1000 ng of plasmid DNA) of six different plasmid construct DNA for 24 hours prior to total RNA extraction. The highest mRln1 expression was measured by normalisation with housekeeping gene 60S acidic ribosomal protein (Rplp0) in C2C12 cells transfected with the pTet On-NCO mRln1 plasmid with tetracycline present (**Figure 3.7A**). **Figure 4.2B** shows specific melting curve with CO mRln1 primer, NCO mRln1 primer and Rplp0 primer indicate only one amplicon is produced.

Some of the RT-qPCR amplicon from the same experiment shown in **Figure 4.2** was run on agarose gel electrophoresis for further identification on the amplicon size. The gel image (**Figure 4.3**) indicate the specific band size of amplicon ~100bp with CO mRln1 and ~150bp NCO mRln1 targeting primer. There are certain basal level of *mRln1* is expression in the C2C12 cells. Both of the transfected samples with either CO mRln1 or NCO mRln1 plasmids have shown higher *mRln1* expression compare to the samples without transfection.

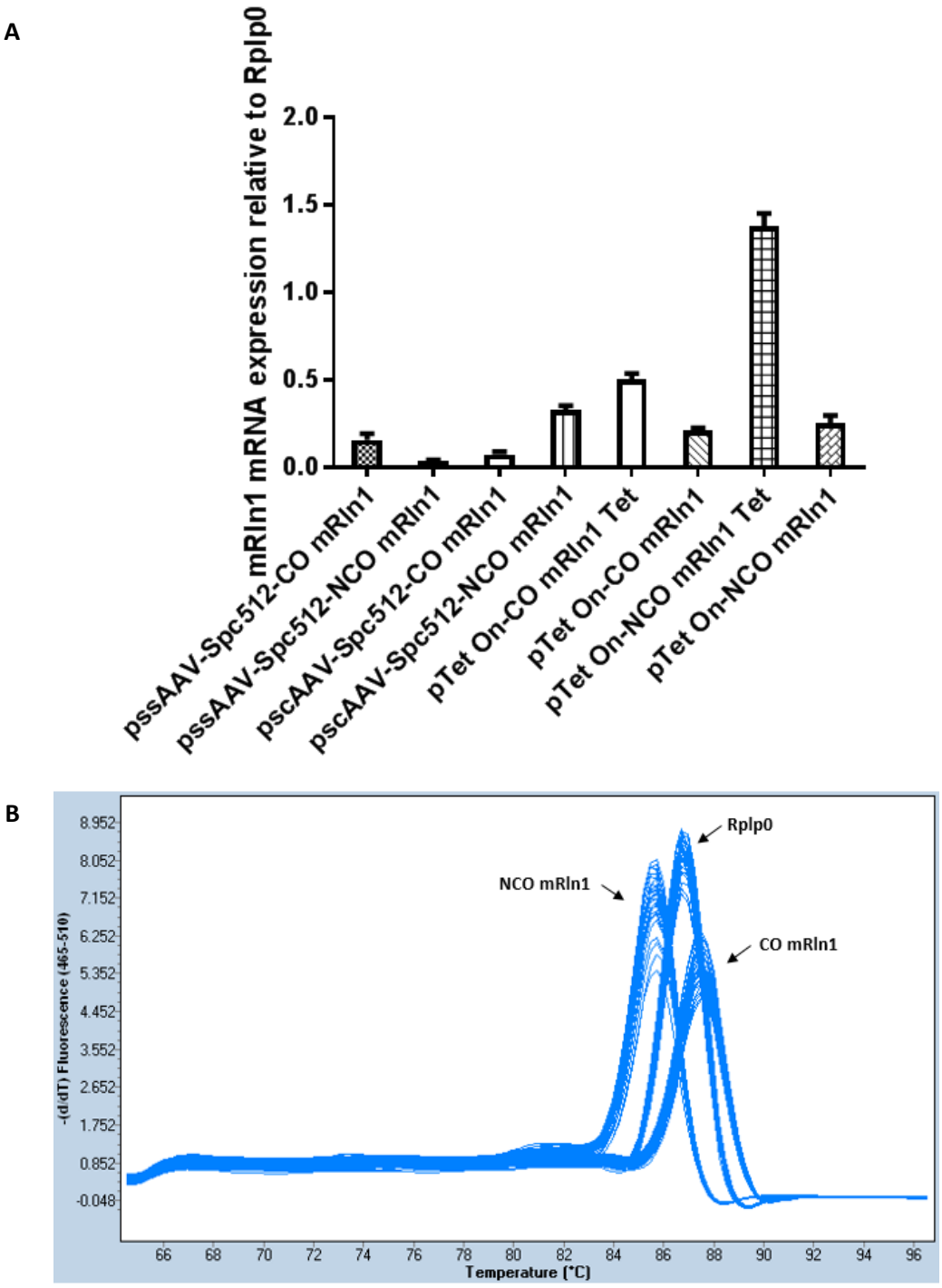

Figure 4.2 Comparison between the m*Rln1* mRNA expressions with different plasmid construct. The C2C12 cells are transfected with CO mRln1 or NCO mRln1 plasmid with tetracycline inducible expression system (Tet on) for 24 hours. The relative quantified mRNA expression of CO mRln1 or NCO mRln1 genes was compared to the level of Rplp0 housekeeping gene shown in (**A.**). The melting curve of RT-qPCR of three different set of primer with specific melting temperature shown in (**B.**).

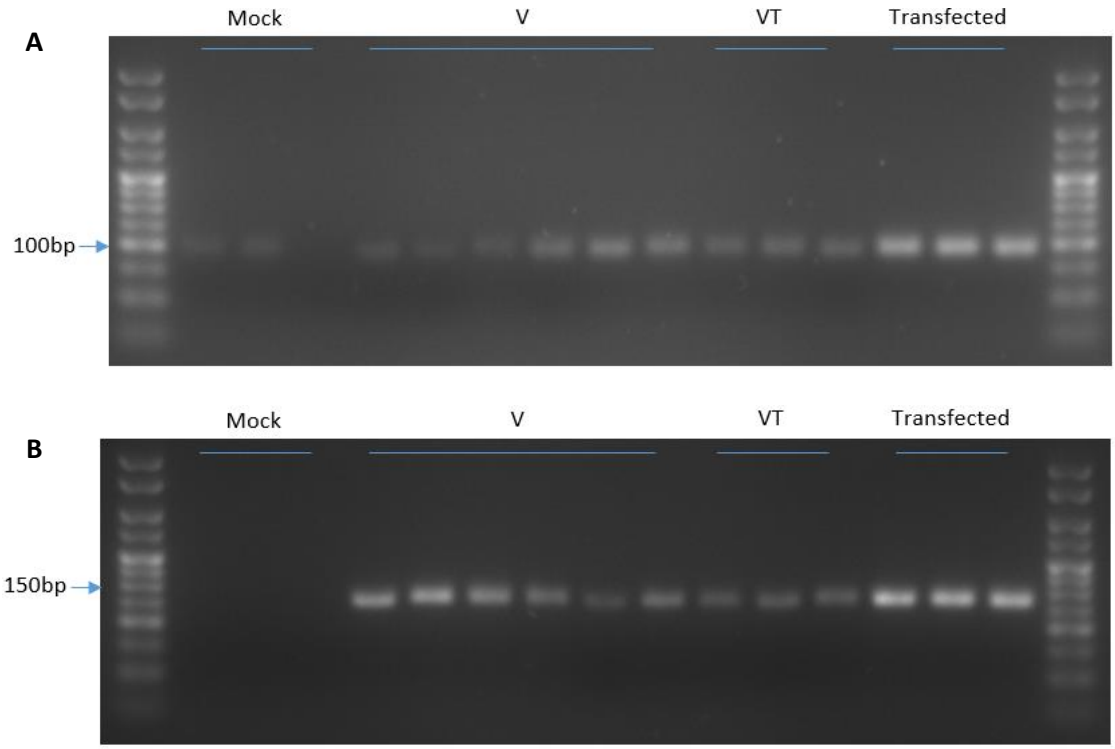

Figure 4.3 Gel Image of RT-qPCR amplicon targeting mRln1. The RT-qPCR amplicon targeting CO mRln1 (**A.**) and NCO mRln1 (**B.**) from **Figure 4.2** were used as a samples to run gel electrophoresis. The analysis of the amplicon was performed with 3.5% (w/v) agarose TAE gel for 65V for 60 minutes and 70V for 40 minutes. The samples that are untransfected (**Mock**), treated with Viafect (**V**), treated with both Viafect and 40ng/ml Tetracycline (**VT**), transfected samples with either CO mRln1 (**A.**) or NCO mRln1 plasmid (**B.**) (**Transfected**) and 25bp ladder (500bp to 25bp).

4.2.3 Optimization of western blot analysis for mRln1 protein detection

The optimization of western blotting is required to obtain optimal results for the analysis. We explored how the SDS-PAGE transferred onto the 2 µm nitrocellulose membrane with different transfer condition, followed by the Ponceau S stain to detect the total protein present on the membrane. This is to make sure all the protein on SDS-PAGE gel have successful transfer onto the membrane before proceeding to next stage. Next, we optimized the blocking conditions with various blocking buffers to reduce the non-specific signal that might interfere with the primary and secondary antibody stain. The 3% BSA 0.1% PBS Triton X100 is the optimal blocking condition buffer, as this condition can block most of the non-specific binding.

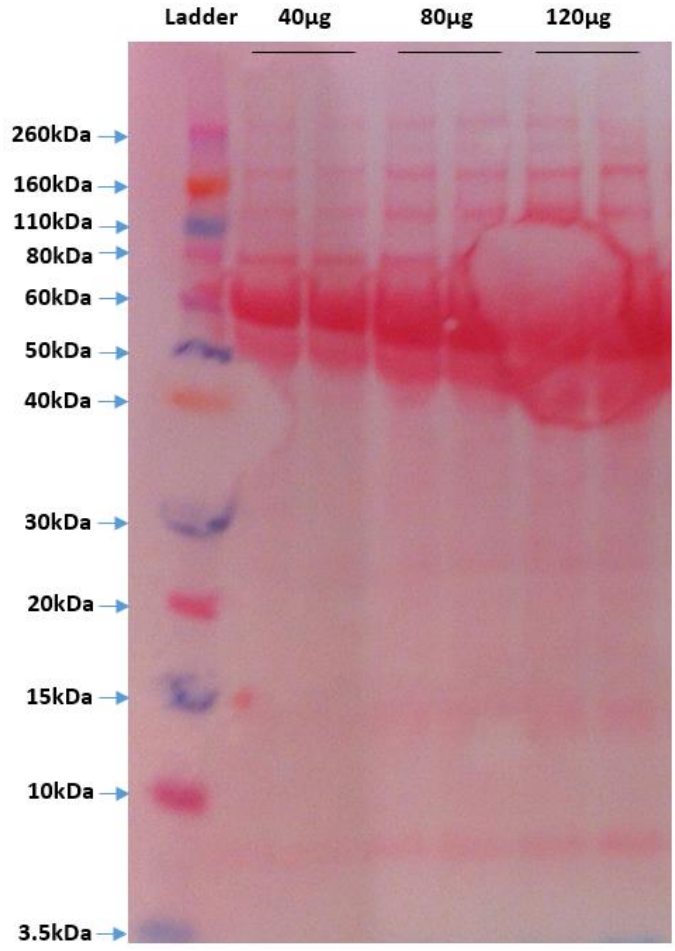

Figure 4.4 Ponceau S staining for transferring optimization. A Ponceau S stain 0.1% (w/v) in 5% acetic acid was apply to investigate on the protein after transferring onto 2µm nitrocellulose membrane. The staining of membrane was performed for 1 to 2 minutes followed by four round of destaining was with water until the background is clear. The protein samples were collected from supernatant of C2C12 cell line through methanol chloroform protein precipitation. A range of protein with different amount protein (40µg, 80µg and 120µg) together with the Novex Sharp Pre-stained 3.5kDa – 260kDa protein standard (Thermofisher) was run on 10% Bis-Tris gel onto 2µm nitrocellulose membrane.

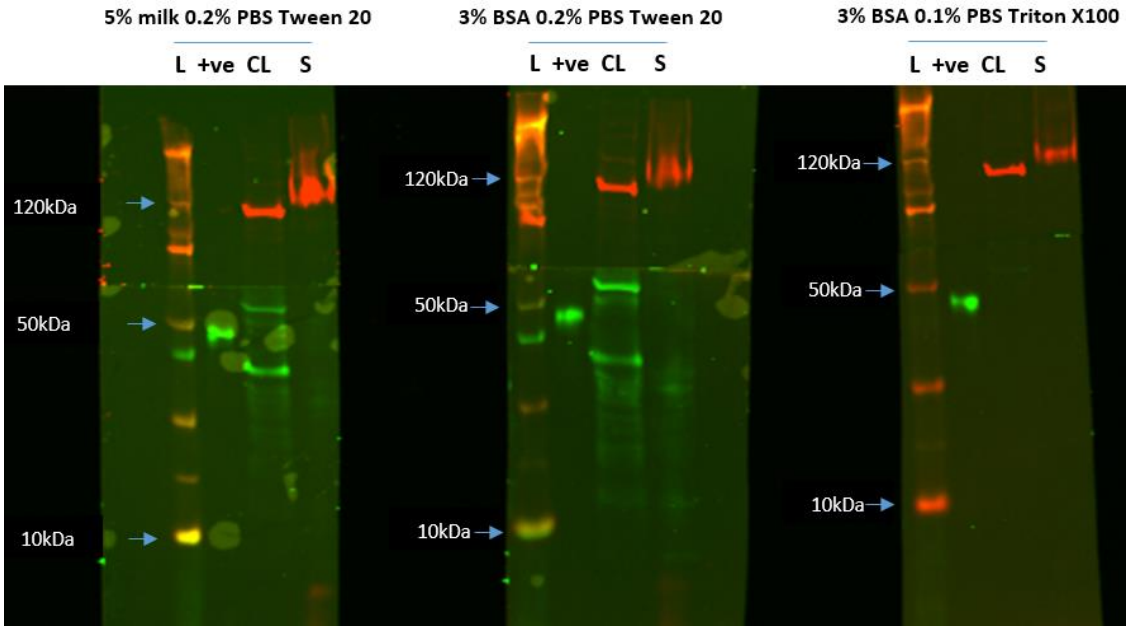

Figure 4.5 Western blot blocking buffer optimization. The protein samples was collected from C2C12 cells transfected with pTet On-NCO mRln1 plasmid with tetracycline present for 24 hours through methanol chloroform protein precipitation. The protein samples are run on 10% Bis-Tris gel and transferred to 0.2 µM nitrocellulose membrane: Novex Sharp Pre-stained 3.5kDa – 260kDa protein standard (Thermofisher, LC5800)(**L**), 0.5µl E.coli cell lysate (Abcam ab5395) with recombinant protein express HA tag (**+ve**), 50µg cell lysate samples (**CL**) and 50µg protein precipitation samples from culture media (**S**) were loaded onto each well. The membrane was cut into half on the size of 60kDa protein ladder. The blot was probed separately with primary antibody mouse anti-HA tag (1:1000) on the <60kDa membrane detected with secondary antibody IRDye® 800CW Goat anti-mouse IgG (LI-COR P/N 925-32210) shown in green and mouse anti-vinculin (1:10000) on the >60kDa membrane followed by detection with secondary antibody IRDye 680RD Goat anti-Mouse IgG (LI-COR P/N 925-68070) shown in red.

4.2.4 Sustained mRln1 transgene expression studies: Comparison the levels of mRln1 protein expression with transfected pTet On-NCO mRln1 cultures of C2C12 and MH cell line

To investigate whether the expressed mRNA of the mRln1 plasmids is translated into a functional protein that is secreted into the culture medium of C2C12 and MH cells we measured the level of mRln1 protein in the culture medium of transfected cells by western blot. For this study, we directly compared protein expression from codon optimised mRln1 (CO mRln1) or non-codon optimised mRln1 (NCO mRln1) constructs relative to the mock (cell without any treatment).

The western blot analysis (**Figure 4.6**) was to detect mRln1 protein in C2C12 cells transfected with either plasmids pssAAV-Tet On-CO mRln1/HA or pssAAV-Tet On-NCO mRln1/HA for 24 hours with the presence of tetracycline. The result suggest that the HA tag antibodies were able to detect the positive control *E.coli* whole cell lysate with recombinant protein with HA tag (~49kDa) but not mRln1 with HA tag. We then try to use human relaxin 2 targeting antibody to detect mRln1 with transfected with either plasmids pTet On-CO mRln1 or pTet On-NCO mRln1 in C2C12 and MH cells for 24 hours with western blot. The result in **Figure 4.7** shown that mRln1 antibody was able to detect mRln1 in both types of cells suggest the prepro-mRln1 (~21kDa) was detected in the cell lysate protein samples. The protein quantification analysis indicate the pTet On-NCO mRln1 was able to upregulate the protein expression of mRln1 to approximately 1.2 folds compared to the mock in both C2C12 and MH cells. However, the mature mRln1 was not detected in the supernatant of the C2C12 cells and the pTet On-CO mRln1 reduced the mRln1 expression in both types of the cells.

Another western blot investigation was focus on the detection mRln1 in C2C12 and MH cells with human relaxin 2 targeting antibody. The cells were transfected with the either plasmids pTet On-CO mRln1 or pTet On-NCO mRln1 for 24 hours. In **Figure 4.8**, indicates all the protein samples from cell lysate in both types of the cells can detect for the present prepro-mRln1. Western blot quantification of mRln1 shown that the cells transfected with pTet On-NCO

mRln1 in C2C12 was able to increase the mRln1 protein expression to approximately 1.5 folds compare to the mock. In contrast, the mRln1 was not able to increase the mRln1 protein expression in MH cells with either of the plasmids.

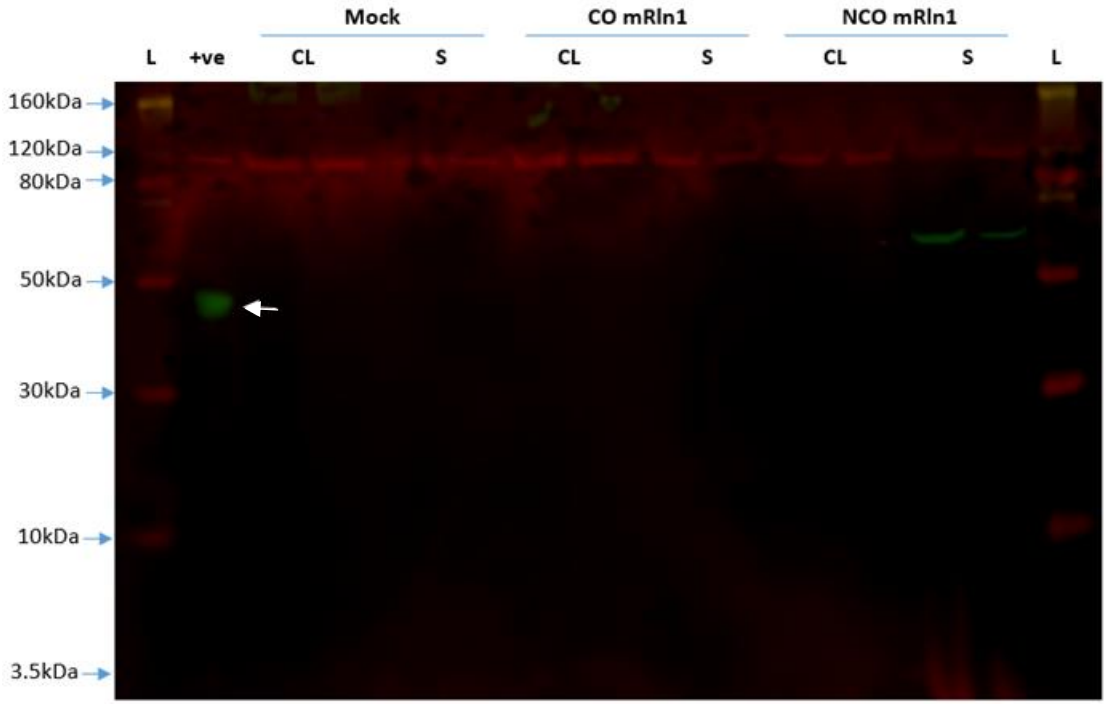

Figure 4.6 Western blot to detect mRln1 with HA tag antibody. The C2C12 cells transfected with either codon optimised mouse relaxin (**CO mRln1**) or non-codon optimised mouse relaxin (**NCO mRln1**) with HA tag plasmid driven by tetracycline inducible promoter with tetracycline present for 24 hours. 40 µg of protein samples that are collected from cell lysate (**CL**) and protein precipitation from supernatant (**S**) are resolved by 10% Bis-Tris gel and transferred to 0.2 µM nitrocellulose membrane. The positive control E.coli cell lysate with recombinant protein with HA tag (**+ve, white arrow**) was used and the protein ladder 3.5kDa to 260kDa (**L**). The red fluorescence represent secondary antibody targeting primary mouse vinculin antibody (117kDa) as housekeeping protein, while the green fluorescence represent secondary antibody targeting primary HA tag antibody.

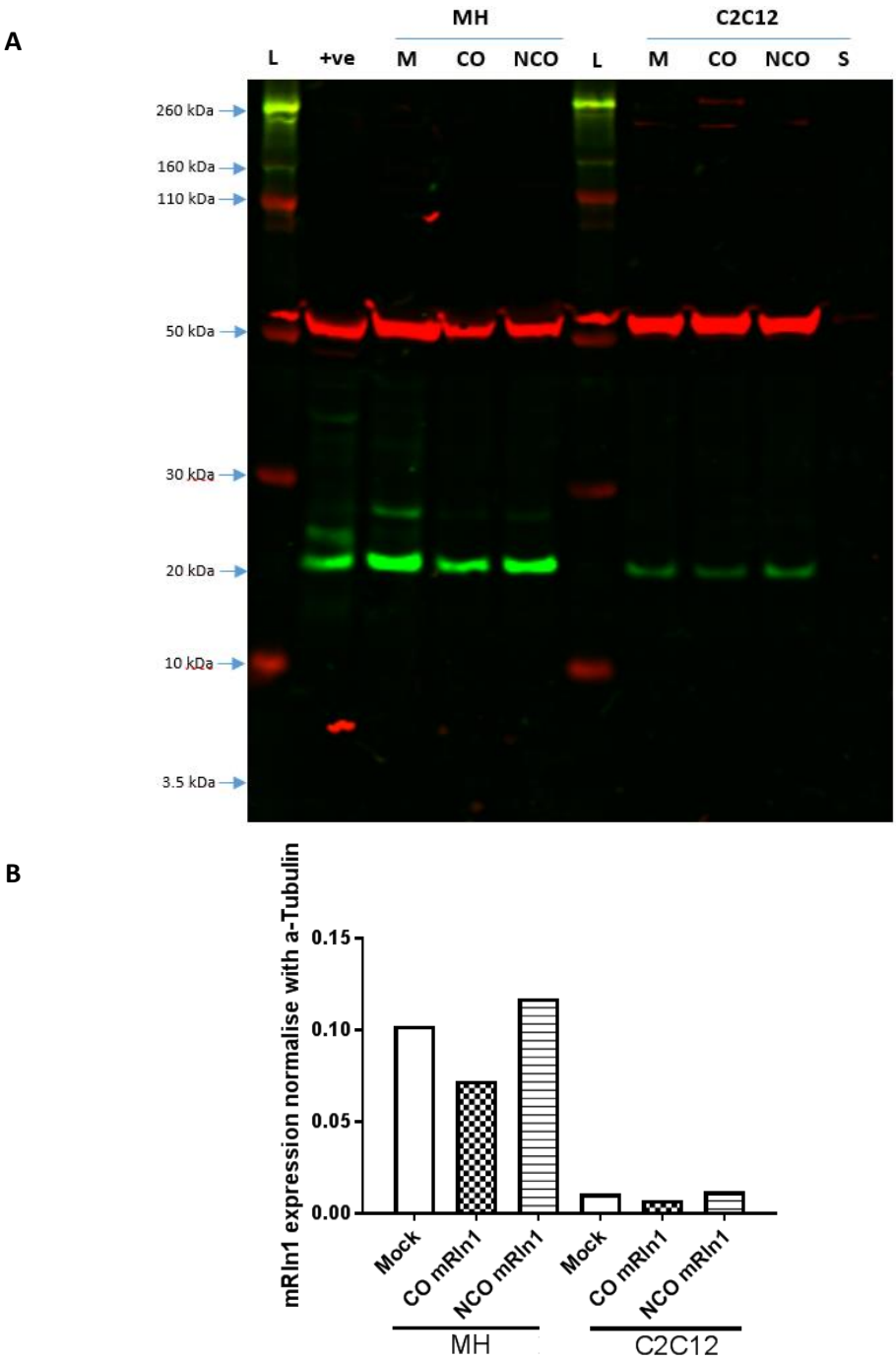

Figure 4.7 Western blot to detect mRln1 with mRln1 targeting antibody. The C2C12 cells were transfected with pTet On-CO mRln1 or pTet On-NCO mRln1; while the MH cells were transfected with the pssAAV-Tet On-CO mRln1 or pssAAV-Tet On-NCO mRln1. The plasmid either codon optimised mouse relaxin 1 (**CO**) or non-codon optimised mouse relaxin 1 (**NCO**) plasmid driven by tetracycline inducible promoter (Tet On) with tetracycline present for 24 hours. The pre-pro-mRln1 protein size is around 21kDa. Western blot result (**A.**) indicate 40µg of protein samples from MH cells cell lysate (**CL**) and C2C12 cells cell lysate, protein samples are precipitation from supernatant (**S**) are resolved by 10% Bis-Tris gel and transferred to 0.2 µM nitrocellulose membrane. The positive control mouse prostate cell lysate samples (**+ve**) was used and the protein ladder 3.5kDa to 260kDa (**L**). The red fluorescence represent secondary antibody targeting primary mouse α-tubulin antibody (50kDa) as housekeeping protein, while the green fluorescence represent secondary antibody targeting primary human relaxin 2 antibody. The western blot quantification (**B.**) shown the level of mRln1 expression comparison between different plasmid construct transfected into MH or C2C12 cells. n = 1

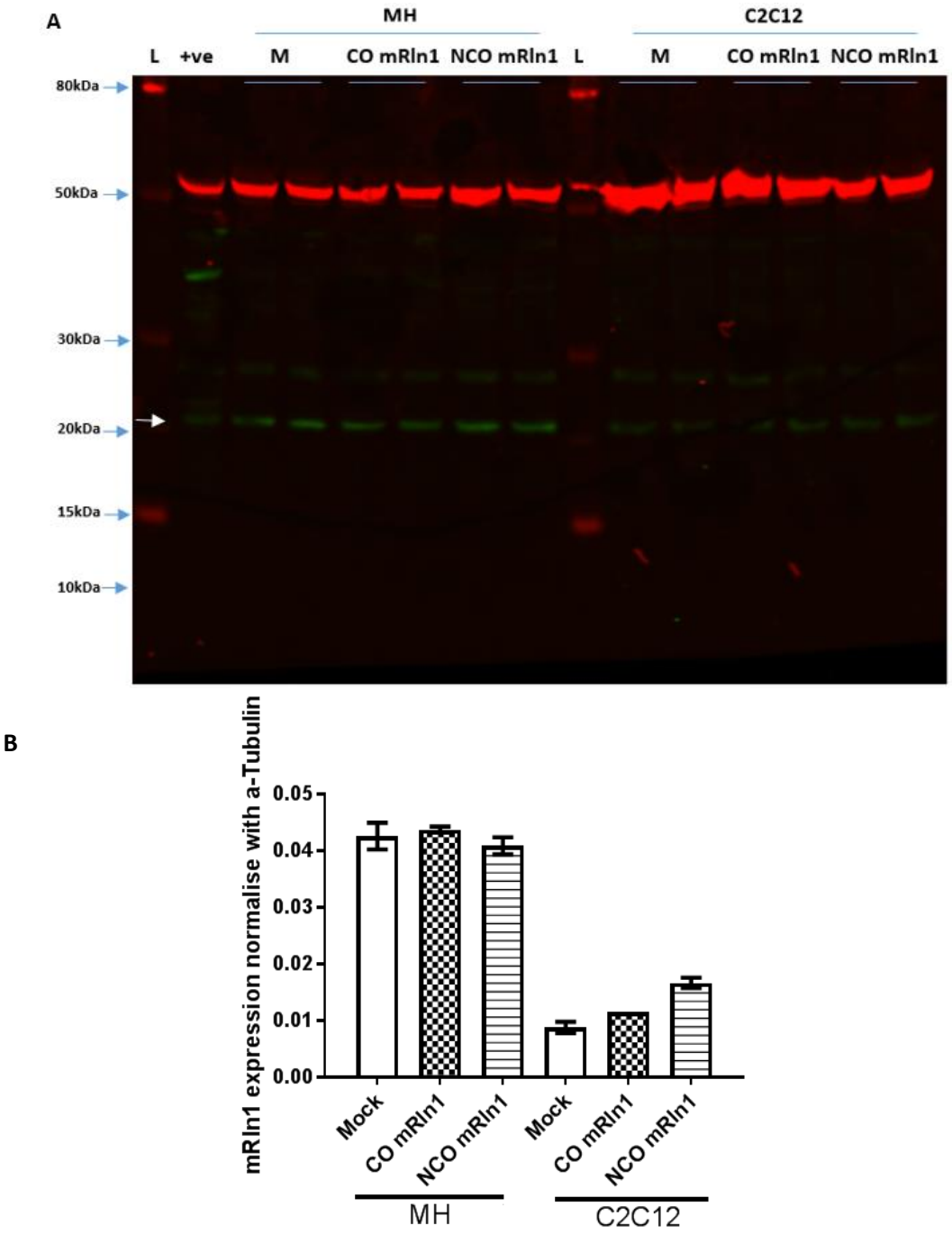

Figure 4.8 Western blot to detect mRln1 in C2C12 and MH cells. The C2C12 and MH cells transfected with either codon optimised mouse relaxin (**CO mRln1**) or non-codon optimised mouse relaxin (**NCO mRln1**) plasmid driven by tetracycline inducible promoter with tetracycline present for 24 hours. The pre-pro-mRln1 protein size is around 21kDa Western blot result (**A.**) indicate 20µg of protein samples from MH cells cell lysate (**CL**) and 20µg of protein samples from C2C12 cells cell lysate are resolved by 10% Bis-Tris gel and transferred to 0.2 µM nitrocellulose membrane. The positive control mouse prostate cell lysate samples (**+ve**) was used and the protein ladder 3.5kDa to 260kDa. The mRln1 transcript level of sample transfected with either CO mRln1 or NCO mRln1 plasmid were compared to the mock (**M**). The red fluorescence represent secondary antibody targeting primary mouse α-tubulin antibody (50kDa) as housekeeping protein, while the green fluorescence represent secondary antibody targeting primary human relaxin 2 antibody. The western blot quantification (**B.**) shown the level of mRln1 expression comparison between different plasmid construct transfected into MH or C2C12 cells. n = 1 or 2.

4.3 DISCUSSION

4.3.1 Gradient PCR and RT-qPCR to detect CO *mRln1* & NCO *mRln1*

In this chapter we have investigated the expression efficiency of vectors that express mouse Relaxin 1 (mRln1) in C2C12 and MH cells. The plasmid constructs contained either codon optimised (CO) mRln1 or non-codon optimised (NCO) mRln1 to increase the expression of relaxin. To detect *mRln1* mRNA expression RT-qPCR was carried out. Gradient RT-PCR was used to test whether the specific amplicon is formed from the designed primer targeting CO mRln1 or NCO mRln1. The gradient RT-PCR result (**Figure 4.1**) indicated that the amplicon was successfully formed with the cDNA template used. The gradient RT-PCR indicated that the optimum annealing temperature for the CO mRln1 primer is ~55^{o}C to 56^{o}C and for NCO mRln1 primer is ~55^{o}C to 57^{o}C. In this way it was verified that the specific size of PCR amplicon can be obtained with the designed primer.

For the RT-qPCR was set on around 60^{o}C optimum annealing temperature as indicated by the IDT OligoAnalyzer analysis software. RT-qPCR result shown in **Figure 4.2** suggested that the cells were transfected with mRln1 plasmids allow *mRln1* expression could be detected. However, in some of the untransfected samples (mock) or control samples with treatment with tetracycline or treatment with both Viafect and tetracycline have some amplicon form, while some is not. The RT-qPCR result indicate the Cq value those mock and control samples are also inconsistent with most appear near to end of the PCR cycles. This might be due to the low amount of the native mouse relaxin 1 expression in *in vitro*. In **Figure 4.2B**, the melting curve shown indicates that only one single melting curve is present, which suggests that only one specific amplicon is amplified. All of the NCO mRln1 plasmids exhibit higher levels of *mRln1* expression compared to the CO mRln1 plasmids. The highest level of *mRln1* expression was detected in C2C12 cells that were transfected with a pscAAV-Spc512-NCO mRln1 plasmids (24 hours after the transfection). It is not clear why the *mRln1* expression in cells transfected with the pscAAV-Spc512-NCO mRln1 construct is higher than in cells transfected with the pssAAV-Spc512-NCO mRln1 construct. Despite the fact that codon optimised mRln1 was designed

through the VectorBuilder codon optimization online software, the expression analysis of the *mRln1* suggests that CO mRln1 is less effective compared to the native mRln1. For further research, several codon optimised versions of the mRln1 shall be designed and compared to the native mRln1. No statistics could be carried out as the n number was 1. In the future, experiment repeats will be enable statistical analysis.

The second highest *mRln1* expression was detected in C2C12 cells transfected with the pTet On-NCO mRln1 plasmid and in the presence of tetracycline. In the absence of tetracycline, both the plasmids (pTet On-CO mRln1 or pTet On-NCO mRln1) exhibit a low level expression of *mRln1* around a third level of expression compared to when tetracycline is present. Many studies have explored the leaky expression of the tetracycline inducible promoter system (Costello *et al*., 2019). In this project, we employed an improved version of the Tet On system where the hybrid TetR- Kruppel associated box (KRAB) system is used to reduce the basal transgene expression compare to Tet On (Szule *et al*., 2006). Our findings indicate in the absence of tetracycline, CO mRln1 and NCO mRln1 expressed *mRln1*. One possible investigation that could be carried out is to use a pTet On-eGFP plasmid to evaluate the efficiency and leakage of the Tet On system. Additionally, a dose dependent investigation with tetracycline is required to establish the optimum dosage to activate the Tet On system for mRln1 expression without causing toxicity to both C2C12 and MH cells.

To further analyse the RT-qPCR amplicon from **Figure 4.2,** the PCR product was run on agarose gel electrophoresis. The gel image (**Figure 4.3**) shows that cells transfected either pTet On-CO mRln1 or pTet On-NCO mRln1 express m*Rln1* in the presence of tetracycline, compared to when tetracycline is absent. We used the untreated or transfected mock samples as a negative control. The results from the RT-qPCR indicate that the amplicon produced with C2C12 samples with the presence of Viafect or treated both with Viafect and tetracycline have a high Cq value near the end of the total PCR cycles. The high Cq value suggest that the Viafect, tetracycline or both might contribute to the activation of low level of native genomic *mRln1*

expression. As low levels of *mRln1* expression in the negative controls, the RT-qPCR quantification (**Figure 4.2A**) was analysed by normalising the expression of *mRln1* to the housekeeping gene (Rplp0).

Another issue with the performed RT-qPCR is the CO mRln1 primer set is shown to target the native *mRln1* expression. Although the CO mRln1 forward primer (5'-GAAGACCCTGCACGACAA-3') is similar to the GAAAACTCTCCATGATAA at the position of 387 to 404 with 13/18 nucleotide with native *mRln1* similarity and CO mRln1 reverse primer (5'-TCTCCCTCTTCTTCCTGCT-3') to the TCACGGAAAAAGAGGGAGT at the position 466 to 484 with 4/19 similarity with native *mRln1*. Despite the low similarity on the CO mRln1 reverse primer, there are some amplicons produced at the same size by PCR amplification caused by cross contamination. The CO mRln1 primer should be redesigned and tested before the RT-qPCR. However, due to the high similarity between the nucleotide sequences of codon optimised *mRln1* and non-codon optimised *mRln1*, it would be challenging to design primers only targeting the codon optimised *mRln1* without amplifying the non-codon optimised *mRln1*. A possible method to specifically detect CO *mRln1* expression is with a designed Taqman probe. Unlike Sybr Green, a non-specific double stranded DNA binding dye to emitted fluorescence, Taqman probes provide a specific fluorescent detection between the hybridization of probe and target unique nucleotide sequence (Arikawa *et al*., 2008). On the other hand, the RNA purity was measured using a spectrophotometer, where $OD_{260/280}$ value for pure RNA is 2.1 and around 1.8 to 2.0 was considered acceptable and used to construct cDNA but there are no information regarding RNA integrity. The RNA integrity should be determined as a better measure of RNA degradation before any downstream application (Taylor *et al*., 2010).

4.3.2 Western blot optimization

The next focus was the detection of relaxin protein through western blot. Firstly, the western blot protocol was optimized. The transfer efficiency of proteins transfer from SDS-PAGE gel on the nitrocellulose membrane were visualising by Ponceau S stain. Although the transfer

process was successful, transfer could be improved to avoid air bubbles. The air bubbles was reduce on the following transfer process as more precaution has been taking to remove air bubbles between SDS-PAGE gel and nitrocellulose membrane. The optimum transfer condition was 30V for 90 minutes at 4^{o}C, the result (**Figure 4.4**) indicates that protein sample were successfully transferred onto the nitrocellulose membrane. This suggests that to transfer small size proteins (<40kDa) lower voltages and low temperatures are preferable.

Following this, the blocking conditions were optimized to reduce non-specific antibody binding. Two of the routinely used blocking buffers contain either 3% (w/v) or 5% (w/v) bovine serum albumin (BSA) or 5% non-fat dried milk in phosphate buffer saline (PBS). Besides that, there are small amounts (e.g. 0.05% (v/v) to 0.1% (v/v)) of surfactant (e.g. Tween 20 or Triton X100) present in the blocking buffer and in the washing buffer to further reduce background signalling (Alegria *et al*., 2009). The surfactants either prevent the antibody binding to the non-specific proteins and/or block the hydrophobic sites on the membrane (Alegria, p. 573 - 599). The optimisation of the western blot blocking buffer (**Figure 4.5**) shows that the blocking buffer 3% (w/v) BSA with 0.1% (v/v) Triton X100 in PBS can reduce most of the background signalling after primary and secondary antibody staining compared with 5% non-fat milk 0.2% Tween 20 PBS and 3% non-fat milk 0.2% Tween 20 PBS. Although this might not be the best optimization for blocking buffer as we change both parameter together, however, are able to shown reduced background signal with one of the blocking buffer.

4.3.3 Western blot detect mRln1 protein expression evaluation

The western blot analysis represent the protein samples (either cell lysate or supernatant) collected from C2C12 cells transfected with plasmids (either pTet On-CO mRln1/HA or pTet On-NCO mRln1/HA) for 24 hours with tetracycline present. The result in **Figure 4.6**, suggests that the HA tag antibodies only bind to the positive control *E.coli* whole cells lysate with recombinant protein with HA tag (~49kDa) but not cell lysate or proteins samples

with mRln1 protein with HA tag. This positive control confirms that the HA tag antibody was able to detect HA tagged proteins. One explanation might be that the HA tag nucleotide sequence might not be present or the nucleotide sequence is not correct within the designed plasmid and therefore further investigations into this are needed. To assess whether the HA tag nucleotide sequence is correct, a PCR targeting the HA tag nucleotide sequence should be carried out and further identified with sequencing. The epitope tagging normally designed to the N- or C terminus of the protein of interest might interfere with protein function, trafficking processing or folding (Zordan *et al*., 2015). Besides, the amount of protein samples loaded on the gel might be insufficient to be detectable, and this shall be repeated with higher amounts of protein. We should include an investigation with a gradient of protein concentration sensitivity to detect mRln1 protein (pre-pro or mature form).

The next western blot analysis focuses on the detection of mRln1 in cells transfected with the following plasmids: either pTet On-CO mRln1 or pTet On-NCO mRln1 in C2C12; pssAAV-Tet On-CO mRln1 or pssAAV-Tet On-NCO mRln1 in MH cells. The western blot result shown in **Figure 4.7A** indicates that the pre-pro mouse relaxin 1 (mRln1) with size ~21kDa can be detected with the human relaxin 2 targeting antibody. All of the samples that are either transfected with plasmids or mock cell lysate samples show mRln1 protein expression in C2C12 and MH cells. However, there is no detection of any form of mRln1 protein in the supernatant samples from C2C12 cells and MH cells (data not shown). Western blot quantification (**Figure 4.7B**) shows that the mRln1 protein is expressed more in both C2C12 and MH cells transfected with the pTet On-NCO mRln1 compared to the pTet On-CO mRln1 with the presence of tetracycline. Transfection with The pTet On- CO mRln1 leads to ~20% more mRln1 protein being expressed compare to the mock. Both of the RT-qPCR result (**Figure 4.2**) and western analysis (**Figure 4.7B**) shows that the NCO mRln1 construct appears to express more mRln1 compared to CO mRln1 construct. In contrast, the CO mRln1 construct had around 30% lower expression level of mRln1 compared to the mock. The pTet On-CO mRln1 has a reduction for mRln1 expression compare to the mock in both C2C12 and MH cells.

A similar western blot (**Figure 4.8A**) was performed with protein samples collected from another batch of C2C12 cells transfected with either pTet On-CO mRln1 or pTet On-NCO mRln1, and of MH cells transfected with either pssAAV-Tet On-CO mRln1 or pssAAV-Tet On-NCO mRln1 for 24 hours prior to protein sample collection for western blot. The western blot quantification analysis (**Figure 4.8B**) shows both of the plasmids pTet On-CO mRln1 (~20%) and pTet-NCO mRln1 (~40%) were able to increase the level of mRln1 expression in C2C12 cells compared to the mock. On the other hand, both of the plasmids (pssAAV-Tet On-CO mRln1 or pssAAV-Tet On-NCO mRln1) did not show any difference in the mRln1 expression compared to mock. Although similar transfection conditions with the plasmids (pTet On-CO mRln1) were investigated twice, the western blot results indicated that the level of mRln1 expression was not consistent. The second western blot result shows that the CO mRln1 construct was able to upregulate mRln1 expression in C2C12, while the first western blot shows a reduction of mRln1 compared to mock; similar experiment shall be conducted for more detailed information. Plasmids pssAAV-Tet On-CO mRln1 and pssAAV-Tet On-NCO mRln1 did not shown any effect on the mRln1 expression in the MH cells on the second western blot. No statistics could be carried out as the n number was 1 or 2. In the future, more experiment repeats will enable statistical analysis.

The rat prostate samples harvest from rat prostate contains rat pre-pro Rln1 (~21kDa) and rat mature Rln1 (~6.5kDa), and rat pro-Rln1 in vas deferens are detected through western blot (Cardoso *et al*., 2002). We used mouse prostate protein samples as a positive control and only managed to detect pre-pro mouse Rln1 form but not the pro mouse Rln1 (~16-17kDa) or mature mouse Rln1 (~6.5kDa) with human relaxin 2 targeting antibody raised to detect residue 1 - 100 amino acid of human and rat relaxin 1. Although the human relaxin 2 antibody that we used was claimed can detect mouse relaxin 1 (mRln1), rat relaxin 1 and human relaxin 2; but we were not able to detect mRln1 with this antibody. It is suspected the antibody was unable to target the mouse relaxin 1 due to differences in the amino acid sequence. There is only 48.09% amino acids sequence similarity between the mouse relaxin 1 similarity and the human relaxin 2 (**Figure 3.14**), this might be the reason that the human relaxin 2 targeting antibody that we

used in our investigation might not able to target the mature mouse relaxin 1. Another explanation might be due to low amount of protein loaded in western blot, as Cardoso *et al*., 2002 have shown that 100ug of rat prostate was loaded in western blots. We should repeat our investigation with higher concentrations protein samples (for example 100µg).

In **Figure 4.6**, in all samples show vinculin (cell surface protein responsible for cytoskeleton and adhesion) (Peng *et al*., 2011) was detected in all the supernatant samples, which suggests cell debris might be present in the supernatant. An additional step such as centrifugation, filtering with a 0.22µm filter (Lobb *et al*., 2015) or with protein size exclusion spin filter column (Sartorius Vivaspin turbo, 2019) could remove specific size of protein and applied to remove apoptotic bodies or cell debris and increase the concentration of protein samples from supernatant before western blot. Further investigation could be carried out with recombinant mature mRln1 protein as a positive control for western blot to check whether the antibody can detect the mature mRln1. Additionally, a gradient time course of expression could be investigated as the short life spans of the relaxin 1 protein of less than 4 minutes (Jung *et al*., 2017) and recombinant human relaxin 2 of less than 10 minutes (Kanai *et al*., 2019) have been reported.

It is vital to show that the expression of transgenic mouse relaxin 1 (mRln1) hormone can be secreted from myogenic cell line or fibroblasts cell line. Here are few suggestions regarding the detection of secreted mRln1 in vitro, as the RT-qPCR can detect the mRln1 mRNA expression indicates the successful transfection of plasmids with mRln1 mRNA upregulation in the C2C12 and MH cell line. The western blot shall be carried out with recombinant mRln1 protein as a positive control with mRln1 specific targeting antibody to make sure the antibody that we are using was able to target mature mRln1 protein. If the antibody that we used in our investigation was not able to detect mature mRln1, we should try to get a mouse relaxin 1 targeting antibody. Apart from that, Cardoso et al., 2010 have shown that mature rat relaxin 1 (~6.5kDa) was able to detect in 100µg of rat prostate samples, which suggest the amount of

supernatant samples (maximum 40µg) that we used is lower (100µg) compared to Cardoso (Cardoso, *et al*., 2010). Besides, a more sensitive ELISA method can be applied to detect a low amount of mRln1 protein. Finally, a time course detection of mRln1 mRNA or secreted mRln1 after transfection with mRln1 express plasmids shall be investigated, as the mRln1 hormone have a short half-life less than 10 minutes. This might provide an idea on when the protein will be secreted from the cell.

Chapter 5: STUDIES DOWNSTREAM EFFECT OF RELAXIN AND IN *in vitro* WOUND SCRATCH ASSAY

CHAPTER 5 STUDIES DOWNSTREAM EFFECT OF RELAXIN AND in *in vitro* WOUND SCRATCH ASSAY

5.1 INTRODUCTION

Activated fibroblasts play a vital role in the wound healing process through the production, deposition and reconstruction of the extracellular matrix (ECM) (Kendell and Feghali-Bostwick, 2014). During the wound healing process, fibroblasts migrate to the injured site and become activated or parenchymal cells on the injured site undergo epithelial or endothelial mesenchyme transition into myofibroblast for ECM component synthesis (Quaggin and Kapus, 2011). In the normal wound healing process, fibroblast activity is reduced to basal level when the wound is healed, however this process is not regulated in some events such as chronic inflammation or fibrosis (Thomas, 2011). In fibrosis, the excessive number of fibroblast and ECM components have caused the hardening and replacement of the parenchyma cells which affect their normal function. In DMD, muscle regeneration does not keep up the pace with the muscle degradation as dystrophic muscle is more susceptible to damage cause by motion and are surrounded with fibrosis and inflammation (Verhaart and Aastsma-Rus, 2019). In this chapter, we focus on utilising wound scratch assays to observe how the presence of mRln1 affects the migration rate of mouse muscle-derived fibroblast (MH cells).

In vitro scratch assays utilise a direct, simple and inexpensive protocol involving observation of cell migration in response to a scratch wound induced in a confluent monolayer of cells and subsequently, cells will start to migrate and fill up the “scratch” gap (Liang *et al*., 2007). The type of cell used in this experiment is either sheets of cells (such as endothelial and epithelial cells) or loosely connected populations (such as fibroblasts cells). Cell migration rate is captured with microscopy images over a specific period of time (for example microscopy imaging after wound scratch, 24 hours and 48 hours post wound scratch) throughout the experiment. The wound scratch assay investigates how different types of treatments (such as drug treatment, phosphorodiamidate morpholino oligomer or plasmid transfection) affect cell migration rates. The limitations of this technique are that large amount of cells are required and

the experiment has a long duration (~5 days in total). In contrast, the advantage of the wound scratch assay are that it is easy to set-up and does not require additional expensive equipment (equipment remains the same as standard tissue culture work).

Transforming growth factor – β1 (TGF-β) is a multifunctional cytokine involved in processes such as growth, proliferation, differentiation, apoptosis and wound healing (Massagué, 2012). In skeletal muscle and other type tissues fibrosis (liver, kidney and lung), TGF-β is the primary pro-fibrotic signal (Ceco and McNally, 2013). TGF-β1 will bind to the TGF-β receptor II and activate the SMAD2 and SMAD3 signalling pathway and lead to the transcriptional activation of downstream pro-fibrotic genes such as collagen I (Hu *et al*., 2018). Li and colleagues have shown that exogenous TGF-β1 treatment in C2C12 cell led to increase in TGF-β secretion act an autocrine manner, where it contributes to reduce expression of myogenic proteins (Li, *et al*., 2004). Besides, TGF-β is also the key regulator for fibroblast activation to become myofibroblasts, the main cell type that synthesises ECM components during wound healing and fibrosis (Akhmetshina *et al*., 2012). In contrast, interferon-γ (IFN-γ) inhibits TGF-β signalling, collagen I expression (Kähäri *et al*., 1990) and reduces the activation and migration of fibroblasts (Bansel *et al*., 2012). Therefore, we investigated the effect of TGF-β1, IFN-γ, mRln1 gene addition on the migration rate of MH cells with the wound scratch assay.

We also investigated the downstream effect of upregulation of mRln1 mRNA expression. The downstream pro-fibrotic related genes of interest were alpha smooth muscle actin (*Acta2*), Collagen I (*Col1a1*), Fibronection 1 (*Fn1*), matrix metallopeptidase 9 (MMP9), Periostin (Postn), Tissue inhibitor of metalloproteinases 1 (*TIMP1*) and Tissue inhibitor of metalloproteinases 2 (*TIMP2*). The ECM components (Col1a1, Fn1 and Postn) are synthesised by fibroblasts, while Acta2 is the surface marker which is upregulated in myofibroblasts compared to fibroblasts (Baun and Duffy, 2011). The balance of ECM component production is regulated by MMPs (degrading enzymes can breakdown various ECM components) and TIMPs (neutralizing enzyme

that inhibits MMP activity); these enzymes therefore play a vital role in wound healing and fibrosis (Kalluri, 2016).

In this chapter, we describe the effects of mRln1 upregulation via plasmid transfection with mRln1 expressing plasmid on downstream pro-fibrotic genes at the level of transcription in C2C12 and MH cell lines. In addition, we also look into how mRln1 upregulation affects the migration rate of MH cells via wound scratch assay. Our *in vitro* studies provide an insight into how mRln1 upregulation might contribute to reducing muscle fibrosis.

5.2 RESULTS

5.2.1 Effect of mRln1 on downstream fibrotic related gene expression assessed using RT-qPCR analysis

We investigated the effect of upregulation of mRln1 expression using plasmid transfection with pTet On-NCO mRln1 plasmids into C2C12 and MH cells. C2C12 or MH cells were transfected with 1000ng of pTet On-NCO mRln1 plasmids with the presence of 200ng/ml tetracycline for 24 hours. Subsequently, total RNA was extracted and 600ng of total RNA was used for cDNA synthesis and RT-qPCR. The *Acta2* was used as a cell surface marker of myofibroblasts, while *Col1a1*, *Postn* and *Fn1* as the extracellular matrix (ECM) component, MMP9 as the metalloproteinase capable to degrade ECM, TIMP1 and TIMP2 are metalloproteinase inhibitor.

In C2C12 cells, RT-qPCR analysis (**Figure 5.3**) has shown a slight reduction in the transcript level of *Acta2* after transfected with pTet On-NCO mRln1 plasmid with tetracycline presence. The other 5 downstream genes *Col1a1*, *Fn1*, *MMP9*, *Postn* and *TIMP2* have remained at a similar transcription level as the mock (C2C12 without transfection). There is a 1 folds increase of transcript level of TIMP1 after transfection compared to untransfected mock sample.

The amplicons formed through RT-qPCR were analysed with a melting curve (**Figure 5.1** and **Figure 5.2**) suggested only one amplicon is formed with Acta2 primer, Col1a1 primer, Fn1 primer, MMP9 primer, Postn primer, TIMP1 primer and TIMP2 primer and Rplp0 primer. The amplicon was further analysed by using agarose gel electrophoresis to examine specificity of amplicon size and stringency. **Figure 5.4** shows a representative gel image, where the specific band size of the amplicon with primers targeting *Acta2* (~129bp), *Fn1* (~96bp), *Col1a1* (~134bp), *MMP9* (~125bp), *Postn* (~97bp), *TIMP1* (~129bp), *TIMP2* (~119bp) and *Rplp0* (~147bp) can be seen. There were primer dimers formed with the *TIMP2* targeting primer set which are suspected to be primer-dimers (**Figure 5.2B**) in non-template control samples with a melting peak at lower temperature and the identity was further confirmed through agarose gel electrophoresis (**Figure 5.4D left**) with a band size <50bp.

The RT-qPCR analysis (**Figure 5.5**) indicate the transcript levels of three targeted genes (*Acta2*, *Fn1* and *Postn*). The total mRNA samples were from MH cell transfection with pTet On-NCO mRln1 for 48 hours in the presence of 200ng/ml tetracycline. When in the presence of human recombinant Transforming growth factor β1 (hrTGF-β1), the transcript level of the *Acta2* was slightly reduced, Fn1 increased and Postn remained unchanged when compared to mock (MH cell without transfection). In contrast, the cells transfected with pTet On-NCO mRln1 with tetracycline presence have reduced mRNA expression of three of the targeted genes compared to mock. The pTet On-NCO mRln1 is the plasmid that able to express highest *mRln1* expression compare to other mRln1 plasmids construct (**Section 2.2.2**) that we designed. Finally, we observed that the transfected mRln1 expressing plasmids can reduce the mRNA expression of three target genes (*Acta2*, *Fn1* and *Postn*) even with the presence of hrTGF-β1.

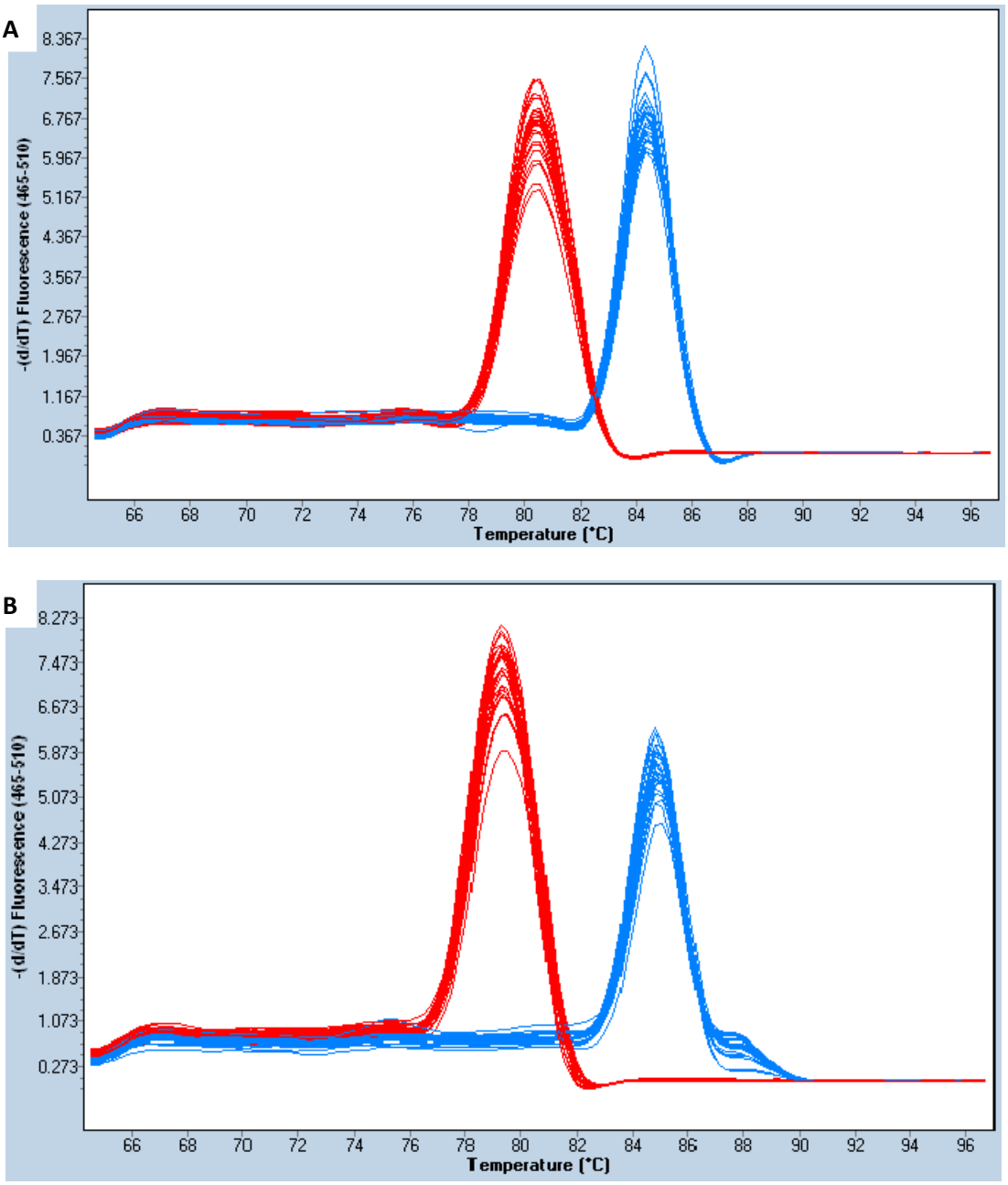

Figure 5.1 Melting Curve of RT-qPCR targeting downstream fibrotic related genes. The RT-qPCR melting curve analysis indicates amplicons are produced at specific melting curve peak with 4 downstream fibrotic related primer targeting ***Acta2*** (**A.** Blue peak), ***Col1a1*** (**B.** Blue peak), ***Fn1*** (**A.** Red peak) and ***Postn*** (**B.** Red peak). The one specific melting curve peak indicates there is only one specific amplicon that is formed with primers through RT-qPCR.

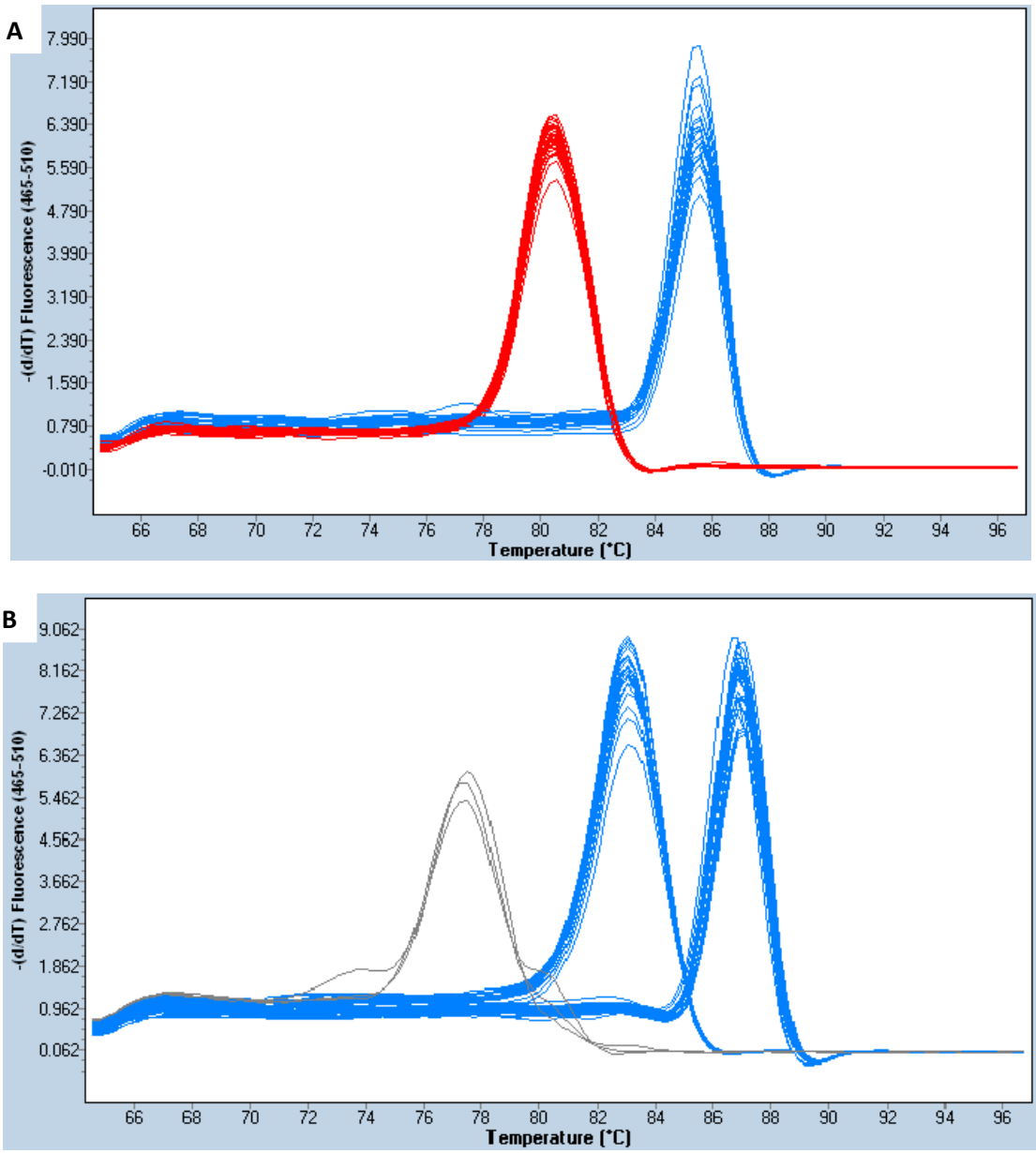

Figure 5.2 Melting Curve of RT-qPCR targeting downstream fibrotic relate genes. The RT-qPCR melting curve analysis indicates amplicon are produced at specific melting curve peak with 3 downstream fibrotic relate primer targeting ***MMP9*** (**A**. Blue peak), ***TIMP1*** (**A.** Red peak), ***TIMP2*** (**B.** Blue peak on left) and housekeeping gene ***Rplp0*** (**B.** Blue peak on right). The one melting curve peak indicates there is only one specific amplicon formed with primers through RT-qPCR. There are amplicons formed on the non-template control (without cDNA) with *TIMP2* primer set (**B**. grey peak on left).

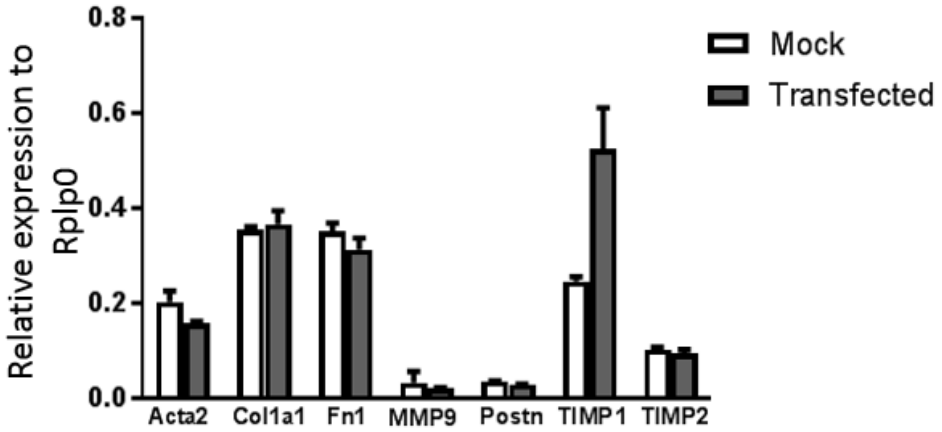

Figure 5.1 RT-qPCR analysis of downstream fibrosis-related genes of RNA harvested from C2C12 cells transfected with mRln1 expressing plasmid. The mouse muscle myogenic cells (C2C12) were transfected with pTet On-NCO mRln1 plasmid in the presence 200ng/ml tetracycline hydrochloride for 24 hours prior to total RNA extraction, cDNA construction and qPCR. The mRNA expression of 7 downstream fibrotic related genes (***Acta2***, ***Col1a1***, ***Fn1***, ***MMP9***, ***Postn***, ***TIMP1*** & ***TIMP2***) was relatively quantified against the expression level of Rplp0 housekeeping gene in untransfected C2C12 cells (**Mock**) and transfected MH cells with pTet On-NCO mRln1 plasmid (**Transfected**). Data are the mean ± SEM of three repeats in one independent experiment. n = 1.

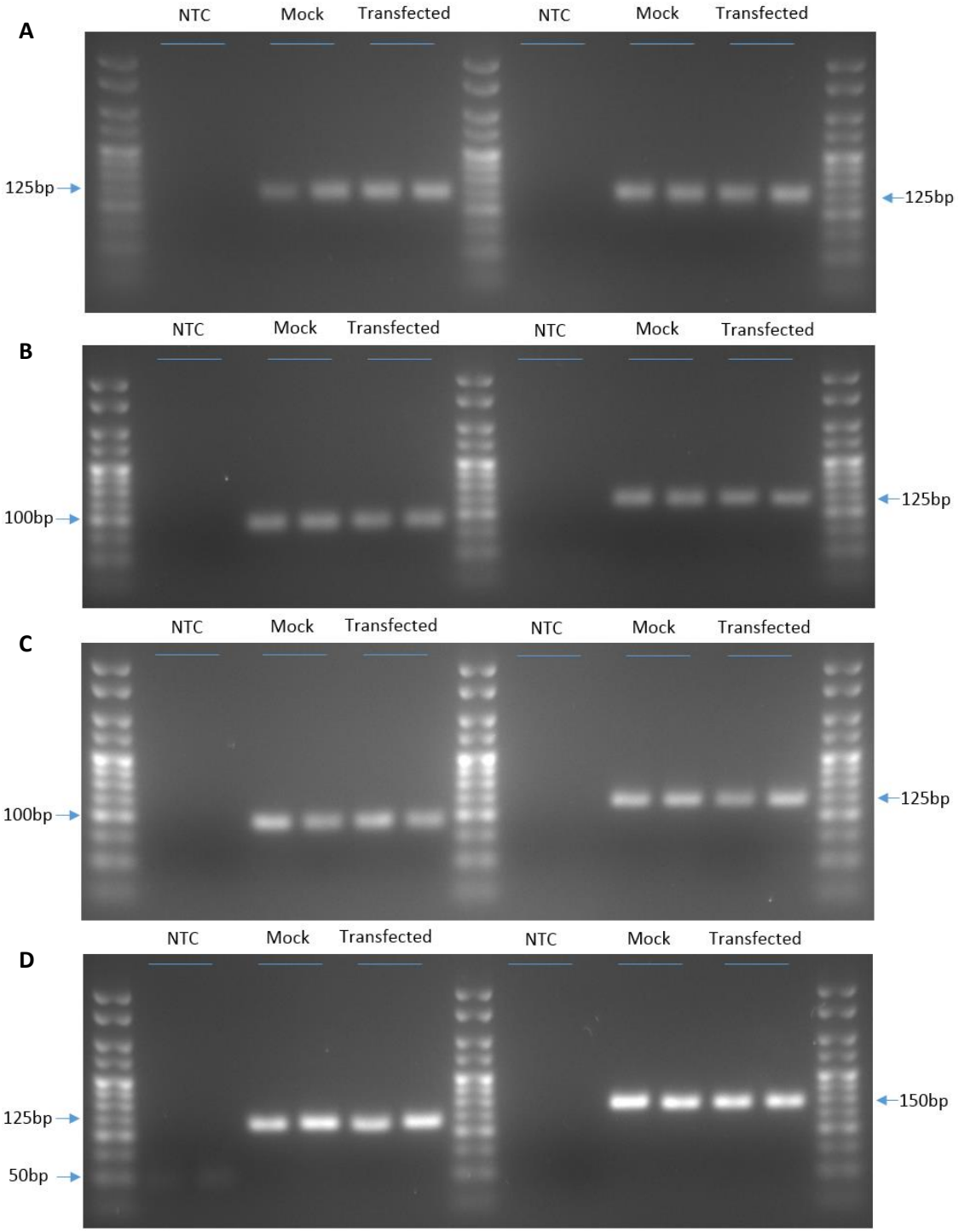

Figure 5.4 Gel Image with RT-qPCR amplicon targeting downstream fibrotic relate genes. The size of RT-qPCR amplicon targeting *Acta2* (**A. left**), *Col1a1* (**A. right**), *MMP9* (**B. left**), *Fn1* (**B. right**), *Postn* (**C. left**), *TIMP1* (**C. right**), *TIMP2* (**D. left**) and *Rplp0* (**D. right**) from **Figure 5.1** electrophoresed on a 3.5% (w/v) agarose TAE gel for 65V for 60 minutes and 70V for 40 minutes. The samples shown are untransfected C2C12 cells without any treatment (**Mock**), transfected with pTet On-NCO mRln1 with the presence of tetracycline (**Transfected**), non-template control (**NTC**) and 25bp DNA ladder (500bp to 25bp). There are primer dimer are formed with the NTC samples with TIMP2 primer.

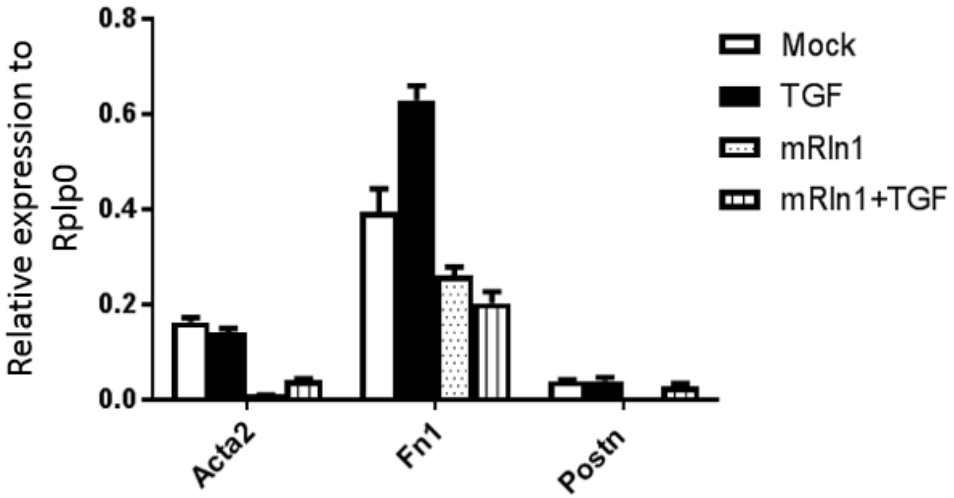

Figure 5.5 RT-qPCR targeting 3 downstream fibrotic related genes affected by mRln1 in MH cells. The mouse muscle derived fibroblast (MH) cells are transfected with pTet On-NCO mRln1 plasmid with the presence 200ng/ml tetracycline hydrochloride for 24 hours prior to total RNA extraction, follow by cDNA construction and RT-qPCR. The relative quantified mRNA expression of 3 downstream fibrotic related genes (***Acta2***, ***Fn1*** and ***Postn***) was compared to the level of Rplp0 housekeeping gene. The untransfected MH cells (**Mock**), presence of 40ng/ml hrTGF-β1 (**TGF**), transfected MH cells with pTet On-NCO mRln1 plasmid with the presence of tetracycline (**mRln1**) and transfected MH cells with pTet On-NCO mRln1 plasmid with the presence of tetracycline and 40ng/ml hrTGF-β1 (**mRln1+TGF**). Data are the mean ± SD of one independent experiment (n = 1, 2 – 3 technical repeats).

5.2.2 Wound scratch assay studies with MH cells

The wound scratch assay was carried out as shown in the represent of the schematic timeframe (**Figure 5.6A**).

5.2.2.1 Effect of TGF-β1 on wound closure.

We assessed the effect of 40 ng/ml human recombinant transforming growth factor β1 (hrTGF-β1) on cell migration of MH cells after a wound scratch. We were also interested in whether the presence of 200 ng/ml of murine recombinant interferon γ (mrIFN-γ) is a TGF-β1 inhibitor would reduce the effect of TGF-β1 on MH cell migration. A wound scratch was performed and the cells scratch closure assessed for 48 hours with treatment of either 40 ng/ml hrTGF-β1, or 200 ng/ml of mrIFN-γ and both after the wound scratch was induced. The microscopy imaging was captured with the area of wound closure on day 0 (T0), day 1 (T24) and day 2 (T48) and percentage of wound closure is shown in **Figure 5.6B**. The presence of TGF-β1 resulted in around ~68% wound closure after 48 hours; no treatment (mock) showed similar wound closure (around ~71%). The presence of hrTGF-β1 also showed the highest wound closure (~30%) between the day 1 (T24) and day 2 (T48) after the wound scratch compared with other samples. On the other hand, the presence of mrIFN-γ had the lowest (~41%) wound closure after 48 hours. Finally, the presence of both 40 ng/ml TGF-β1 and 200 ng/ml mrIFN-γ led to ~40% wound closure after 48 hours. The treatment with either only tetracycline or transfection reagent (Viafect) resulted in a wound closure of ~57% on both treatments. The representative phase contrast microscopy images of the wound gaps before and after treatment are shown in **Figure 5.7**.

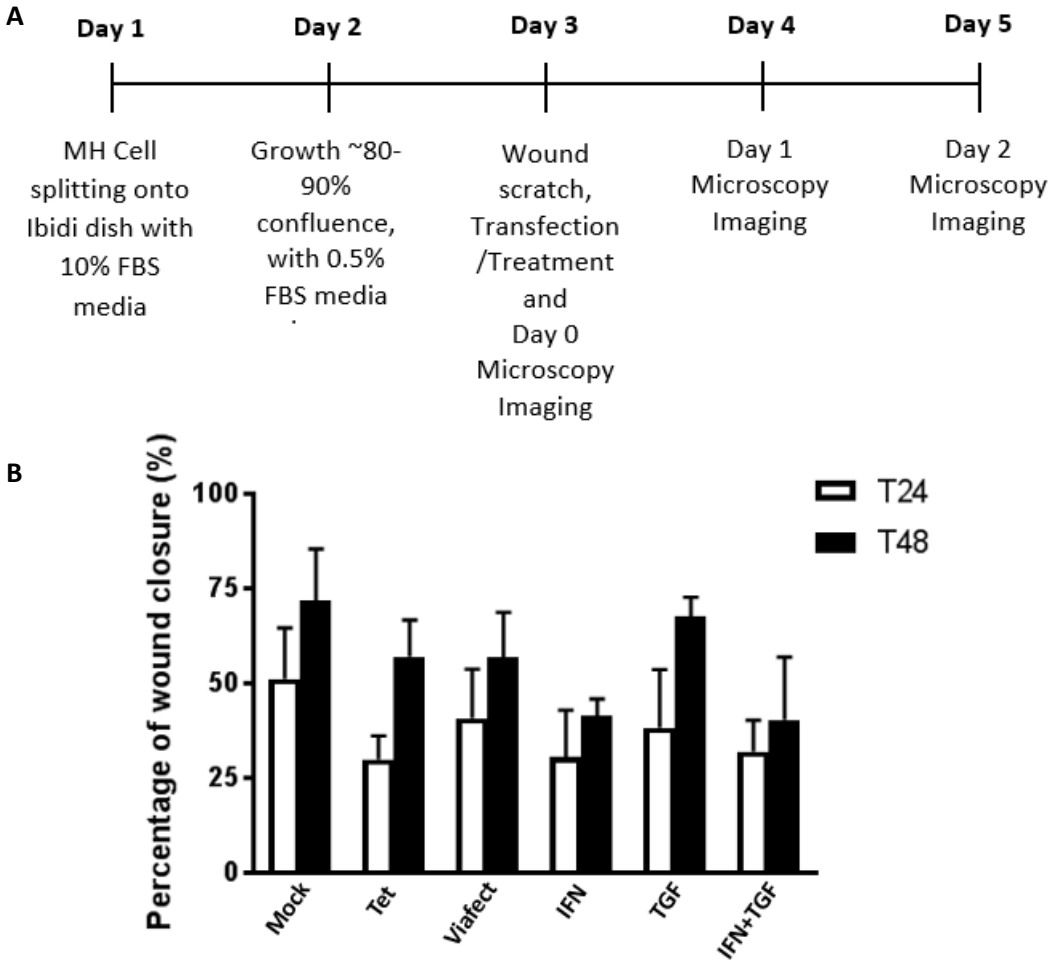

Figure 5.6 ***In vitro*** **assessment of wound closure in MH cell with hrTGF-β1. A.** Schematic timeframe of wound scratch assay. On day 1, mouse muscle derived fibroblast (MH) cells were seeded onto Ibidi dishes (1.2 x 10^5 cells per well) with 10% FBS media. On the second day, the MH cells were grown to around 80% - 90% confluency and the media was replaced with 0.5% FBS media to minimise cell proliferation. On the third day, the wound scratch was induced with 20µl pipette tips followed by plasmid transfection, treatment or both and microscopy imaging as Day 0 (T0). The microscopy imaging was performed on day 1 (T24) and day 2 (T48) after the wound scratch. **B.** The percentage of wound closure with MH cells transfected with pTet On-NCO mRln1 plasmids over a period of 48 hours. The wound was induced on day 0 (T0) and together with different treatment with the presence of 40ng/ml human recombinant transforming growth factor β1 (hrTGF-β1), presence of 200ng/ml murine recombinant interferon γ (mrIFN-γ) or presence of both hrTGF-β1 and IFN-γ. The wound closure was captured with microscopy imaging on day 1 (**T24**) and day 2 (**T48**). The area of wound closure was highlighted with ImageJ and the result shown indicate the percentage of area wound closure. MH cells with no treatment (**Mock**), MH cells treated with 100ng/µl tetracycline (**Tet**), MH cells with the presence of transfection reagent Viafect (**Viafect**), MH cells with the presence of 40ng/ml hrTGF-β1 (**TGF**), MH cells with the presence of 200ng/ml mrIFN-γ (**IFN**) and MH cells with the presence of both 40ng/ml hrTGF-β1 and 200ng/ml mrIFN-γ (**IFN+TGF**). Data are the mean ± SD of one independent experiment (n = 1, 2 – 3 technical repeats).

Samples	T0	T48
Mock	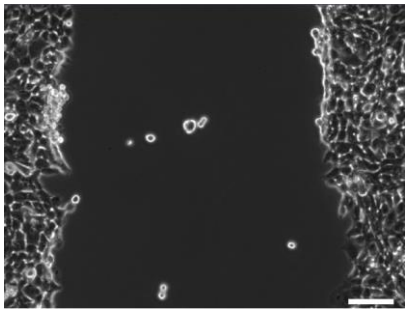	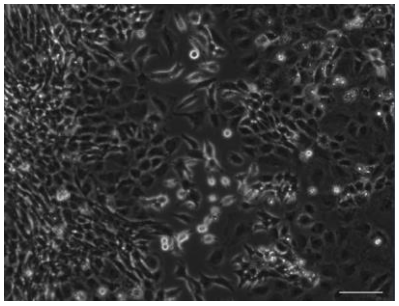
T+	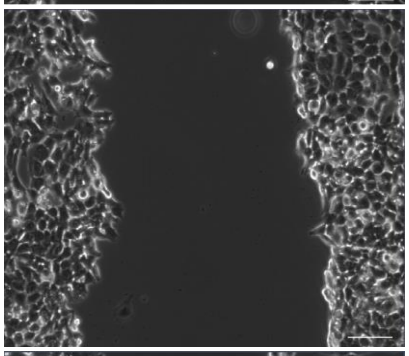	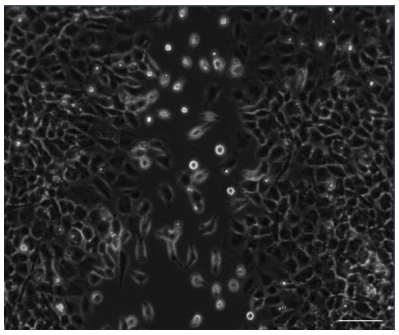
V	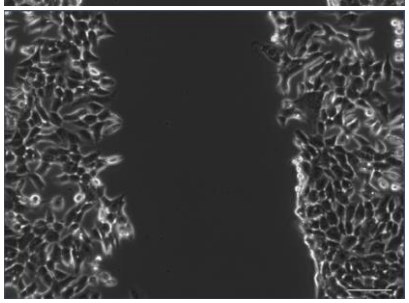	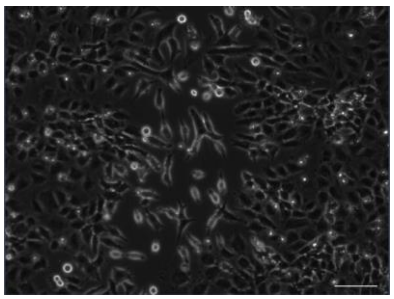
B	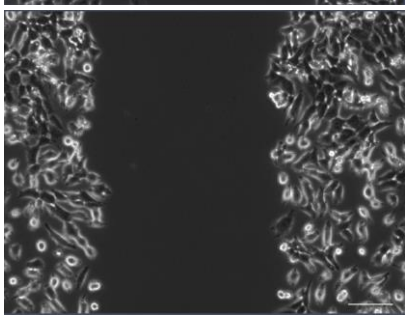	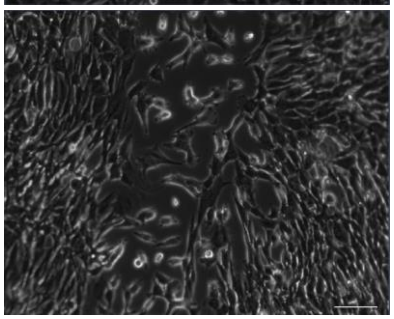
Y	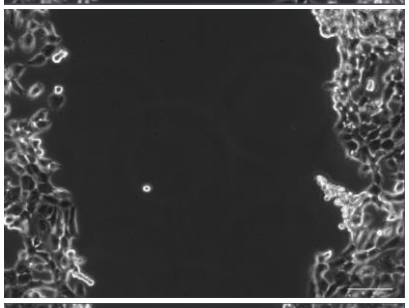	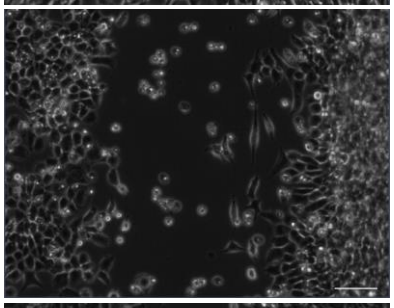
BY	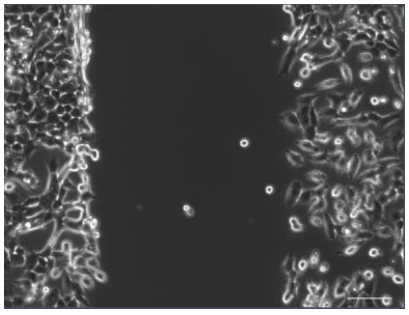	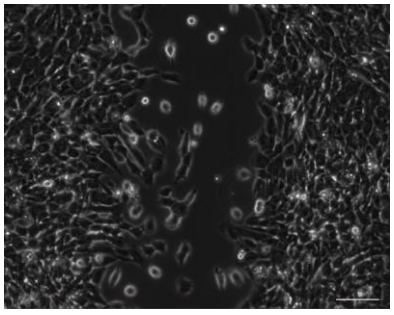

Figure 5.7 Representative phase contrast images of cell wound scratch assay. The microscopy imaging was captured after wound scratch induction and different treatment on day 0 (**T0**). The microscopy imaging was captured again on 48 hours (**T48**) after wound scratch induction. The representative bright field microscopy images of control without treatment (**mock**), presence of 200ng/ml Tetracycline hydrochloride (**T+**), presence of transfection reagent Viafect (**V**), presence of 40 ng/ml transforming growth factor β1 (**B**), presence of 200 ng/ml mrIFN-γ (**Y**) and presence of both 40 ng/ml hrTGF-β1 and 200 ng/ml mrIFN-γ (**BY**). There are morphological changes with TGF-β1 treatment (elongated cell shape) compare to mock (round cell shape). Scale bar = 100µm.

5.2.2.2 Effect of mRln1 on wound closure

We assessed the effect of the presence of 40 ng/ml hrTGF-β1 on cell migration of MH cells with a wound scratch assay. We were also interested whether the transfection of 1000 µg of pTet On-NCO mRln1 plasmids reduced the effect of hrTGF-β1 on MH cell migration. A wound scratch assay was carried out for 48 hours with the treatment of either 40 ng/ml hrTGF-β1, transfected with mRln1 plasmid or both after the wound scratch was induced. The microscopy imaging was captured to assess the area of wound closure on day 0 (T0), day 1 (T24) and day 2 (T48) and percentage of wound closure is shown in **Figure 5.8**. The presence of the either hrTGF-β1 treatment or tetracycline resulted in around ~93% of wound closure after 48 hours, while no treatment (mock) had around ~82% wound closure. The presence of hrTGF-β1 also showed the highest wound closure (~53%) between the day 1 (T24) and day 2 (T48) after the wound scratch was compared with other samples. On the other hand, the presence of mRln1 had the lowest wound closure (~54%) after 48 hours. Finally, the presence of both 40 ng/ml TGF-β1 and mRln1led to wound closure 76%. The representative Brightfield microscopy images of the wound gaps before and after treatment are shown in **Figure 5.9**.

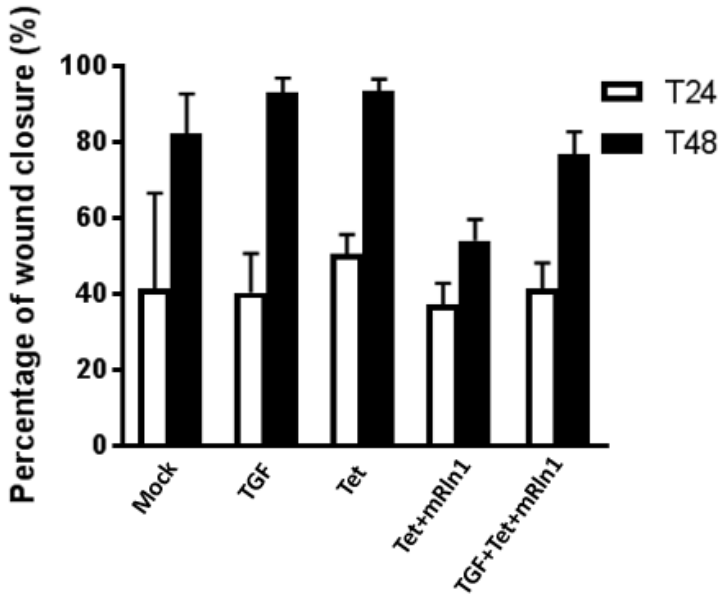

Figure 5.8 *In vitro* assessment of wound closure in MH cell with hrTGF-β1 and mRln1. A wound scratch assay with mouse muscle derived fibroblast cells (MH) transfected with pTet On-NCO mRln1 plasmids with tetracycline presence over a period of 48 hours was carried out. The wound was induced on day 0 (T0) and together with different treatments with the presence or absence of hrTGF-β1. The wound closure was captured with microscopy imaging on day 1 (**T24**) and day 2 (**T48**). The area of wound closure was highlighted with ImageJ and the result shown indicates the percentage area of wound closure. MH cells with no transfection or treatment (**Mock**), MH cells with the presence of 40ng/ml human recombinant transforming growth factor β1 (hrTGF-β1) (**TGF**), MH cells with the presence of 100ng/µl tetracycline (**Tet**), MH cells transfected with pTet On-NCO mRln1 plasmid and the presence of 100ng/µl tetracycline (**Tet+mRln1**) and MH cells transfected with pTet On-NCO mRln1 plasmid and the presence of both 100ng/µl tetracycline & 40ng/ml hrTGF-β1 (**TGT+Tet+mRln1**). Data are the mean ± SD of one independent experiment (n=1, 2 – 3 technical repeats).

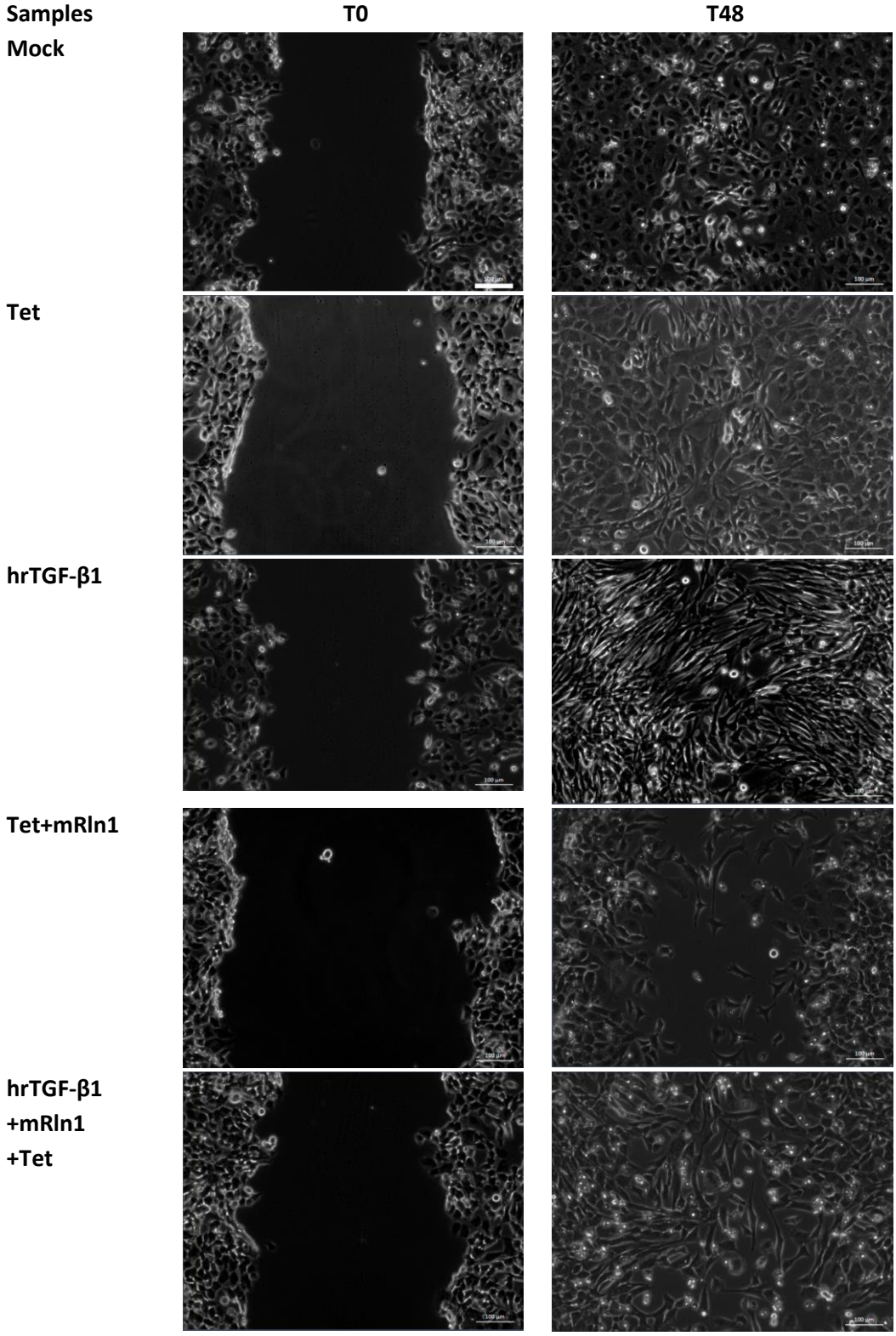

Figure 5.9 Representative Bright field microscopy images of wound scratch assay. The microscopy imaging was captured after wound scratch induction and different treatment on day 0 (**T0**). The microscopy imaging was captured again on 48 hours (**T48**) after wound scratch induction. The representative bright field microscopy images of control without treatment (**mock**), presence of 200ng/ml Tetracycline hydrochloride (**Tet**), presence of 40ng/ml transforming growth factor β1 (**hrTGF-β1**), transfected with plasmid pTet On-NCO mRln1 & presence of 200ng/µl tetracycline hydrochloride (**Tet+mRln1**), transfected with plasmid pTet On-NCO mRln1 & presence of 40ng/ml hrTGF-β1 (**mRln1+hrTGF-β1**) and transfected with plasmid pTet On-NCO mRln1 & presence of both 200ng/ml tetracycline hydrochloride, 40ng/ml

hrTGF-β1 (**Tet+mRln1+hrTGF-β1**). There are morphological changes with TGF-β1 treatment (elongate cell shape) compare to mock (round cell shape). Scale bar = 100μm.

5.3 DISCUSSION

5.3.1 The effect of mRln1 on downstream fibrotic related genes and wound scratch assay

In this chapter, we tried to evaluate on the effect of mRln1 expression in C2C12 and MH cell line by transfecting pTet On-NCO mRln1 plasmids in the presence of tetracycline. RT-qPCR methods were able to provide an insight into how upregulations of mRln1 have an effect on the transcript level of downstream fibrotic related genes. Li and colleagues (Li *et al*., 2004) have shown the expression of Acta2 and Fn1 protein increase after 8 hours of treatment with exogenous hrTGF-β1. While our investigation was carried out for 24 hours, our results do not seem to match theirs, with a slight reduction on the transcript level of Acta2 and Fn1. Further investigations such as investigation of the protein level of Acta2 and Fn1 should be considered for more information. Our results showed a 1-fold increase of the TIMP1 transcript level after mRln1 upregulation for 24 hours. The TIMP1 mRNA upregulation might link to the suppression activity of MMP9, where the TIMP1 is an inhibitor to MMP9 (Morgan *et al*., 2010). Besides, high levels of MMP9 in C2C12 cells have been shown in improving the migration rate (Morgan *et al*., 2010). On the other hand, a gradient of time course of investigation can be performed on how upregulation of mRln1 at different time point. We should also investigate the effect of TGF-β1 presence in cells transfected with mRln1 expressing plasmid or both in C2C12. Li and colleagues shown the presence of TGF-β1 can reduce the myogenic protein expression (such as myogenin, myoD and desmin) and increase Acta2, Fn1 protein expression (Li *et al*., 2004). Overall we have shown that the mRln1 upregulation in C2C12 cells can reduce the transcript level of Acta2 and Fn1.

The downstream fibrotic related genes (*Acta2*, *Fn1* and *Postn*) transcript level is reduced with the mRln1 upregulations compared to mock. This results suggested mRln1 can reduce expression of the myofibroblast cell surface marker (Acta2), and also reduces the transcript level

of ECM components (Fn1 and Postn). In contrast, the presence of TGF-β1 can increase the transcript level expression of *Fn1*, while *Acta2* and *Postn* remain similar compared to mock. It is not sure why the effect of TGF-β does not affect *Acta2* and *Postn* expression. Our result have shown the effect of hrTGF-β1 can be reduced with the mRln1 upregulation. Our results are similar to Zanotti *et* al., (2016) who report that the presence of pirfenidone (anti-fibrotic drug) can reduce the transcript level of *Fn1* in primary mdx active myofibroblasts. Further investigation on the protein level of the three genes mentioned earlier or other related proteins shall be examined for more accurate outcome on the effect of mRln1. A gradient of TGF-β1 dose treatment and duration of treatment shall be investigated further on the transcript level or protein expression of downstream fibrotic related genes. Overall, we have shown that the mRln1 upregulation might reduce the activity of TGF-β1. However, no statistics could be carried out as the n number was 1 or 2. In the future, experiment repeat with more n number will enable statistical analysis.

5.3.2 The effect of TGF-β1 and mRln1 on wound closure in wound scratch assay

To determine the effects of the TGF-β1 on MH cells with wound scratch, we applied exogenous hrTGF-β1 in the culture media. Our results indicate that hrTGF-β1 can increase the speed of wound closure compared to untreated samples; in contrast the presence of IFN-γ reduced the rate of wound closure. When both hrTGF-β1 and IFN-γ are present in the culture medium of MH cells in wound scratch assay, the activity of hrTGF-β1 is inhibited due to the presence of IFN-γ. On the other hand, the upregulation of mRln1 is capable in reducing the effect of TGF-β1. This is further supported by the fact that mRln1 might contribute with its anti-fibrotic property. In the future, investigations shall be focused on related proteins affected by the mRln1 upregulation. On the other hand, the collagen content in the culture media and intracellular collagen content might be an interesting point to look into as this can indicate the amount of

ECM production and secretion. The TGF-β1 has been shown here to change the morphology of MH cells in both wound scratch assay investigation; further investigation such as gene and protein expression (α-SMA as a biomarker of myofibroblast or ECM secretion) comparison with MH cell would be interesting. Apart from that, a concentration gradient shall be investigated with a range of doses of TGF-β1 and IFN-γ with MH cells for optimum response.

There are few challenges during the wound scratch assay experiment, where it is difficult to split the cells in a well even distributed manner on ibidi dishes. Next, the wound scratch induced manually with the pipette tip is not consistent; it could be improved with a more consistent automatic wound induction system (Incucyte) across 96-wells plate (Roddy *et al*., 2016). In order to improve the accuracy of data collect, microscopy live-imaging provide video camera recording on wound scratch assay such as more consistent imaging on the same fix targeting location microscopy imaging at specific time point or with continued microscopy video recording system (Roddy *et al*., 2016). Although latest technology can improve the outcome of wound scratch assays, limitations such as different cell densities due to the accumulation of cells at the side of wound scratch might not be able to overcome (Vang and Jenssen, 2018). On the other hand, the sample size shall be increased for the experiment.

In conclusion, our data indicate that the mRln1 upregulation is able to reduce MH cell migration rate and the mRNA expression of downstream fibrotic related genes. However, the mRln1 protein might not expressed so well, we should therefore try to compare our transfection with mRln1 expressing plasmids to the presence of mouse recombinant relaxin 1 protein as a positive control in *in vitro* investigation or western blot. Apart from that, it is important to show mouse relaxin 1 receptor (RXFP1) is presence in both MH and C2C12 cells. This demonstrates the mRln1 upregulation might be a potential treatment for muscle fibrosis in Duchenne muscular dystrophy. On top of that, relaxin has been shown to have other beneficial effects: reduced inflammation in cardiovascular diseases, control MMP expression and promote satellite cell mobilization in muscle healing. In muscular dystrophies, muscle fibrosis and inflammation is

an unregulated process which contributes to the second pathology. Further *in vitro* studies regard using primary mdx myogenic, muscle-derived fibroblasts or both types of cells shall be investigated before proceeding to *in vivo*.

CHAPTER 6: GENERAL DISCUSSION

Chapter 6: GENERAL DISCUSSION

6.1 Project overview

Many studies have shown that skeletal muscle is capable of synthesizing and correct processing of a variety of proteins (Kessler *et al*., 1996). Skeletal muscle targeting gene therapy is also considered to be the first regulatory approval of gene therapy (Sarcar et al., 2019). We aim to use adeno-associated viral vector as a vehicle to deliver mouse relaxin 1 (mRln1) isoform as a muscle targeting gene therapy to reduce muscle fibrosis in DMD. In this thesis, we evaluated the potential of mouse relaxin 1 expression to reduce muscle fibrosis through an in vitro study using mRln1 plasmid delivery. We were particularly interested in investigating the hypothesis that muscle-derived mRln1 secretion acts in an autocrine and paracrine manner and could potentially reduce the activation of muscle-derived fibroblasts in response to a fibrotic stimulus. In the following investigation, experimental data were assessed:

In Chapter 3, we have showed the mRln1 plasmids construct are designed and verification the identity of the plasmid. The transfection efficiency is highest with transfection reagent Viafect in C2C12 and MH cells. In Chapter 4, our results suggested that the mRln1 mRNA expression with RT-qPCR analysis show that mRln1 transcript level is express with mRln1 plasmids construct with codon optimised mRln1 (CO mRln1) or non-codon optimised mRln1 (NCO mRln1). The highest mRln1 mRNA expression was shown with plasmids pTet On-NCO mRln1, a NCO mRln1 plasmid driven by the tetracycline-inducible promoter (Tet-On). Next, the pre-pro-mRln1 protein (~21kDa) was detected with the cell lysate samples was success detected via western blot, but the mRln1 targeting antibody cannot detect any mature form of mRln1 protein in the cell culture medium.

In Chapter 5, we demonstrated that the downstream effects of mRln1 upregulation in C2C12 and MH cells. The RT-qPCR targeting 7 downstream fibrotic relate genes (Acta2, Col1a1, Fn1, MMP9, Postn, TIMP1 and TIMP2) in C2C12 cell. Our result suggested the mRln1 upregulation can reduce the transcript level of Acta2 and Fn1, increase TIMP1 expression in C2C12 cell. On the other hand, the RT-qPCR analysis indicate a reduce in 3 downstream fibrotic

relate genes (Acta2, Fn1 and Postn) in MH cell. Furthermore, the effect of the presence of TGF-β1 (a pro-fibrotic factor) can be reduced with the mRln1 upregulation and lower the expression of the three downstream fibrotic relate genes. Next, we utilize wound scratch with MH cells shown that the migration rate is reduced with the presence of IFN-γ or transfected with mRln1 expressing plasmids. In contrast, TGF-β1 increase the migration rate of MH cells and lead to a 10% more on wound closure. The effect of both IFN-γ (TGF-β1 inhibitor) and upregulations of mRln1 can also inhibit the effect of the presence of TGF-β1 on the migration rate of MH cells.

6.2 Limitation of the work present and relevance to the field of gene therapy for DMD and muscle fibrosis

6.2.1 Limitation of present work

In the current project, we performed an in vitro investigation in a mouse myogenic cell line (C2C12) and a mouse muscle-derived fibroblast cell line (MH). Although we show upregulation of mRln1 mRNA expression from mRln1 express plasmids in C2C12 and MH cells through RT-qPCR, we are unable to show mature mRln1 protein is secreted into the culture medium using western blot. We suggest that further investigation using western blotting with another specific mouse relaxin 1 antibody instead of the human relaxin 2 targeting antibody we had used, loading higher protein amounts and using mRln1 recombinant protein as a positive control might contribute to the success of secreted mRln1 detection. Further investigation could focus on the change in level of downstream fibrotic related protein (such as Acta2, Col1a1, Fn1, MMP9, Postn, TIMP1 and TIMP2), and intracellular and soluble collagen content as a result of relaxin expression.

We suspect the mRln1 protein expressed from both the codon and non-codon optimized constructs may not secreted into the cell culture media. Both of the codon and non-codon optimized mRln1 constructs are based on the native mRln1 amino acids sequence (Uniprot,

P47932). We have tried to relate insulin with relaxin as both of these proteins share similar B-C-A protein structures. A study has shown that mature insulin is not secreted from muscle targeting gene therapy; mature insulin is only secreted by pancreatic β cell due to the presence of a specific group of prohormone convertase that can cleave and remove the insulin pro-peptide (Niessen et al., 2012). In both canine modified insulin (Niessen et al., 2012) and human-modified insulin (Shaw et al., 2002) have shown that mutation on original prohormone convertase 3 targeting site and prohormone convertase 2 targeting site into furin (ubiquitous prohormone convertase) targeting site has to allow modified canine and human insulin secreted in C2C12 cell (**Figure 6.1 top**). Although we try to investigate which prohormone convertase might be responsible for the LS amino acids sequence (C-terminal of B-chain and N-terminal of pro-peptide of mRln1) cleavage and compared with some of the secretome protein, there is no information regarding the cleavage of amino acids sequence or types of prohormone convertase targeting it. Therefore, we propose modification of the original prohormone convertase targeting site in the native mRln1 amino acids sequences in between the end of B-chain and before pro-peptide with a furin cleavage site might contribute to the pro-peptide cleavage (**Figure 6.1 bottom**), resulting in mature mRln1 secretion in the myogenic cell line.

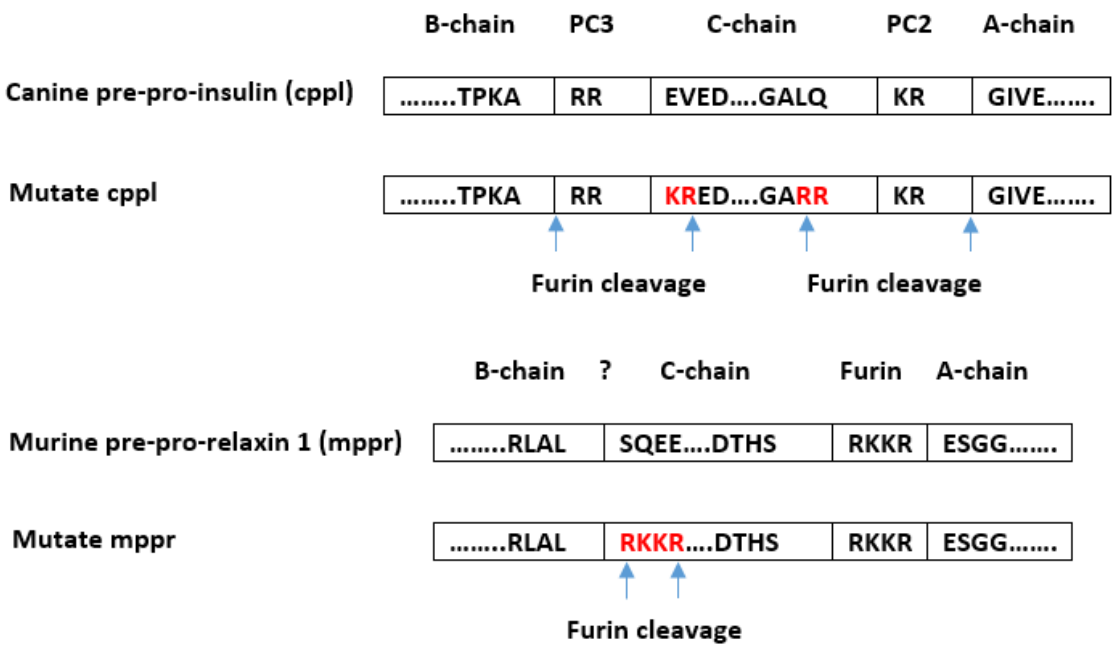

Figure 6.1 Comparison between amino acid sequence of canine pre-pro-insulin and murine pre-pro-relaxin. The canine pre-pro-insulin (**cppl**) (top) have two cleavage site target by prohormone convertase 2 (**PC2**) and prohormone convertase 3 (**PC3**). The mutate cppl are generate through 4 amino acids mutation (**Red**) which allow cleavage by furin (ubiquitous prohormone convertase) (Niessen et al., 2012). The murine pre-pro-relaxin 1 (**mppr**) (bottom) have two cleavage site target by unknown prohormone convertase (**?**) and furin. The mutate mppr are generate through 4 amino acids mutation (**Red**) which allow both cleavage site target by furin.

Both the C2C12 and MH cell lines are normal cell line from mouse, which is different compared to myogenic and fibroblasts from both mdx mouse and DMD patient. Further *in vitro* investigation should be focus on much closer murine H2kb *mdx* myoblast cell line (Morgan *et al*., 1994) and isolating primary muscle-derived fibroblasts/myofibroblasts from *mdx* mice. A study has shown that quiescent fibroblasts can be activated to become active fibroblasts (myofibroblasts) during circumstances (such as wound healing or stress) to proliferate and promote secretion of extracellular matrix component (ECM); activated fibroblasts can be reversible to become quiescent fibroblast or undergo apoptosis (Kalluri, 2016). However, the activated fibroblast in cancer or fibrosis can be irreversible in cancerous/fibrosis activated fibroblasts with ability to enhanced secretion and proliferation (Kalluri, 2016). On the other hand, the high level of transforming growth factor-β (TGF-β) from macrophages cause fibro/adipogenic progenitors to differentiate into myofibroblasts in mdx mice might also be

considered as a source of activating fibroblasts (Lemon et al., 2015). One study has shown that the TGF-β1 kinase inhibitor is able to reverse the proliferating cardiac myofibroblasts but not non-proliferating cardiac myofibroblasts (Driesen *et al*.,2019). It is interesting to investigate whether the irreversible activated muscle derived fibroblasts from mdx mice or DMD exhibit the similar characteristic or not. The investigation on the effect of mRln1 on irreversible myofibroblasts can provide insight into a much closer characteristic of myofibroblast in DMD.

The manual wound scratch assay provides only limited detail on the migration rate of the mouse muscle-derived fibroblasts (MH cell). By using primary mdx muscle fibroblast for wound scratch assay which has the morphology and activity much closer in DMD compare to control mouse muscle-derived fibroblasts (MH cells). Although the wound scratch assay is a cheap, easy and direct technique, it is hard to produce a consistent result (Grada et al., 2017). Other limitations of wound scratch assay is absence of cell to cell adhesion and lack of extracellular matrix effect (Stamm et al., 2016). Besides, the wound scratch does not represent the actual wound (Grada et al., 2017) or muscle fibrosis in DMD (Kharraz et al., 2014). It is unlikely that wound scratch assay with just limited observation on cell migration of fibroblasts can provide a full complex picture on the interaction between different types of cells and extracellular matrix in DMD.

In the 2D cell culture system involved in the wound scratch assay, the limitation is that the single monolayer cell line has more contact with medium and plastic compared to 3D in vivo structure (Antoni et al., 2015). Skeletal muscle wound healing or fibrosis is a complex process involving the interaction of multiple types of cells (such as myogenic cells, fibroblasts, myofibroblasts and leukocyte) with various elements such as chemokines, cytokines, growth factors and inflammatory mediators (Kharraz et al., 2014). TGF-β improved myogenesis in 3D muscle cell cultures but not in the 2D monolayer muscle cell culture, where both of the myogenin gene expression and myotube formation was reduced (Krieger et al., 2018). This study has shown an example of the limitations of the 2D *in vitro* model is not as accurate 3D *in vitro*

model which is similar to *in vivo*. Besides, the presence of more than one of the elements (such as chemokines, cytokines, growth factors and inflammatory mediators) in the culture media of 3D *in vitro* model during the investigation might contribute to much more closely mimic environment that takes place in Mdx mice or DMD patients (Kalluri, 2016).

On top of that, exosome derived from muscle fibroblasts of DMD patients have an elevated miRNA-199a-5p (a pro-fibrotic miRNA) which can promote the activation of fibroblasts (Zanotti et al., 2018). The presence of muscle-derived exosome from muscle fibroblast promotes myofibroblasts phenotype such as Acta2 expression, cell proliferation and collagen production. This might suggest the factors such as miRNA might also affect the muscle fibrosis as well as other elements (such as chemokines, cytokines, growth factors and inflammatory mediators). Therefore it is important to test the effect of mRln1 upregulation with a much more suitable in vitro 3D model with pro-fibrotic secretome and various elements that contribute to muscle fibrosis to give a much closer cellular environment to DMD patients (Krieger et al., 2018).

In fibrosis, there are many strategies targeting for a single factor that have been involve in either extracellular or intracellular factors. Most of the anti-fibrosis strategy focus on the inhibition of growth factors, cytokine, MMP and fibrotic relate miRNA (March *et al*., 2018). One of the main target is transforming growth factor β (master regulator for fibrosis) was the focus. The TGF-β1 contribute to the activation of fibroblast to promoter ECM production which is one of the main pathology in fibrosis. The TGF-β1 inhibition (such as halofuginone), suppression (such as decorin) antagonist (such as tumor necrosis factor-α) strategy have been adapted in order to target TGF-β1 to reduce fibrosis in multiple types of tissue fibrosis (Lichtman *et al*., 2016).

Connective tissue growth factor (CTGF) is a matricellular matrix protein that is upregulated in relation to fibrosis in several chronic diseases. In fibrosis, CTGF promote the proliferation of fibroblast to produce more extracellular matrix (ECM) component. Studies have shown that over expression of CTGF can induce skeletal muscle to produce ECM in *in vivo*

(Morales *et* al., 2011). Besides, it suggested CTGF have been related to the downstream action on TGF-β to exacerbate pro-fibrotic effects (Mori *et al*., 1999). On the other hand, Morales *et al* 2013 also showed that the FG-3019 suppression on CTGF does not affect the TGF-β, pERK1/2 and p38 signalling in mdx mouse. FG-3019 (Pamrevlunab) is a neutralizing antibody target CTGF for and can ameliorate muscle fibrosis in mdx mice, reduce fibrosis in different types of tissue (liver, cardiac and lung) (Morales *et* al., 2013) and currently waiting for Phase II clinical trial in DMD (Fibrogen, 2019). In one of the *in vivo* study have shown that the co-treatment of TGF-β and CTGF cause fibrosis compare to injection with either one of TGF-β or CTGF. (Wang *et al*., 2011). Furthermore, the TGF-β and CTGF immunohistochemical staining of muscle biopsy samples from DMD patients (age between 3 to 13) indicate both integral optical density value is around 115 times more intense compare to normal (Song *et al*., 2017). By summary some of the study on CTGF, we suggested to set up *in vitro* and *in vivo* study that is similar to fibrosis with co-treatment of TGF-β and CTGF together with treatment to inhibit both TGF-β and CTGF.

The pro-fibrotic miRNA have also been study as a strategy to target in order to reduce fibrosis. The studies on miRNA that is involved in fibrosis are such as miR-21 (pro fibrotic role) and miR-29 (anti-fibrotic role) dysregulation in muscle fibrosis (Zanotti *et al*., 2015), miR-125 involve in cardiac fibroblast activation (Zanotti *et al*., 2018), both miR-208a and miR34 relate to cardiac fibrosis (March *et al*., 2018), miR-17-5p upregulated in fibrosis (Meng *et al*., 2016b). The fibrotic miRNA can reduce the fibrotic-related mRNA expression of fibrotic tissue and should compare with muscle fibrosis in DMD.

One of the current published study have shown that by utilizing cell therapy with leukemia inhibit factor (LIF) expression in leukocyte progenitors into dystrophin mouse (Welc *et al*., 2019). The LIF is a member of interleukin-6 class cytokine which exhibit either promote or inhibit process such as cell growth, proliferation or differentiation (Nicola and Babon, 2015). The transplantation of LIF expressing leukocyte progenitor cell can reduce the fibrosis pathology by not favour macrophages for CD163+/CD206 phenotype and decrease T helper cells type 2 (Th2)

cytokines production in muscle (Welc *et al*., 2019), resulting in inhibit TGF-β signalling. This study can provide an insight into how the macrophage and T helper cells involve in muscle fibrosis.

The early detection of the first symptom of DMD in patient play a vital role to start the treatment before fibrosis and inflammation take place in dystrophic muscle (Cordova *et al*., 2018). As the first symptoms start around two to three years old should be noticed with early detection (Bushby *et al*., 2010). Besides, the early dystrophin restoration therapy could minimise the pathology of DMD and maximise the effect of therapeutic therapy. One of the key is the timing to performed therapy for DMD, where the treatment should be started before a plateau in muscle loss around four to six years old is recommended (Sienkiewicz *et al*., 2015).

6.3 CONCLUSIONS

Introduction of muscle targeting as an autocrine, paracrine or endocrine manner with transgene expression offer a therapeutic effect in gene therapy can eliminate repeated administration or daily intake of a therapeutic protein, including Duchenne Muscular Dystrophy. Our project hopes to focus on gene addition for mouse relaxin 1 secretion via muscle to reduce muscle fibrosis. We aim to reduce the muscle fibrosis in DMD with relaxin might combine with other anti-fibrotic strategy to target one of the secondary pathologies of DMD. In future we hope that our work on systemic mouse relaxin 1 expression with AAV in muscle targeting gene therapy should be investigate much more details in 3D models or in vivo models for more information regarding reducing fibrosis before as a supportive therapy together with other strategy target other secondary pathology and the main primary dystrophin restoration multiple factors combinational therapy to cure DMD. In conclusion, DMD research is moving forward with some clinical trials to target primary and secondary pathology represents data collection toward better treatment. An ideal combinational therapy that able targeting both primary and secondary pathology as early as possible would be most likely provide maximise therapeutic effect to DMD.

REFERENCES

Abdul-Razak, H., Malerba, A., & Dickson, G. (2016). Advances in gene therapy for muscular dystrophies. *F1000Research*, *5*.

Alam, M. A., Nayab, M., Azeez, A., Quamri, M. A., & Ansari, A. N. (2014). Muscular Dystrophy (Istirkha) and its management through Unani Medicine: A Review. *International Journal of Herbal Medicine*, 2(4), 1-5.

Alberts, B., Johnson, A., Lewis, J., Raff, M., Roberts, K., Walter, P. (2008) *Molecular Biology of the Cell*. New York: Garland Science.

Alegria-Schaffer, A., Lodge, A. and Vattem, K., 2009. Performing and optimizing Western blots with an emphasis on chemiluminescent detection. In *Methods in enzymology* (Vol. 463, pp. 573-599). Academic Press.

Akhmetshina, A., Palumbo, K., Dees, C., Bergmann, C., Venalis, P., Zerr, P., Horn, A., Kireva, T., Beyer, C., Zwerina, J. and Schneider, H., 2012. Activation of canonical Wnt signalling is required for TGF-β-mediated fibrosis. *Nature communications*, *3*, p.735.

Aminzadeh, M.A., Rogers, R.G., Fournier, M., Tobin, R.E., Guan, X., Childers, M.K., Andres, A.M., Taylor, D.J., Ibrahim, A., Ding, X. and Torrente, A., (2018). Exosome-mediated benefits of cell therapy in mouse and human models of Duchenne muscular dystrophy. *Stem cell reports*, *10*(3), pp.942-955.

Andreetta, F., Bernasconi, P., Baggi F., et al. (2006). Immunomodulation of TGF-beta 1 in mdx mouse inhibits connective tissue proliferation in diaphragm but increases inflammatory response: implications for antifibrotic therapy. *J Neuroimmunol*. 175:77–86.

Anguela, X.M. and High, K.A., 2019. Entering the modern era of gene therapy. *Annual review of medicine*, *70*, pp.273-288.

Antoni, D., Burckel, H., Josset, E. and Noel, G., 2015. Three-dimensional cell culture: a breakthrough in vivo. International journal of molecular sciences, 16(3), pp.5517-5527.

Arikawa, E., Sun, Y., Wang, J., Zhou, Q., Ning, B., Dial, S.L., Guo, L. and Yang, J., 2008. Cross-platform comparison of SYBR® Green real-time PCR with TaqMan PCR, microarrays and other gene expression measurement technologies evaluated in the MicroArray Quality Control (MAQC) study. *BMC genomics*, *9*(1), p.328.

Atchison, R. W., Casto, B. C., & Hammon, W. M. (1965). Adenovirus-associated defective virus particles. *Science*, *149*(3685), 754-755.

Athey, J., Alexaki, A., Osipova, E., Rostovtsev, A., Santana-Quintero, L.V., Katneni, U., Simonyan, V. and Kimchi-Sarfaty, C., 2017. A new and updated resource for codon usage tables. *BMC bioinformatics*, *18*(1), p.391.

Balcı, B. and Dinçer, P., 2009. Efficient transfection of mouse-derived C2C12 myoblasts using a matrigel basement membrane matrix. *Biotechnology Journal: Healthcare Nutrition Technology*, *4*(7), pp.1042-1045.

Bansal, R., Tomar, T., Ostman, A., Poelstra, K., Prakash, J. (2012) Selective targeting of interferon gamma to stromal fibroblasts and pericytes as a novel therapeutic approach to inhibit angiogenesis and tumor growth. *Molecular Cancer Therapeutics*, **11**, 2419-2428. DOI: 10.1158/1535-7136.MCT-11-0758

Bathgate, R.A., Samuel, C.S., Burazin, T.C., Gundlach, A.L. and Tregear, G.W., 2003. Relaxin: new peptides, receptors and novel actions. *Trends in Endocrinology & Metabolism*, *14*(5), pp.207-213.

Bathgate, R. A. D., Lekgabe, E. D., McGuane, J. T., Su, Y., Pham, T., Ferraro, T., et al. (2008). Adenovirus-mediated delivery of relaxin reverses cardiac fibrosis. *Molecular and cellular endocrinology*, *280*(1), 30-38.

Bathgate, R. A. D., Halls, M. L., Van Der Westhuizen, E. T., Callander, G. E., Kocan, M., & Summers, R. J. (2013). Relaxin family peptides and their receptors. *Physiological reviews*, *93*(1), 405-480.

Baum, J. and Duffy, H.S., 2011. Fibroblasts and myofibroblasts: what are we talking about?. *Journal of cardiovascular pharmacology*, *57*(4), p.376.

Bizario, J. C., Cerri , D. G., Rodrigues, L. C., et al. (2009). Imatinib mesylate ameliorates the dystrophic phenotype in exercised mdx mice. *J Neuroimmunol*. 212:93–101.

Bordignon, C., Notarangelo, L. D., Nobili, N., Ferrari, G., Casorati, G., Panina, P., ... & Ugazio, A. G. (1995). Gene therapy in peripheral blood lymphocytes and bone marrow for ADA–immunodeficient patients. *Science*, *270*(5235), 470-475.

Brack, A.S., Conboy, M.J., Roy, S., Lee, M., Kuo, C.J., Keller, C. and Rando, T.A., 2007. Increased Wnt signaling during aging alters muscle stem cell fate and increases fibrosis. *Science*, *317*(5839), pp.807-810.

Bulfield, G., Siller, W.G., Wight, P.A. and Moore, K.J., 1984. X chromosome-linked muscular dystrophy (mdx) in the mouse. *Proceedings of the National Academy of Sciences*, *81*(4), pp.1189-1192.

Büning, H., Perabo, L., Coutelle, O., Quadt-Humme, S., & Hallek, M. (2008). Recent developments in adeno-associated virus vector technology. *The journal of gene medicine*, 10(7), 717-733.

Bushby, K., Finkel, R., Birnkrant, D.J., Case, L.E., Clemens, P.R., Cripe, L., Kaul, A., Kinnett, K., McDonald, C., Pandya, S. and Poysky, J., (2010). Diagnosis and management of Duchenne muscular dystrophy, part 1: diagnosis, and pharmacological and psychosocial management. *The Lancet Neurology*, *9*(1), pp.77-93.

Briggs, D., & Morgan, J. E. (2013). Recent progress in satellite cell/myoblast engraftment–relevance for therapy. *The FEBS journal*, *280*(17), 4281-4293.

Brizzard, B., 2008. Epitope tagging. *Biotechniques*, *44*(5), pp.693-695.

Cardoso, L.C., Nascimento, A.R., Royer, C., Porto, C.S. and Lazari, M.F.M., 2010. Locally produced relaxin may affect testis and vas deferens function in rats. *Reproduction*, *139*(1), p.185.

Ceco, E. and McNally, E.M., 2013. Modifying muscular dystrophy through transforming growth factor-β. *The FEBS journal*, *280*(17), pp.4198-4209.

Chakrabarty, P., Rosario, A., Cruz, P., Siemienski, Z., Ceballos-Diaz, C., Crosby, K., Jansen, K., Borchelt, D.R., Kim, J.Y., Jankowsky, J.L. and Golde, T.E., 2013. Capsid serotype and timing of injection determines AAV transduction in the neonatal mice brain. *PloS one*, *8*(6), p.e67680.

Chamova, T., Guergueltcheva, V., Raycheva, M., Todorov, T., Genova, J., Bichev, S., Bojinova, V., Mitev, V., Tournev, I. and Todorova, A., 2013. Association between loss of Dp140 and cognitive impairment in Duchenne and Becker dystrophies. *Balkan Journal of Medical Genetics*, *16*(1), pp.21-29.

Chan, L.J., Rosengren, K.J., Layfield, S.L., Bathgate, R.A., Separovic, F., Samuel, C.S., Hossain, M.A. and Wade, J.D., 2012. Identification of key residues essential for the structural fold and receptor selectivity within the A-chain of H2 relaxin. *Journal of Biological Chemistry*, pp.jbc-M112.

Chen, Z., Tan, W., Zhang, L., Tan, Q., & Yang, J. (2015). Beneficial impact of bFGF antisense therapy in a rat model of pulmonary fibrosis. *Sarcoidosis vasculitis and diffuse lung disease*, *32*(1), 22-31.

Clinical Trials 2017 *Duchenne Muscular Dystrophy*. [online] Available at: https://www.clinicaltrials.gov/ [Accessed 24/1/2017]

Ciciliot, S., & Schiaffino, S. (2010). Regeneration of mammalian skeletal muscle: basic mechanisms and clinical implications. *Current pharmaceutical design*, *16*(8), 906-914.

Cordova, G., Negroni, E., Cabello-Verrugio, C., Mouly, V. and Trollet, C., 2018. Combined therapies for Duchenne muscular dystrophy to optimize treatment efficacy. *Frontiers in genetics*, *9*, p.114.

Conrad, K. P. (2011). Maternal vasodilation in pregnancy: the emerging role of relaxin. *American Journal of Physiology-Regulatory, Integrative and Comparative Physiology*, 301(2), R267-R275.

Cormack, B.P., Valdivia, R.H. and Falkow, S., 1996. FACS-optimized mutants of the green fluorescent protein (GFP). *Gene*, *173*(1), pp.33-38.

Costello, A., Lao, N.T., Gallagher, C., Capella Roca, B., Julius, L.A., Suda, S., Ducrée, J., King, D., Wagner, R., Barron, N. and Clynes, M., 2019. Leaky expression of the TET-On system hinders control of endogenous miRNA abundance. *Biotechnology journal*, *14*(3), p.1800219.

Dalby, B., Cates, S., Harris, A., Ohki, E.C., Tilkins, M.L., Price, P.J. and Ciccarone, V.C., 2004. Advanced transfection with Lipofectamine 2000 reagent: primary neurons, siRNA, and high-throughput applications. *Methods*, *33*(2), pp.95-103.

Daya, S., & Berns, K. I. (2008). Gene therapy using adeno-associated virus vectors. *Clinical microbiology reviews*, 21(4), 583-593.

Dellavalle, A., Sampaolesi, M., Tonlorenzi, R., Tagliafico, E., Sacchetti, B., Perani, L., Innocenzi, A., Galvez, B.G., Messina, G., Morosetti, R. and Li, S., 2007. Pericytes of human skeletal muscle are myogenic precursors distinct from satellite cells. *Nature cell biology*, *9*(3), p.255.

Devarakonda, T. and Salloum, F.N., 2018. Heart Disease and Relaxin: New Actions for an Old Hormone. *Trends in Endocrinology & Metabolism*.

Dhawan, J., & Rando, T. A. (2005). Stem cells in postnatal myogenesis: molecular mechanisms of satellite cell quiescence, activation and replenishment. *Trends in cell biology*, *15*(12), 666-673.

Dickson, G., Voit, T., Moullier, P. and Le Guiner, C., GENETHON, Royal Holloway and Bedford New College, (2017). *Efficient systemic treatment of dystrophic muscle pathologies*. U.S. Patent Application 15/321,416.

Doerfler, W., 2011. Epigenetic consequences of foreign DNA insertions: de novo methylation and global alterations of methylation patterns in recipient genomes. *Reviews in medical virology*, *21*(6), pp.336-346.

Draghia-Akli, R. and Schwartz, R., Baylor College of Medicine and ADViSYS Inc, 2004. *Synthetic muscle promoters with activities exceeding naturally occurring regulatory sequences in cardiac cells*. U.S. Patent Application 10/699,597.

Driesen, R.B., Nagaraju, C.K., Abi-Char, J., Coenen, T., Lijnen, P.J., Fagard, R.H., Sipido, K.R. and Petrov, V.V., 2013. Reversible and irreversible differentiation of cardiac fibroblasts. *Cardiovascular research*, *101*(3), pp.411-422.

Dschietzig, T., Bartsch, C., Greinwald, M., Baumann, G., & Stangl, K. (2005). The pregnancy hormone relaxin binds to and activates the human glucocorticoid receptor. *Annals of the New York Academy of Sciences*, *1041*(1), 256-271.

Duan, D., (2018). Systemic AAV micro-dystrophin gene therapy for Duchenne muscular dystrophy. *Molecular Therapy*.

Dumont, N.A. and Rudnicki, M.A., 2016. Targeting muscle stem cell intrinsic defects to treat Duchenne muscular dystrophy. *NPJ Regenerative medicine*, *1*, p.16006.

England, S.B., Nicholson, L.V.B., Johnson, M.A., Forrest, S.M., Love, D.R., Zubrzycka-Gaarn, E.E., Bulman, D.E., Harris, J.B. and Davies, K.E., 1990. Very mild muscular dystrophy associated with the deletion of 46% of dystrophin. *Nature*, *343*(6254), p.180.

Evans, V. C., Graham, I. R., Athanasopoulos, T., Galley, D. J., Jackson, C. L., Simons, J. P et al. (2011). Adeno-associated virus serotypes 7 and 8 outperform serotype 9 in expressing atheroprotective human apoE3 from mouse skeletal muscle. *Metabolism*, 60(4), 491-498.

Fairclough, R. J., Wood, M. J., & Davies, K. E. (2013). Therapy for Duchenne muscular dystrophy: renewed optimism from genetic approaches. *Nature Reviews Genetics*, *14*(6), 373-378.

Felgner, P.L., Gadek, T.R., Holm, M., Roman, R., Chan, H.W., Wenz, M., Northrop, J.P., Ringold, G.M. and Danielsen, M., 1987. Lipofection: a highly efficient, lipid-mediated DNA-transfection procedure. *Proceedings of the National Academy of Sciences*, *84*(21), pp.7413-7417.

FibroGen 2019 *Pamrevlumab Trials*. [online] Available at: http://www.fibrogen.com/pamrevlumab-trials/ [Accessed 12/9/2019]

Foster, K., Graham, I. R,, Otto, A., Foster, H,, Trollet, C., Yaworsky, P. J., Walsh, F. S., Bickham, D., Curtin, N. A., Kawar, S, L,, Patel, K., Dickson, G. (2009). Adeno-associated virus-8-mediated intravenous transfer of myostatin propeptide leads to systemic functional improvements of slow but not fast muscle. *Rejuvenation Res*.12(2):85-94.

Gangadaran, P., Hong, C.M. and Ahn, B.C., 2017. Current perspectives on in vivo noninvasive tracking of extracellular vesicles with molecular imaging. *BioMed research international*, *2017*.

Gehrig, S. M., van der Poel, C., Hoeflich, A., Naim, T., Lynch, G. S., Metzger, F. (2012). Therapeutic potential of PEGylated insulin-like growth factor I for skeletal muscle disease evaluated in two murine models of muscular dystrophy. *Growth Horm IGF Res*.22(2):69-75

Gene and Cell Therapy FAQ's (2018) American Society of Gene and Cell Therapy [online] Available at: https://www.asgct.org/education/gene-and-cell-therapy-faqs [Accessed 4/5/2018]

Gene Therapy Net (2017) *Viral vectors*. [online] Available at: http://www.genetherapynet.com/viral-vectors.html [accessed 20/1/2016]

Georgia Highlands College (2011) *The Muscular System: Micro and Macro Anatomy*. [online] Available

at:http://www2.highlands.edu/academics/divisions/scipe/biology/faculty/harnden/2121/images/musfiber.jpg [Accessed 30/6/2017]

Gill, D.R., Pringle, I.A. and Hyde, S.C., 2009. Progress and prospects: the design and production of plasmid vectors. *Gene therapy*, *16*(2), p.165.

Gillies, A. R., & Lieber, R. L. (2011). Structure and function of the skeletal muscle extracellular matrix. *Muscle & nerve*, *44*(3), 318-331.

Gossen, M., Freundlieb, S., Bender, G., Muller, G., Hillen, W. and Bujard, H., 1995. Transcriptional activation by tetracyclines in mammalian cells. *Science*, *268*(5218), pp.1766-1769.

Grada, A., Otero-Vinas, M., Prieto-Castrillo, F., Obagi, Z. and Falanga, V., 2017. Research techniques made simple: analysis of collective cell migration using the wound healing assay. Journal of Investigative Dermatology, 137(2), pp.e11-e16.

Gray, S.J., Foti, S.B., Schwartz, J.W., Bachaboina, L., Taylor-Blake, B., Coleman, J., Ehlers, M.D., Zylka, M.J., McCown, T.J. and Samulski, R.J., 2011. Optimizing promoters for recombinant adeno-associated virus-mediated gene expression in the peripheral and central nervous system using self-complementary vectors. *Human gene therapy*, *22*(9), pp.1143-1153.

Guiraud, S., & Davies, K. E. (2017). Pharmacological advances for treatment in Duchenne muscular dystrophy. *Current opinion in pharmacology*, *34*, 36-48.

Gumerson, J. D., Michele, D. E. (2011). The dystrophin-glycoprotein complex in the prevention of muscle damage. *J Biomed Biotechnol*. 2011:210797.

Gustafsson, C., Minshull, J., Govindarajan, S., Ness, J., Villalobos, A., & Welch, M. (2012). Engineering genes for predictable protein expression. *Protein expression and purification*, *83*(1), 37-46.

Hartwig, S., Raschke, S., Knebel, B., Scheler, M., Irmler, M., Passlack, W., Muller, S., Hanisch, F.G., Franz, T., Li, X. and Dicken, H.D., (2014). Secretome profiling of primary human skeletal

muscle cells. *Biochimica et Biophysica Acta (BBA)-Proteins and Proteomics*, *1844*(5), pp.1011-1017.

Hathout, Y., Conklin, L.S., Seol, H., Gordish-Dressman, H., Brown, K.J., Morgenroth, L.P., Nagaraju, K., Heier, C.R., Damsker, J.M., Van Den Anker, J.N. and Henricson, E., 2016. Serum pharmacodynamic biomarkers for chronic corticosteroid treatment of children. *Scientific reports*, *6*, p.31727.

Hisaw, F.L., 1926. Experimental relaxation of the pubic ligament of the guinea pig. *Proceedings of the Society for Experimental Biology and Medicine*, *23*(8), pp.661-663.

Ho, S.C., Koh, E.Y., Soo, B.P., Chao, S.H. and Yang, Y., 2016. Evaluating the use of a CpG free promoter for long-term recombinant protein expression stability in Chinese hamster ovary cells. *BMC biotechnology*, *16*(1), p.71.

Hoffman, E. P., Brown, R. H., & Kunkel, L. M. (1987). Dystrophin: the protein product of the Duchenne muscular dystrophy locus. *Cell*, *51*(6), 919-928.

Hsu, S.Y., Nakabayashi, K., Nishi, S., Kumagai, J., Kudo, M., Sherwood, O.D. and Hsueh, A.J., (2002). Activation of orphan receptors by the hormone relaxin. *Science*, *295*(5555), pp.671-674.

Hu, H.H., Chen, D.Q., Wang, Y.N., Feng, Y.L., Cao, G., Vaziri, N.D. and Zhao, Y.Y., 2018. New insights into TGF-β/Smad signaling in tissue fibrosis. *Chemico-biological interactions*, *292*, pp.76-83.

Johnson, E. K., Li, B., Yoon, J. H., Flanigan, K. M., Martin, P. T., Ervasti, J., & Montanaro, F. (2013). Identification of new dystroglycan complexes in skeletal muscle. *PLoS One*, *8*(8), e73224.

Jung, B.K., Lee, W.J., Kang, E., Ahn, H.M., Kim, Y.O., Rah, D.K., Yun, C.O. and Yun, I.S., 2017. Effect of Relaxin Expressing Adenovirus on Scar Remodeling: A Preliminary Study. *Archives of craniofacial surgery*, *18*(1), p.9.

Kähäri, V.M., Chen, Y.Q., Su, M.W., Ramirez, F., Uitto, J. (1990) Tumor necrosis factor-alpha and interferon-gamma suppress the activation of human type I collagen gene expression by transforming growth factor-beta 1. Evidence for two distinct mechanisms of inhibition at the transcriptional and posttranscriptional levels. *The Journal of Clinical Investigation*, **86**, 1489- 1495.

Kalluri, R., 2016. The biology and function of fibroblasts in cancer. *Nature Reviews Cancer*, *16*(9), p.582.

Kendall, R.T. and Feghali-Bostwick, C.A., 2014. Fibroblasts in fibrosis: novel roles and mediators. *Frontiers in pharmacology*, *5*, p.123.

Kallunki, T., Barisic, M., Jäättelä, M. and Liu, B., 2019. How to Choose the Right Inducible Gene Expression System for Mammalian Studies?. *Cells*, *8*(8), p.796.

Kanai, A.J., Konieczko, E.M., Bennett, R.G., Samuel, C.S. and Royce, S.G., 2019. Relaxin and fibrosis: Emerging targets, challenges, and future directions. *Molecular and cellular endocrinology*.

Kang, J. K., Malerba, A., Popplewell, L., Foster, K., Dickson, G. (2011). Antisense-induced myostatin exon skipping leads to muscle hypertrophy in mice following octa-guanidine morpholino oligomer treatment. *Mol Ther*. 19(1):159-64.

Katwal, A.B., Konkalmatt, P.R., Piras, B.A., Hazarika, S., Li, S.S., Lye, R.J., Sanders, J.M., Ferrante, E.A., Yan, Z., Annex, B.H. and French, B.A., (2013). Adeno-associated virus serotype 9 efficiently targets ischemic skeletal muscle following systemic delivery. *Gene therapy*, *20*(9), p.930.

Kawecka, K., Theodoulides, M., Hasoglu, Y., Jarmin, S., Kymalainen, H., Le-Heron, A., et al. (2015). Adeno-associated virus (AAV) mediated dystrophin gene transfer studies and exon skipping strategies for Duchenne muscular dystrophy (DMD). *Current gene therapy*, 15(4), 395-415.

Ke, Xu. (2011) Viral Gene Therapy, Intech, Available from: http://www.intechopen.com/books/viral-gene-therapy/progress-and-challenges-in-aav-mediated-gene-therapy-for-duchenne-muscular-dystrophy [Accessed 19 January 2017]

Kessler, P.D., Podsakoff, G.M., Chen, X., McQuiston, S.A., Colosi, P.C., Matelis, L.A., Kurtzman, G.J. and Byrne, B.J., 1996. Gene delivery to skeletal muscle results in sustained expression and systemic delivery of a therapeutic protein. *Proceedings of the National Academy of Sciences*, *93*(24), pp.14082-14087.

Kinali, M., Main, M., Mercuri, E., & Muntoni, F. (2007). Evolution of abnormal postures in Duchenne muscular dystrophy. *Annals of Indian Academy of Neurology*, *10*(5), 44.

Kharraz, Y., Guerra, J., Pessina, P., Serrano, A.L. and Muñoz-Cánoves, P., 2014. Understanding the process of fibrosis in Duchenne muscular dystrophy. BioMed research international, 2014.

Klymiuk, N., Blutke, A., Graf, A., Krause, S., Burkhardt, K., Wuensch, A., et al. (2013). Dystrophin-deficient pigs provide new insights into the hierarchy of physiological derangements of dystrophic muscle. *Human molecular genetics*, *22*(21), 4368-4382.

Kong, R.C., Shilling, P.J., Lobb, D.K., Gooley, P.R. and Bathgate, R.A., 2010. Membrane receptors: structure and function of the relaxin family peptide receptors. *Molecular and cellular endocrinology*, *320*(1), pp.1-15.

Kornegay, J.N., Childers, M.K., Bogan, D.J., Bogan, J.R., Nghiem, P., Wang, J., Fan, Z., Howard, J.F., Schatzberg, S.J., Dow, J.L. and Grange, R.W., (2012a). The paradox of muscle hypertrophy in muscular dystrophy. *Physical Medicine and Rehabilitation Clinics*, *23*(1), 149-172.

Kornegay, J.N., Bogan, J.R., Bogan, D.J., Childers, M.K., Li, J., Nghiem, P., Detwiler, D.A., Larsen, C.A., Grange, R.W., Bhavaraju-Sanka, R.K. and Tou, S., (2012b). Canine models of Duchenne muscular dystrophy and their use in therapeutic strategies. *Mammalian genome*, *23*(1-2), pp.85-108.

Kota, J., Handy, C.R., Haidet, A.M., Montgomery, C.L., Eagle, A., Rodino-Klapac, L.R., Tucker, D., Shilling, C.J., Therlfall, W.R., Walker, C.M. and Weisbrode, S.E., (2009). Follistatin gene delivery enhances muscle growth and strength in nonhuman primates. *Science translational medicine*, *1*(6), pp.6ra15-6ra15.

Kudla, G., Murray, A.W., Tollervey, D. and Plotkin, J.B., 2009. Coding-sequence determinants of gene expression in Escherichia coli. *science*, *324*(5924), pp.255-258.

Kumar, A. and Pal, D., 2016. Green fluorescent protein and their applications in advance research. *Res. J. Appl. Sci. Eng. Tech*, *1*, pp.42-46.

Krieger, J., Park, B.W., Lambert, C.R. and Malcuit, C., 2018. 3D skeletal muscle fascicle engineering is improved with TGF-β1 treatment of myogenic cells and their co-culture with myofibroblasts. PeerJ, 6, p.e4939.

Lancelot, C., Carnac, G., Nonclercq, D., Delrée, P., Coppée, F., & Belayew, A. (2013). Development of fibrosis and its impact on muscle regeneration in FSHD muscle.

Larcher, T., Lafoux, A., Tesson, L., Remy, S., Thepenier, V., François, V., et al. (2014). Characterization of dystrophin deficient rats: a new model for Duchenne muscular dystrophy. *PloS one*, *9*(10), e110371.

Le Guiner, C., Servais, L., Montus, M., Larcher, T., Fraysse, B., Moullec, S., Allais, M., François, V., Dutilleul, M., Malerba, A. and Koo, T., 2017. Long-term microdystrophin gene therapy is effective in a canine model of Duchenne muscular dystrophy. *Nature communications*, *8*, p.16105.

Lee, H. J., Kao, C. Y., Lin, S. C., Xu, M., Xie, X., Tsai, S. Y., & Tsai, M. J. (2017). Dysregulation of nuclear receptor COUP-TFII impairs skeletal muscle development. *Scientific Reports*, *7*.

Lemos, D.R., Babaeijandaghi, F., Low, M., Chang, C.K., Lee, S.T., Fiore, D., Zhang, R.H., Natarajan, A., Nedospasov, S.A. and Rossi, F.M., 2015. Nilotinib reduces muscle fibrosis in chronic

muscle injury by promoting TNF-mediated apoptosis of fibro/adipogenic progenitors. Nature medicine, 21(7), p.786.

Lenselink, E. A. (2015). Role of fibronectin in normal wound healing. *International wound journal*, *12*(3), 313-316.

Li, X., Eastman, E. M., Schwartz, R. J., & Draghia-Akli, R. (1999). Synthetic muscle promoters: activities exceeding naturally occurring regulatory sequences. *Nature biotechnology*, *17*(3), 241.

Li, Y., Foster, W., Deasy, B.M., Chan, Y., Prisk, V., Tang, Y., Cummins, J. and Huard, J., 2004. Transforming growth factor-β1 induces the differentiation of myogenic cells into fibrotic cells in injured skeletal muscle: a key event in muscle fibrogenesis. *The American journal of pathology*, *164*(3), pp.1007-1019.

Liang, C. C., Park, A. Y., & Guan, J. L. (2007). In vitro scratch assay: a convenient and inexpensive method for analysis of cell migration in vitro. *Nature protocols*, *2*(2), 329.

Lichtman, M.K., Otero-Vinas, M. and Falanga, V., 2016. Transforming growth factor beta (TGF-β) isoforms in wound healing and fibrosis. *Wound Repair and Regeneration*, *24*(2), pp.215-222.

Lieber, R. L., & Ward, S. R. (2013). Cellular mechanisms of tissue fibrosis. 4. Structural and functional consequences of skeletal muscle fibrosis. *American Journal of Physiology-Cell Physiology*, *305*(3), C241-C252.

Lobb, R.J., Becker, M., Wen Wen, S., Wong, C.S., Wiegmans, A.P., Leimgruber, A. and Möller, A., 2015. Optimized exosome isolation protocol for cell culture supernatant and human plasma. *Journal of extracellular vesicles*, *4*(1), p.27031.

Lodish H, Berk A, Zipursky SL, et al. Molecular Cell Biology. 4th edition. New York: W. H. Freeman; 2000. Section 7.1, DNA Cloning with Plasmid Vectors. Available from: https://www.ncbi.nlm.nih.gov/books/NBK21498/

Lodish, H., Berk, A., Kaiser, C. A., Krieger, M., Scott, M. P., Bretscher, A., Ploegh, H., and Matsudaira 2007. *Molecular cell biology*. WH Freeman.

Longo, P. A., Kavran, J. M., Kim, M. S., & Leahy, D. J. (2013). Transient mammalian cell transfection with polyethylenimine (PEI). In *Methods in enzymology* (Vol. 529, pp. 227-240). Academic Press.

LONZA 2013 4D-nucleofector™ Protocol C2C12 cells [online] Available at: https://bioscience.lonza.com/lonza_bs/CH/en/document/download/21276 [Accessed 25 August 2019]

Lu-Nguyen, N. B., Jarmin, S. A., Saleh, A. F., Popplewell, L., Gait, M. J., & Dickson, G. (2015). Combination antisense treatment for destructive exon skipping of myostatin and open reading frame rescue of dystrophin in neonatal mdx mice. *Molecular Therapy*, *23*(8), 1341-1348.

Makihara, N., Arimura, K., Ago, T., Tachibana, M., Nishimura, A., Nakamura, K., ... & Kamouchi, M. (2015). Involvement of platelet-derived growth factor receptor β in fibrosis through extracellular matrix protein production after ischemic stroke. *Experimental neurology*, *264*, 127-134.

Malerba, A., Kang, J. K., McClorey, G., Saleh, A. F., Popplewell, L., Gait, M. J., Wood, M. J., Dickson, G. (2012). Dual Myostatin and Dystrophin Exon Skipping by Morpholino Nucleic Acid Oligomers Conjugated to a Cell-penetrating Peptide Is a Promising Therapeutic Strategy for the Treatment of Duchenne Muscular Dystrophy. *Mol Ther Nucleic Acids*. 1:e62.

Malik, V., Rodino-Klapac, L. R., & Mendell, J. R. (2012). Emerging drugs for Duchenne muscular dystrophy. *Expert opinion on emerging drugs*, 17(2), 261-277.

Mann, C. J., Perdiguero, E., Kharraz, Y., Aguilar, S., Pessina, P., Serrano, A. L., & Muñoz-Cánoves, P. (2011). Aberrant repair and fibrosis development in skeletal muscle. *Skeletal muscle*, *1*(1), 21.

March, J., Golshirazi, G., Cernisova, V., Carr, H., Leong, Y., Lu-Nguyen, N. and Popplewell, L., (2018). Targeting TGFβ Signaling to Address Fibrosis Using Antisense Oligonucleotides. *Biomedicines*, *6*(3), p.74.

Masotti, A., Mossa, G., Cametti, C., Ortaggi, G., Bianco, A., Del Grosso, N., Malizia, D. and Esposito, C., 2009. Comparison of different commercially available cationic liposome–DNA lipoplexes: Parameters influencing toxicity and transfection efficiency. *Colloids and Surfaces B: Biointerfaces*, *68*(2), pp.136-144..

Massagué, J., 2012. TGFβ signalling in context. *Nature reviews Molecular cell biology*, *13*(10), p.616.

Matsakas, A., Foster, K., Otto, A., Macharia, R., Elashry, M. I., Feist, S., Graham, I., Foster, H., Yaworsky, P., Walsh, F., Dickson, G., Patel, K. (2009). Molecular, cellular and physiological investigation of myostatin propeptide-mediated muscle growth in adult mice. *Neuromuscul Disord*. 19(7):489-99.

Matsumura, K., Yamada, H., Shimizu, T., Campbell, K. P. (1993a). Differential expression of dystrophin, utrophin and dystrophin-associated proteins in peripheral nerve. *FEBS Lett*. 334(3):281-5.

Matsumura, K., Campbell, K. P., & Nonaka, I. (1993b). Abnormal expression of dystrophin-associated proteins in Fukuyama-type congenital muscular dystrophy. *The Lancet*, *341*(8844), 521-522.

McCarty, D. M., Young Jr, S. M., & Samulski, R. J. (2004). Integration of adeno-associated virus (AAV) and recombinant AAV vectors. *Annu. Rev. Genet.*, *38*, 819-845.

Meliani, A., Boisgerault, F., Fitzpatrick, Z., Marmier, S., Leborgne, C., Collaud, F., Sola, M.S., Charles, S., Ronzitti, G., Vignaud, A. and van Wittenberghe, L., (2017). Enhanced liver gene transfer and evasion of preexisting humoral immunity with exosome-enveloped AAV vectors. *Blood advances*, *1*(23), pp.2019-2031.

Mendell, J. R., Campbell, K., Rodino-Klapac, L., Sahenk, Z., Shilling, C., Lewis, S., et al & Malik, V. (2010). Dystrophin immunity in Duchenne's muscular dystrophy. *New England Journal of Medicine*, *363*(15), 1429-1437.

Mendell, J.R., Rodino-Klapac, L.R., Sahenk, Z., Roush, K., Bird, L., Lowes, L.P., Alfano, L., Gomez, A.M., Lewis, S., Kota, J. and Malik, V., 2013. Eteplirsen for the treatment of Duchenne muscular dystrophy. *Annals of neurology*, *74*(5), pp.637-647.

Meng, X., Jiang, Q., Chang, N., Wang, X., Liu, C., Xiong, J., Cao, H. and Liang, Z., (2016a). Small activating RNA binds to the genomic target site in a seed-region-dependent manner. *Nucleic acids research*, *44*(5), 2274-2282.

Meng, X. M., Nikolic-Paterson, D. J., & Lan, H. Y. (2016b). TGF-[beta]: the master regulator of fibrosis. *Nature Reviews Nephrology*, *12*(6), 325-338.

Mercuri, E., & Muntoni, F. (2013). Muscular dystrophies. *The Lancet*, *381*(9869), 845-860.

Midoux, P., Breuzard, G., Gomez, J.P. and Pichon, C., 2008. Polymer-based gene delivery: a current review on the uptake and intracellular trafficking of polyplexes. *Current gene therapy*, *8*(5), pp.335-352.

Mihpatte (2012) *Duchenne Muscular Dystrophy Inheritance Pattern*. [online] Available on: http://mihpatte.com/duchenne-muscular-dystrophy-inheritance-pattern/ [Accessed 23/6/2017]

Morales, M.G., Cabello-Verrugio, C., Santander, C., Cabrera, D., Goldschmeding, R. and Brandan, E., 2011. CTGF/CCN-2 over-expression can directly induce features of skeletal muscle dystrophy. *The Journal of pathology*, *225*(4), pp.490-501.

Morales, M.G., Gutierrez, J., Cabello-Verrugio, C., Cabrera, D., Lipson, K.E., Goldschmeding, R. and Brandan, E., 2013. Reducing CTGF/CCN2 slows down mdx muscle dystrophy and improves cell therapy. *Human molecular genetics*, *22*(24), pp.4938-4951.

Morales, M. G., Cabrera, D., Céspedes, C., Vio, C. P., Vazquez, Y., Brandan, E., & Cabello-Verrugio, C. (2013). Inhibition of the angiotensin-converting enzyme decreases skeletal muscle fibrosis in dystrophic mice by a diminution in the expression and activity of connective tissue growth factor (CTGF/CCN-2). *Cell and tissue research*, *353*(1), 173-187.

Morgan, J.E., Beauchamp, J.R., Pagel, C.N., Peckham, M., Ataliotis, P., Jat, P.S., Noble, M.D., Farmer, K. and Partridge, T.A., 1994. Myogenic cell lines derived from transgenic mice carrying a thermolabile T antigen: a model system for the derivation of tissue-specific and mutation-specific cell lines. *Developmental biology*, *162*(2), pp.486-498.

Morgan, J., Rouche, A., Bausero, P., Houssaïni, A., Gross, J., Fiszman, M.Y. and Alameddine, H.S., 2010. MMP-9 overexpression improves myogenic cell migration and engraftment. *Muscle & nerve*, *42*(4), pp.584-595.

Mori, T., Kawara, S., Shinozaki, M., Hayashi, N., Kakinuma, T., Igarashi, A., Takigawa, M., Nakanishi, T. and Takehara, K., 1999. Role and interaction of connective tissue growth factor with transforming growth factor-β in persistent fibrosis: A mouse fibrosis model. *Journal of cellular physiology*, *181*(1), pp.153-159.

Morrison, C., 2015. $1-million price tag set for Glybera gene therapy.

Mu, X., Urso, M. L., Murray, K., Fu, F., & Li, Y. (2010). Relaxin regulates MMP expression and promotes satellite cell mobilization during muscle healing in both young and aged mice. The *American journal of pathology*, 177(5), 2399-2410

Muir, L. A., & Chamberlain, J. S. (2009). Emerging strategies for cell and gene therapy of the muscular dystrophies. *Expert reviews in molecular medicine*, *11*.

Mullis, K., Faloona, F., Scharf, S., Saiki, R.K., Horn, G.T. and Erlich, H., 1986, January. Specific enzymatic amplification of DNA in vitro: the polymerase chain reaction. In *Cold Spring Harbor symposia on quantitative biology* (Vol. 51, pp. 263-273). Cold Spring Harbor Laboratory Press.

Münch, R.C., Muth, A., Muik, A., Friedel, T., Schmatz, J., Dreier, B., Trkola, A., Plückthun, A., Büning, H. and Buchholz, C.J., 2015. Off-target-free gene delivery by affinity-purified receptor-targeted viral vectors. *Nature communications*, *6*, p.6246.

Muntoni, F., Torelli, S., Ferlini, A. (2003). Dystrophin and mutations: one gene, several proteins, multiple phenotypes. *Lancet Neurol*. 2(12):731-40.

Murphy, K. T., Ryall, J. G., Snell, S. M., Nair, L., Koopman, R., Krasney, P. A., Ibebunjo, C., Holden, K. S., Loria, P. M., Salatto, C. T., Lynch, G. S. (2010). Antibody-directed myostatin inhibition improves diaphragm pathology in young but not adult dystrophic mdx mice. *Am J Pathol*. 176(5):2425-34.

Muscular System Anatomy (2018) Medicalook [Online] Available at: http://www.medicalook.com/human_anatomy/systems/Muscular_system.html [[Accessed 4/5/2018]

Nakamura, K., Fujii, W., Tsuboi, M., Tanihata, J., Teramoto, N., Takeuchi, S., et al. (2014). Generation of muscular dystrophy model rats with a CRISPR/Cas system. *Scientific reports*, *4*, 5635.

Naldini, L., 2015. Gene therapy returns to centre stage. *Nature*, *526*(7573), p.351.

Naso, M.F., Tomkowicz, B., Perry, W.L. and Strohl, W.R., 2017. Adeno-associated virus (AAV) as a vector for gene therapy. *BioDrugs*, *31*(4), pp.317-334.

NCBI (2017) *dystrophin Dp427m isoform [Homo sapiens]*. [online] Available at: https://www.ncbi.nlm.nih.gov/protein/NP_003997.1 [Accessed 27/6/2017]

Neary, R., Watson, C. J., & Baugh, J. A. (2015). Epigenetics and the overhealing wound: the role of DNA methylation in fibrosis. *Fibrogenesis & tissue repair*, *8*(1), 18.

Negishi, S., Li, Y., Usas, A., Fu, F. H., & Huard, J. (2005). The effect of relaxin treatment on skeletal muscle injuries. *The American journal of sports medicine*, 33(12), 1816-1824.

Negroni, E., Gidaro, T., Bigot, A., Butler-Browne, G. S., Mouly, V., & Trollet, C. (2015). Invited review: Stem cells and muscle diseases: advances in cell therapy strategies. *Neuropathology and applied neurobiology*, *41*(3), 270-287.

Niessen, S.J.M., Fernandez-Fuente, M., Mahmoud, A., Campbell, S.C., Aldibbiat, A., Huggins, C., Brown, A.E., Holder, A., Piercy, R.J., Catchpole, B. and Shaw, J.A.M., 2012. Novel diabetes mellitus treatment: mature canine insulin production by canine striated muscle through gene therapy. Domestic animal endocrinology, 43(1), pp.16-25.

Neto, M.F. and Figueiredo, M.L., 2016. Skeletal muscle signal peptide optimization for enhancing propeptide or cytokine secretion. *Journal of theoretical biology*, *409*, pp.11-17.

Nicola, N.A. and Babon, J.J., 2015. Leukemia inhibitory factor (LIF). *Cytokine & growth factor reviews*, *26*(5), pp.533-544.

Nirenberg, M.W., (1967). Will society be prepared?. *Science*, *157*(3789), pp.633-633.

Nonneman, D. J., Brown-Brandl, T., Jones, S. A., Wiedmann, R. T., & Rohrer, G. A. (2012). A defect in dystrophin causes a novel porcine stress syndrome. *BMC genomics*, *13*(1), 233.

Ohlendieck, K., Ervasti, J. M., Snook, J. B., & Campbell, K. P. (1991). Dystrophin-glycoprotein complex is highly enriched in isolated skeletal muscle sarcolemma. *The Journal of cell biology*, *112*(1), 135-148.

Ormö, M., Cubitt, A.B., Kallio, K., Gross, L.A., Tsien, R.Y. and Remington, S.J., 1996. Crystal structure of the Aequorea victoria green fluorescent protein. *Science*, *273*(5280), pp.1392-1395.

Orth, P., Schnappinger, D., Hillen, W., Saenger, W. and Hinrichs, W., 2000. Structural basis of gene regulation by the tetracycline inducible Tet repressor–operator system. Nature structural & molecular biology, 7(3), p.215.

Özdemir, C., Akpulat, U., Sharafi, P., Yıldız, Y., Onbaşılar, İ., & Kocaefe, Ç. (2014). Periostin is temporally expressed as an extracellular matrix component in skeletal muscle regeneration and differentiation. *Gene*, *553*(2), 130-139.

Pallafacchina, G., Blaauw, B., & Schiaffino, S. (2013). Role of satellite cells in muscle growth and maintenance of muscle mass. *Nutrition, Metabolism and Cardiovascular Diseases*, *23*, S12-S18.

Paulk, N.K., Pekrun, K., Charville, G.W., Maguire-Nguyen, K., Wosczyna, M.N., Xu, J., Zhang, Y., Lisowski, L., Yoo, B., Vilches-Moure, J.G. and Lee, G.K., 2018. Bioengineered Viral Platform for Intramuscular Passive Vaccine Delivery to Human Skeletal Muscle. *Molecular Therapy-Methods & Clinical Development*, *10*, pp.144-155.

Peng, X., Nelson, E.S., Maiers, J.L. and DeMali, K.A., 2011. New insights into vinculin function and regulation. In *International review of cell and molecular biology* (Vol. 287, pp. 191-231). Academic Press.

Pessina, P., Cabrera, D., Morales, M. G., Riquelme, C. A., Gutiérrez, J., Serrano, A. L., et al., (2014). Novel and optimized strategies for inducing fibrosis in vivo: focus on Duchenne Muscular Dystrophy. *Skeletal muscle*, *4*(1), 7.

Puzzo, F., Colella, P., Biferi, M.G., Bali, D., Paulk, N.K., Vidal, P., Collaud, F., Simon-Sola, M., Charles, S., Hardet, R. and Leborgne, C., 2017. Rescue of Pompe disease in mice by AAV-mediated liver delivery of secretable acid α-glucosidase. *Science translational medicine*, *9*(418), p.eaam6375.

Qiu, J., & Pintel, D. (2008). Processing of adeno-associated virus RNA. *Front Biosci*, *13*, 3101-3115.

Quaggin, S.E. and Kapus, A., 2011. Scar wars: mapping the fate of epithelial–mesenchymal–myofibroblast transition. *Kidney international*, *80*(1), pp.41-50.

Quax, T. E., Claassens, N. J., Söll, D., & van der Oost, J. (2015). Codon bias as a means to fine-tune gene expression. *Molecular cell*, *59*(2), 149-161.

Rahimov, F., & Kunkel, L. M. (2013). Cellular and molecular mechanisms underlying muscular dystrophy. *J Cell Biol*, *201*(4), 499-510.

Ramamoorth, M. and Narvekar, A., 2015. Non-viral vectors in gene therapy-an overview. *Journal of clinical and diagnostic research: JCDR*, *9*(1), p.GE01.

Randolph, M.E. and Pavlath, G.K., 2015. A muscle stem cell for every muscle: variability of satellite cell biology among different muscle groups. *Frontiers in aging neuroscience*, *7*, p.190.

Reed, C. C., Iozzo, R. V. (2002). The role of decorin in collagen fibrillogenesis and skin homeostasis. *Glycoconj J*. 19:249–55.

Roddy, M., Nelson, T., Appledorn, D.M., and Groppi, V., 2016 IncuCyte™ 96-well real-time cell migration and invasion assays [online]. *Essen Bioscience* Publisher. Available from: http://www.essenbioscience.com/media/uploads/files/8000-0083-H00_-_Scratch_Wound_ Migration_Invassion_App_Note.pfd. [Accessed 19 August 2019].

Rodríguez-García, A., Combes, P., Perez-Redondo, R., Smith, M.C. and Smith, M.C., 2005. Natural and synthetic tetracycline-inducible promoters for use in the antibiotic-producing bacteria Streptomyces. *Nucleic acids research*, *33*(9), pp.e87-e87.

Rudeck, S., Etard, C., Khan, M.M., Rottbauer, W., Rudolf, R., Strähle, U. and Just, S., 2016. A compact unc45b-promoter drives muscle-specific expression in zebrafish and mouse. *genesis*, *54*(8), pp.431-438.

Sakai, N., Nakamura, M., Lipson, K.E., Miyake, T., Kamikawa, Y., Sagara, A., Shinozaki, Y., Kitajima, S., Toyama, T., Hara, A. and Iwata, Y., (2017). Inhibition of CTGF ameliorates peritoneal fibrosis through suppression of fibroblast and myofibroblast accumulation and angiogenesis. *Scientific reports*, *7*(1), p.5392.

Samuel, C.S., Zhao, C., Bathgate, R.A., Bond, C.P., Burton, M.D., Parry, L.J., Summers, R.J., Tang, M.L., Amento, E.P. and Tregear, G.W., (2003). Relaxin deficiency in mice is associated with an age-related progression of pulmonary fibrosis. *The FASEB Journal*, *17*(1), pp.121-123.

Samuel, C.S., Tian, H., Zhao, L. and Amento, E.P., 2003. Relaxin is a key mediator of prostate growth and male reproductive tract development. Laboratory investigation, 83(7), p.1055.

Samuel, C.S., Zhao, C., Bathgate, R.A., DU, X.J., Summers, R.J., Amento, E.P., Walker, L.L., Mcburnie, M., Zhao, L. and Tregear, G.W., (2005a). The relaxin gene-knockout mouse: a model of progressive fibrosis. *Annals of the New York Academy of Sciences*, *1041*(1), pp.173-181.

Samuel, C.S., Zhao, C., Yang, Q., Wang, H., Tian, H., Tregear, G.W. and Amento, E.P.,(2005b). The relaxin gene knockout mouse: a model of progressive scleroderma. *Journal of investigative dermatology*, *125*(4), pp.692-699.

Samuel, C. S., Cendrawan, S., Gao, X. M., Ming, Z., Zhao, C., Kiriazis, H., Xu, Q., Tregear, G. W., Bathgate, R. A., Du, X. J. (2011). Relaxin remodels fibrotic healing following myocardial infarction. *Lab Invest*. 91(5):675-90.

Samuel, C. S., Royce, S. G., Hewitson, T. D., Denton, K. M., Cooney, T. E., & Bennett, R. G. (2016). Anti-fibrotic actions of relaxin. *British journal of pharmacology*.

Samuel, C. S., Summers, R. J., & Hewitson, T. D. (2016). Antifibrotic actions of serelaxin–new roles for an old player. *Trends in pharmacological sciences*, *37*(6), 485-497.

Salva, M. Z., Himeda, C. L., Tai, P. W., Nishiuchi, E., Gregorevic, P., Allen, J. M., et al. (2007). Design of tissue-specific regulatory cassettes for high-level rAAV-mediated expression in skeletal and cardiac muscle. *Molecular Therapy*, 15(2), 320-329.

Saraiva, J., Nobre, R. J., & de Almeida, L. P. (2016). Gene therapy for the CNS using AAVs: the impact of systemic delivery by AAV9. *Journal of Controlled Release*, *241*, 94-109.

Sarcar, S., Tulalamba, W., Rincon, M.Y., Tipanee, J., Pham, H.Q., Evens, H., Boon, D., Samara-Kuko, E., Keyaerts, M., Loperfido, M. and Berardi, E., 2019. Next-generation muscle-directed gene therapy by in silico vector design. Nature communications, 10(1), p.492.

Sarepta (2018) *News* [online] Available at:http://investorrelations.sarepta.com/news-releases/news-release-details/sarepta-therapeutics-announces-its-first-rd-day-jerry-mendell-md [Accessed 31/8/2018]

Sartorius, *Vivapsin turbo*, Available at: http://www.sartorius.com/shop/ww/en/usd/applications-laboratory-filtrationultrafiltration/vivaspin-turbo> [Accessed 4 July 2019]

Serrano, A.L. and Muñoz-Cánoves, P., 2010. Regulation and dysregulation of fibrosis in skeletal muscle. *Experimental cell research*, *316*(18), pp.3050-3058.

Schembri, L., Dalibart, R., Tomasello, F., Legembre, P., Ichas, F. and De Giorgi, F., 2007. The HA tag is cleaved and loses immunoreactivity during apoptosis. *Nature methods*, *4*(2), p.107.

Senior, M., 2017. After Glybera's withdrawal, what's next for gene therapy?.

Shi-Wen, X., Parapuram, S. K., Pala, D., Chen, Y., Carter, D. E., Eastwood, M., ... & Leask, A. (2009). Requirement of transforming growth factor β–activated kinase 1 for transforming growth factor β–induced α-smooth muscle actin expression and extracellular matrix contraction in fibroblasts. *Arthritis & Rheumatology*, *60*(1), 234-241.

Sibbald, B. (2001). Death but one unintended consequence of gene-therapy trial. *Canadian Medical Association. Journal*, *164*(11), 1612.

Song, Y., Yao, S., Liu, Y., Long, L., Yang, H., Li, Q., Liang, J., Li, X., Lu, Y., Zhu, H. and Zhang, N., 2017. Expression levels of TGF−β1 and CTGF are associated with the severity of Duchenne muscular dystrophy. *Experimental and therapeutic medicine*, *13*(4), pp.1209-1214.

Sonntag, F., Schmidt, K., & Kleinschmidt, J. A. (2010). A viral assembly factor promotes AAV2 capsid formation in the nucleolus. *Proceedings of the National Academy of Sciences*, *107*(22), 10220-10225.

Spinazzola, J.M. and Kunkel, L.M., 2016. Pharmacological therapeutics targeting the secondary defects and downstream pathology of Duchenne muscular dystrophy. *Expert opinion on orphan drugs*, *4*(11), pp.1179-1194.

Stamm, A., Reimers, K., Strauß, S., Vogt, P., Scheper, T. and Pepelanova, I., 2016. In vitro wound healing assays–state of the art. BioNanoMaterials, 17(1-2), pp.79-87.

Su, X., Jin, Y., Shen, Y., Ju, C., Cai, J., Liu, Y., Kim, I.M., Wang, Y., Yu, H., Weintraub, N.L. and Jiang, M., 2018. Exosome-derived dystrophin from allograft myogenic progenitors improves cardiac function in duchenne muscular dystrophic mice. *Journal of cardiovascular translational research*, *11*(5), pp.412-419.

Sun, Y., Wang, H., Li, Y., Liu, S., Chen, J., & Ying, H. (2018). miR-24 and miR-122 negatively regulate transforming growth factor-β/Smad signaling pathway in skeletal muscle fibrosis. *Molecular Therapy-Nucleic Acids*.

Szulc, J., Wiznerowicz, M., Sauvain, M.O., Trono, D. and Aebischer, P., 2006. A versatile tool for conditional gene expression and knockdown. *Nature methods*, *3*(2), p.109.

T Das, A., Tenenbaum, L. and Berkhout, B., 2016. Tet-On systems for doxycycline-inducible gene expression. Current gene therapy, 16(3), pp.156-167.

Taylor, S., Wakem, M., Dijkman, G., Alsarraj, M. and Nguyen, M., 2010. A practical approach to RT-qPCR—publishing data that conform to the MIQE guidelines. *Methods*, *50*(4), pp.S1-S5.

Teerlink, J.R., Cotter, G., Davison, B.A., Felker, G.M., Filippatos, G., Greenberg, B.H., Ponikowski, P., Unemori, E., Voors, A.A., Adams Jr, K.F. and Dorobantu, M.I., 2013. Serelaxin,

recombinant human relaxin-2, for treatment of acute heart failure (RELAX-AHF): a randomised, placebo-controlled trial. *The Lancet*, *381*(9860), pp.29-39.

Thomas, C.E., Ehrhardt, A. and Kay, M.A., 2003. Progress and problems with the use of viral vectors for gene therapy. *Nature Reviews Genetics*, *4*(5), p.346.

Thomas, Christopher M; and, Summers, David (2008) Bacterial Plasmids. In: Encyclopedia of Life Sciences (ELS). John Wiley & Sons, Ltd: Chichester.

Townsend, D. (2014). Finding the Sweet Spot: Assembly and Glycosylation of the Dystrophin-Associated Glycoprotein Complex. *The Anatomical Record*, *297*(9), 1694-1705.

Treat-NMD (2017) *Overview of current trails on DMD.* [online] Available at: http://www.treat-nmd.eu/research/clinical-research/overview-current-trials-dmd/ [accessed 24/1/2017]

Tsien, R.Y., 1998. The green fluorescent protein.

Van Putten, M., Hulsker, M., Nadarajah, V.D., van Heiningen, S.H., Van Huizen, E., Van Iterson, M., Admiraal, P., Messemaker, T., Den Dunnen, J.T., AC't Hoen, P. and Aartsma-Rus, A., 2012. The effects of low levels of dystrophin on mouse muscle function and pathology. *PloS one*, *7*(2), p.e31937.

Vectors Used in Gene Therapy Clinical Trials (2017). Gene Therapy Clinical Trials Worldwide [online] Available at: http://www.abedia.com/wiley/vectors.php [Accessed 3/5/2018]

Vang Mouritzen, M., Jenssen, H. *Optimized Scratch Assay for In Vitro Testing of Cell Migration with an Automated Optical Camera*. *J. Vis. Exp.* (138), e57691. (2018).

Verhaart, I.E. and Aartsma-Rus, A., 2019. Therapeutic developments for Duchenne muscular dystrophy. *Nature Reviews Neurology*, p.1.

Vidal, B., Serrano, A. L., Tjwa, M., et al. Fibrinogen drives dystrophic muscle fibrosis via a TGFbeta/alternative macrophage activation pathway. (2008). *Genes Dev*. 22:1747–52.

Wang, B., Li, J., Fu, F. H., Chen, C., Zhu, X., Zhou, L., et al. (2008). Construction and analysis of compact muscle-specific promoters for AAV vectors. *Gene therapy*, 15(22), 1489-1499.

Wang, C., Kemp-Harper, B.K., Kocan, M., Ang, S.Y., Hewitson, T.D. and Samuel, C.S., 2016. The anti-fibrotic actions of relaxin are mediated through a NO-sGC-cGMP-dependent pathway in renal myofibroblasts in vitro and enhanced by the NO donor, diethylamine NONOate. *Frontiers in pharmacology*, *7*, p.91.

Wang, K., Tang, X., Xie, Z., Zou, X., Li, M., Yuan, H., Guo, N., Ouyang, H., Jiao, H. and Pang, D., (2017). CRISPR/Cas9-mediated knockout of myostatin in Chinese indigenous Erhualian pigs. *Transgenic research*, *26*(6), pp.799-805.

Wang, Q., Usinger, W., Nichols, B., Gray, J., Xu, L., Seeley, T.W., Brenner, M., Guo, G., Zhang, W., Oliver, N. and Lin, A., 2011. Cooperative interaction of CTGF and TGF-β in animal models of fibrotic disease. *Fibrogenesis & tissue repair*, *4*(1), p.4.

Wang, Y.X. and Rudnicki, M.A., (2012). Satellite cells, the engines of muscle repair. *Nature reviews. Molecular cell biology*, 13(2), p.127.

Wang, Y. G., Huang, P. P., Zhang, R., Ma, B. Y., Zhou, X. M., & Sun, Y. F. (2016). Targeting adeno-associated virus and adenoviral gene therapy for hepatocellular carcinoma. *World journal of gastroenterology*, 22(1), 326.

Wang, Z., Zhu, T., Qiao, C., Zhou, L., Wang, B., Zhang, J., et al. (2005). Adeno-associated virus serotype 8 efficiently delivers genes to muscle and heart. *Nature biotechnology*, 23(3), 321-328.

Watanabe, T., Saito, D., Tanabe, K., Suetsugu, R., Nakaya, Y., Nakagawa, S., & Takahashi, Y. (2007). Tet-on inducible system combined with in ovo electroporation dissects multiple roles of genes in somitogenesis of chicken embryos. *Developmental biology*, *305*(2), 625-636.

Welc, S.S., Flores, I., Wehling-Henricks, M., Ramos, J., Wang, Y., Bertoni, C. and Tidball, J.G., 2019. Targeting a therapeutic LIF transgene to muscle via the immune system ameliorates muscular dystrophy. *Nature Communications*, *10*(1), p.2788.

Wells, D.J., 2018. Tracking progress: an update on animal models for Duchenne muscular dystrophy.

Wilkinson, T. N., Speed, T. P., Tregear, G. W., & Bathgate, R. A. (2005). Evolution of the relaxin-like peptide family. *BMC evolutionary biology*, *5*(1), 14.

Wong, M.L. and Medrano, J.F., 2005. Real-time PCR for mRNA quantitation. *Biotechniques*, *39*(1), pp.75-85.

Wu, T., Töpfer, K., Lin, S. W., Li, H., Bian, A., Zhou, X. Y., et al (2012). Self-complementary AAVs induce more potent transgene product-specific immune responses compared to a single-stranded genome. *Molecular Therapy*, *20*(3), 572-579.

Wu, Z., Asokan, A., & Samulski, R. J. (2006). Adeno-associated virus serotypes: vector toolkit for human gene therapy. *Molecular therapy*, 14(3), 316-327.

Wynn, T.A., (2008). Cellular and molecular mechanisms of fibrosis. *The Journal of Pathology: A Journal of the Pathological Society of Great Britain and Ireland*, *214*(2), pp.199-210.

Yang, T.T., Cheng, L. and Kain, S.R., 1996. Optimized codon usage and chromophore mutations provide enhanced sensitivity with the green fluorescent protein. *Nucleic acids research*, *24*(22), pp.4592-4593.

Yoshida, T., Kumagai, H., Suzuki, A., Kobayashi, N., Ohkawa, S., Odamaki, M., Kohsaka, T., Yamamoto, T. and Ikegaya, N., 2011. Relaxin ameliorates salt-sensitive hypertension and renal fibrosis. Nephrology Dialysis Transplantation, 27(6), pp.2190-2197.

Yucel, N., Chang, A.C., Day, J.W., Rosenthal, N. and Blau, H.M., 2018. Humanizing the mdx mouse model of DMD: the long and the short of it. *NPJ Regenerative medicine*, *3*(1), p.4.

Zanotti, S., Gibertini, S., Di Blasi, C., Cappelletti, C., Bernasconi, P., Mantegazza, R., et al. & Mora, M. (2011). Osteopontin is highly expressed in severely dystrophic muscle and seems to play a role in muscle regeneration and fibrosis. *Histopathology*, 59(6), 1215-1228.

Zanotti, S., Gibertini, S., Curcio, M., Savadori, P., Pasanisi, B., Morandi, L., Cornelio, F., Mantegazza, R. and Mora, M., 2015. Opposing roles of miR-21 and miR-29 in the progression of fibrosis in Duchenne muscular dystrophy. *Biochimica et Biophysica Acta (BBA)-Molecular Basis of Disease*, *1852*(7), pp.1451-1464.

Zanotti, S., Bragato, C., Zucchella, A., Maggi, L., Mantegazza, R., Morandi, L., & Mora, M. (2016). Anti-fibrotic effect of pirfenidone in muscle derived-fibroblasts from Duchenne muscular dystrophy patients. *Life sciences*, *145*, 127-136.

Zanotti, S., Gibertini, S., Blasevich, F., Bragato, C., Ruggieri, A., Saredi, S., Fabbri, M., Bernasconi, P., Maggi, L., Mantegazza, R. and Mora, M., (2018). Exosomes and exosomal miRNAs from muscle-derived fibroblasts promote skeletal muscle fibrosis. *Matrix Biology*.

Zhou, L., & Lu, H. (2010). Targeting fibrosis in Duchenne muscular dystrophy. *Journal of Neuropathology & Experimental Neurology*, 69(8), 771-776.

Zinn, E., Pacouret, S., Khaychuk, V., Turunen, H. T., Carvalho, L. S., Andres-Mateos, E., et al. (2015). In silico reconstruction of the viral evolutionary lineage yields a potent gene therapy vector. *Cell reports*, 12(6), 1056-1068.

Zordan, R.E., Beliveau, B.J., Trow, J.A., Craig, N.L. and Cormack, B.P., 2015. Avoiding the ends: internal epitope tagging of proteins using transposon Tn7. *Genetics*, *200*(1), pp.47-58.

Zou, Q., Wang, X., Liu, Y., Ouyang, Z., Long, H., Wei, S., Xin, J., Zhao, B., Lai, S., Shen, J. and Ni, Q., (2015). Generation of gene-target dogs using CRISPR/Cas9 system. *Journal of molecular cell biology*, *7*(6), pp.580-583.